ASSESSING THE INFLUENCE OF BIOMASS ACCESSIBILITY ON ENZYME TRANSPORT AND CATALYSIS

A Dissertation

Presented to the Faculty of the Graduate School

of Cornell University

In Partial Fulfillment of the Requirements for the Degree of

Doctor of Philosophy

by

Dong Yang

August 2014

ASSESSING THE INFLUENCE OF BIOMASS ACCESSIBILITY ON ENZYME TRANSPORT AND CATALYSIS

Dong Yang, Ph.D.

Cornell University 2014

Accessible internal pore surface is a major factor in defining the rate and extent of enzymatic hydrolysis of cellulosic biomass. Steric hindrance within the pore structure can be a major factor limiting the accessibility of cell-wall-degrading-enzymes (CWDEs) to reactive surface area. My research investigated the fundamental mechanisms involved in limiting CWDEs accessibility to reactive surface area from three aspects. First, a high resolution microscopy platform was developed to gain insights into the diffusion hindrance that CWDEs may encounter in crowded environments inside the biomass porous space. The diffusion activity of fluorescently-labeled non-bound dextran probes in pore space of filter paper particles was observed using a high resolution CLSM microscopy platform. A pore grouping diffusion model was developed and modeling results show that 75% of the accessible pore volume is available for fast diffusion without any significant pore hindrance. Second, a novel solute exclusion system was developed to measure specific pore volume and specific surface areas for raw and pretreated mixed-hardwood (MHW) and switchgrass (SG). Replicate measurements of probe concentrations consistently yielded coefficient of variance of less than 1.5%. Particle size reduction had a smaller influence on the specific pore volume distribution of raw biomass. Pore surface area accessible to 5.1 nm probe increased 4-5 folds for pretreated

MHW and SG. A pore size change mechanism was proposed that could explain the influence of size reduction and pretreatment on pore volume measurements. Third, pore size distribution changes during the hydrolysis process were investigated to elucidate the intrinsic hydrolysis mechanisms of CWDEs. Pretreated SG reached the plateau after 12 hr of hydrolysis and showed a faster initial hydrolysis rate than pretreated MHW. Most of the CWDEs have been removed by protease from the system as shown by SDS-PAGE gel and Bradford assay analysis. Results showed a 30% initial declining of specific pore volume for both MHW and SG after the first 2 hours of hydrolysis. The resulting accessible reaction surface drop can directly contribute to the decreasing in hydrolysis rate.

BIOGRAPHICAL SKETCH

Dong Yang was born in Henan Province, China. He and his family happily lived there before he went to Shanghai to attend Jiao Tong University (SJTU) in 2003. He graduated in 2007 with a Bachelor of Science degree in Environmental Engineering. Following this, Dong came to the United States to study renewable chemical production. He graduated from University of California, Davis (UCD) in 2009 with a Master of Science degree in Biosystem Engineering. After that he started to pursue his Doctorate of Philosophy degree in the Department of Biological and Environmental Engineering at Cornell University in Ithaca, New York. In July 2014, he will be getting into the chemical/bio industry to start the next chapter of his life as a Chemical Engineer. He has been happily married for five years and has a little girl who always wants his attention.

To Mom, Shuang and Emma

Three lovely women who always wonder what I did at Cornell

ACKNOWLEDGMENTS

"Learning without thinking leads to confusion, thinking without learning is wasted effort". -- Confucius, ~500 BC

I would like to express my gratitude to my advisor, Dr. Larry Walker, for supporting and mentoring me through my doctoral program. His encouragement, perseverance and his philosophy of balancing learning and thinking made him a great mentor to work with. I would also like to express my sincere appreciation to my other committee members. Dr. Jean-Yves Parlange, Dr. David Wilson and Dr. Matt DeLisa have provided much valuable insights and thoughtful discussions during my stay at Cornell. Also owed thanks are my colleagues in the Walker group for their feedback and support over the years. Thanks must go to Ms. Sue Fredenburg for providing generous help and assistance to my study and life during my stay at Cornell.

I would like to give my greatest gratitude to my dad for his everlasting love and to my mom, my wife Shuang and my precious little girl Emma for their love, hope, company and support.

TABLE OF CONTENTS

LIST OF FIGURES

LIST OF TABLE

1. INTRODUCTION

1.1 Background

Despite the current uncertainty and challenges to the development of second generation biofuels and bioproducts, there remains considerable global interest in the biochemical conversion of biomass into fermentable sugars (Harris et al., 2013). The biochemical conversion process for producing fermentable sugars from lignocellulosic biomass is called saccharification. Saccharification can generate intermediate products for the later biological or chemical process to produce fuels and other chemicals. Aside from bioethanol, the carbohydrates generated from saccharification can also be converted to hydrocarbons for use as liquid transportation fuels. It has been reported that branched hydrocarbons in gasoline and longer chain hydrocarbons in diesel and jet fuels are selectively produced from carbohydrates derived from lignocellulosic biomass. Other monofunctional compounds such as alcohols, ketones and carboxylic acids, can also be produced after saccharification and used as intermediates for fine chemicals and polymers markets (Bond et al., 2010; Gallezot, 2012; Huber et al., 2005; Kunkes et al., 2008).

Progress has been made in lowering the cost of biomass saccharification through process engineering and the innovative application of genomics, protein engineering and other

molecular biology approaches (Gusakov et al., 2005; Irwin et al., 1993; Karlsson et al., 2001; Santhanam and Walker, 2008; Snow and O'Dea, 1981; Wilson, 2012). However, the saccharification of lignocellulosic biomass remains one of the most expensive steps in the production of advanced biofuels (Luterbacher et al., 2010; Lynd et al., 2008; Wang et al., 2012). This is primarily due to the cost associated with high enzyme loadings commonly required for efficient saccharification (Jeoh et al., 2002a; Wilson, 2004). Thus, the successful commercialization of fuels derived from lignocellulosic biomass hinges on lowering the cost of the enzymes through a reduction of enzyme loadings or an increase in the activities of enzyme cocktails (Arantes and Saddler, 2011).

To accomplish these dual goals of lowering cost and improving activity, it is necessary to expand our understand of the enzymatic saccharification process (Saxena and Brown, 2005). However, the fundamentals (e.g. binding mechanisms, rate retardation and diffusion limitation in the porous substrate) of saccharification are still not well understood. At the most fundamental level, saccharification occurs when cellulases bind to and react on the exposed surface of cellulose fibrils (Chanzy et al., 1984; Langan et al., 2001). The surface area available for enzymatic attack and the ease of transport of the enzyme through the porous cellulosic structure are critical in assessing the hydrolysis rate and extent. Therefore, my overall goal is to assess the influence of cellulose accessibility on cellulase transport and catalysis.

1.2. General objective

An over-arching hypothesis for this research is that steric hindrance within the pore structure of cellulosic materials is a major factor limiting the accessibility of cell-wall-degrading enzymes (CWDEs) to reactive surface area and is a major factor in determining the overall reaction rate. This is based on the need for CWDEs to access reactive surface area form the enzyme-substrate complex for hydrolysis to occur. Mechanistically, CWDEs initially diffuse, bind and react on readily accessible cellulose in the macropore space of the cellulose particle. However, the accessibility to the smaller micropores is limited due to the "traffic jam" caused by the interactions between CWDEs and micropore wall and collisions between CWDE molecules in crowded environments (Figure 1.1). In addition, steric hindrance is expected to play a major role in the ability of CWDEs to cooperate in the synergistic degradation on cell wall materials. Synergistic degradation can only occur when the synergistic CWDEs occupy the same reaction space. Given the difference in CWDEs molecular weights, it is possible that pore size and steric hindrance act as a sieving mechanism that limits synergistic activities.

Therefore, the focus of this research program is the investigation of the fundamental mechanisms involved in limiting CWDEs accessibility to reactive surface area. I addressed this problem from three different aspects: (1) the development of a high resolution microscopy platform to observe, measure and analyze diffusive transport for

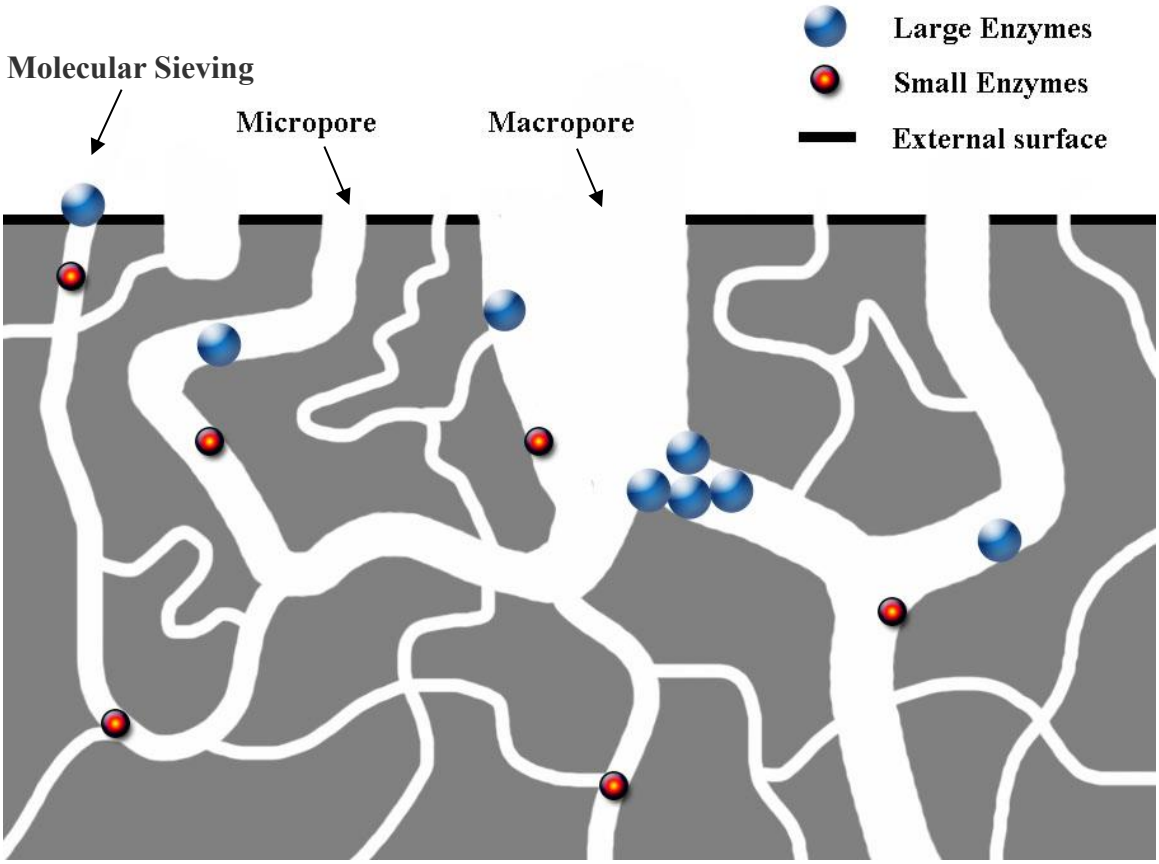

Figure 1.1 Schematic diagram of pore hindered diffusion for enzyme mixtures. Smaller enzymes gain access to more reactive areas than large enzymes.

non-binding species in biomass; (2) the development of a solute exclusion system to measure the pore volume distribution for raw and pretreated mixed hardwoods (MHW) and switchgrass (SG); and (3) the measurement of the temporal changes in pore volume distribution caused by the activities of CWDEs on MHW and SG.

1.3. Objective One: Develop an imaging platform to study the diffusion without binding activities in cellulosic biomass

The molecular diameter of the CWDEs is a key factor in accessing their diffusion into the pore structure of lignocellulosic biomass. However, the process of teasing out diffusive mechanism strictly based on molecular diameter is complicated by the high binding affinity of CWDEs on accessible surface area (Jeoh et al., 2002b; Jung et al., 2002b; Wang et al., 2008). Thus a key research goal is to gain insights into the diffusion hindrance that CWDEs may encounter in crowded environments by observing diffusion of non-binding molecular probes of different sizes into the pore space of cellulosic biomass.

A high resolution microscopy platform was developed to observe and measure the diffusion activity of non-binding species in pore space of a model cellulosic biomass - filter paper particles. In essence, a micro-scale solute exclusion technique is developed for observing and measuring local concentration of fluorescently-labeled dextran as a

model system to observe and measure of these species using confocal laser scanning microscopy (CLSM). Wide-field fluorescence microscopy in combination with high numerical aperture objectives and highly sensitive cameras has allowed high resolution imaging of enzyme-surface interactions (Moran-Mirabal et al., 2011; Moran-Mirabal et al., 2009; Zhu et al., 2011). This approach can provide high spatial and temporal resolution of the three dimensional distributions of fluorescence-labeled dextran probes inside biomass pore space. Two diffusion models, including a simple transient diffusion and a pore grouping diffusion models, were developed. These models and the experimental datasets were used to investigate solute diffusion in macro- and micro-pores. Nonlinear least squares fitting of the datasets to the simple transient model yielded diffusion coefficient estimates that were inadequate for describing the initial fast diffusion and the later slow diffusion rates observed; on the other hand, nonlinear least squares fitting of the datasets to the pore grouping diffusion model yielded estimations of the micro-pore diffusion coefficient that described the inherently porous structure of plant-derived cellulose. In addition, modeling results show that on average 75% of the accessible pore volume is available for fast diffusion without any significant pore hindrance. The method developed can be applied to study the porous structure of plant-derived biomass and help assess the diffusion process for enzymes with known sizes.

1.4. Objective Two: Investigate raw and pretreated biomass pore size distribution to

reveal its impact on accessibility to solute

The study of the biomass porous structure and its role in defining the accessibility of CWDEs to the substrate is very important for understanding the cellulase-cellulose reaction system. Specific pore volume and specific surface area are two important measures of accessibility and a variety of methods have been used to make these measurements. For this study a size exclusion chromatography system was developed to measure specific pore volume and specific surface areas for raw and pretreated mixed-hardwood and switchgrass. This is also an effort to correlate the micro-accessibility studies to the macro results obtained from solute exclusion. Polyethylene glycol (PEG) probes of known molecular diameter (1.8 nm – 13 nm) were allowed to diffuse into the pore structure of the various biomass substrate packed in the column and subsequently eluted to generate high resolution concentration measurements with excellent reproducibility. Replicate measurements of probe concentrations from this system consistently yielded coefficient of variance of less than 1.5%. Results showed that particle size reduction had a smaller influence on the specific pore volume distribution of raw mixed-hardwoods, whereas for switchgrass the larger particles yielded a significantly lower estimate for the pore volume distribution compared to the smaller switchgrass particles. Results also clearly showed that the bi-phasic pretreatment yielded the largest increase in pore volume accessibility for mixed-hardwoods relative to switchgrass. From these results a pore size change mechanism was proposed that could explain the influence

of size reduction and pretreatment on pore volume measurements.

1.5. Objective Three: Assess of pore size distribution change during the hydrolysis process to elucidate the intrinsic hydrolysis mechanisms of CWDEs

Biomass porous structure change during enzymatic hydrolysis is critical for understanding the reaction mechanism and interactions between CWDEs and biomass. Pretreated mixed hardwood and switchgrass samples were hydrolyzed by CWDEs mixtures and the reducing sugar yield was measured by high performance liquid chromatography (HPLC) at different hydrolysis time points. Hydrolyzed biomass was treated with protease to remove bound CWDEs and biomass accessible pore volume was measured by the size exclusion chromatography system. The influence of biomass drying was also evaluated by measuring the pore size distribution of dried biomass samples by rehydrating and repacking them into the chromatography system. Results showed a decreasing trend of accessible porous volume as hydrolysis proceeded, which correlated well with the decreasing rate of hydrolysis. Results also showed that drying could universally decrease the accessible porous volume of pretreated and hydrolyzed biomass by up to 80%, which suggested that drying could cause irreversible pore collapsing.

1.6. References

Arantes, V., Saddler, J. 2011. Cellulose accessibility limits the effectiveness of minimum cellulase loading on the efficient hydrolysis of pretreated lignocellulosic substrates. *Biotechnology for Biofuels*, 4(1), 3.

Bond, J.Q., Alonso, D.M., Wang, D., West, R.M., Dumesic, J.A. 2010. Integrated catalytic conversion of γ-Valerolactone to liquid alkenes for transportation fuels. *Science*, 327(5969), 1110-1114.

Chanzy, H., Henrissat, B., Vuong, R. 1984. Colloidal gold labelling of l,4-β-D-glucan cellobiohydrolase adsorbed on cellulose substrates. *FEBS Letters*, 172(2), 193-197.

Gallezot, P. 2012. Conversion of biomass to selected chemical products. *Chemical Society Reviews*.

Gusakov, A.V., Sinitsyn, A.P., Salanovich, T.N., Bukhtojarov, F.E., Markov, A.V., Ustinov, B.B., Zeijl, C.v., Punt, P., Burlingame, R. 2005. Purification, cloning and characterisation of two forms of thermostable and highly active cellobiohydrolase I (Cel7A) produced by the industrial strain of *Chrysosporium lucknowense*. *Enzyme and Microbial Technology*, 36(1), 57-69.

Huber, G.W., Chheda, J.N., Barrett, C.J., Dumesic, J.A. 2005. Production of liquid alkanes by aqueous-phase processing of biomass-derived carbohydrates. *Science*, 308(5727), 1446-1450.

Irwin, D.C., Spezio, M., Walker, L.P., Wilson, D.B. 1993. Activity studies of eight purified cellulases: Specificity, synergism, and binding domain effects. *Biotechnol Bioeng*, 42(8), 1002-13.

Jeoh, T., Wilson, D.B., Walker, L.P. 2002a. Cooperative and competitive binding in synergistic mixtures of *Thermobifida fusca* Cel5A, Cel6B and Cel9A. *Biotechnology Progress*, 18(4), 760-769.

Jeoh, T., Wilson, D.B., Walker, L.P. 2002b. Cooperative and Competitive Binding in Synergistic Mixtures of Thermobifida fuscaCellulases Cel5A, Cel6B, and Cel9A. *Biotechnology Progress*, 18(4), 760-769.

Jung, H., Wilson, D.B., Walker, L.P. 2002. Binding of Thermobifida fusca CDCel5A, CDCel6B and CDCel48A to easily hydrolysable and recalcitrant cellulose fractions on BMCC. *Enzyme and Microbial Technology*, 31(7), 941-948.

Karlsson, J., Saloheimo, M., Siika-aho, M., Tenkanen, M., Penttilä, M., Tjerneld, F. 2001. Homologous expression and characterization of Cel61A (EG IV) of Trichoderma reesei. *European Journal of Biochemistry*, 268(24), 6498-6507.

Kunkes, E.L., Simonetti, D.A., West, R.M., Serrano-Ruiz, J.C., Gärtner, C.A., Dumesic, J.A. 2008. Catalytic conversion of biomass to monofunctional hydrocarbons and targeted liquid-fuel classes. *Science*, 322(5900), 417-421.

Langan, P., Nishiyama, Y., Chanzy, H. 2001. X-ray Structure of Mercerized Cellulose II at 1 Å Resolution. *Biomacromolecules*, 2(2), 410-416.

Luterbacher, J.S., Tester, J.W., Walker, L.P. 2010. High-solids biphasic CO2–H2O pretreatment of lignocellulosic biomass. *Biotechnology and Bioengineering*, 107(3), 451-460.

Lynd, L.R., Laser, M.S., Bransby, D., Dale, B.E., Davison, B., Hamilton, R., Himmel, M., Keller, M., McMillan, J.D., Sheehan, J., Wyman, C.E. 2008. How biotech can transform biofuels. *Nat Biotech*, 26(2), 169-172.

Moran-Mirabal, J.M., Bolewski, J.C., Walker, L.P. 2011. Reversibility and binding kinetics of Thermobifida fusca cellulases studied through fluorescence recovery after photobleaching microscopy. *Biophysical Chemistry*, 155(1), 20-28.

Moran-Mirabal, J.M., Corgie, S.C., Bolewski, J.C., Smith, H.M., Cipriany, B.R., Craighead, H.G., Walker, L.P. 2009. Labeling and purification of cellulose-binding proteins for high resolution fluorescence applications. *Analytical Chemistry*, 81(19), 7981-7987.

Santhanam, N., Walker, L.P. 2008. A high throughput assay to measure cellulose binding and synergism in ternary mixtures. *Biological Engineering*, 1(1), 1-19.

Saxena, I.M., Brown, R.M.J. 2005. Cellulose biosynthesis: current views and evolving concepts. *Ann Bot*, 96(1), 9-21.

Snow, P., O'Dea, K. 1981. Factors affecting the rate of hydrolysis of starch in food. *The American Journal of Clinical Nutrition*, 34(12), 2721-7.

Wang, J., Dismer, F., Hubbuch, J., Ulbricht, M. 2008. Detailed analysis of membrane adsorber pore structure and protein binding by advanced microscopy. *Journal of Membrane Science*, 320(1-2), 456-467.

Wang, Q.Q., He, Z., Zhu, Z., Zhang, Y.H.P., Ni, Y., Luo, X.L., Zhu, J.Y. 2012. Evaluations of cellulose accessibilities of lignocelluloses by solute exclusion and protein adsorption techniques. *Biotechnology and Bioengineering*, 109(2), 381-389.

Wilson, D. 2012. Processive and nonprocessive cellulases for biofuel production—lessons from bacterial genomes and structural analysis. *Applied Microbiology and Biotechnology*, 93(2), 497-502.

Wilson, D.B. 2004. Studies of Thermobifida fusca plant cell wall degrading enzymes. *The Chemical Record*, 4(2), 72-82.

Zhu, P., Moran-Mirabal, J., Luterbacher, J., Walker, L., Craighead, H. 2011. Observing Thermobifida fusca cellulase binding to pretreated wood particles using time-lapse confocal laser scanning microscopy. *Cellulose*, 18(3), 749-758.

2. LITERATURE REVIEW

2.1. Lignocellulosic biomass

Lignocellulosic biomass mainly includes herbaceous and woody plants, as well as municipal and industrial solid wastes (Atalla and Vanderhart, 1984; Cosgrove, 2005; Wickholm et al., 2001). The recalcitrance feature of plant cell wall prevents enzyme from gaining easy access to and degrading plant tissue, thus makes lignocellulosic biomass hard to degrade (Annis and Goodwin, 1997; Aro et al., 2005; Esquerre-Tugaye et al., 2000; Mendgen et al., 1996; Tonukari, 2003; Toth and Birch, 2005). Therefore, understanding the composition and function of plant cell wall is important for addressing feedstock recalcitrance. The plant cell wall is primarily composed of cellulose, hemicellulose, pectin and lignin in secondary walls (Gilbert, 2010). These components give the plant its mechanical strength and protection from microbial pathogens and enzyme attacks. The cellulose component is organized into elementary fibrils. Surrounding them are hemicellulose components that form a gel matrix by bonding with cellulose and other hemicellulose molecules via noncovalent and covalent bonds (Atalla et al., 1993; Cosgrove, 2005). Lignin provides a matrix coating of cellulose fibrils (Walker and Wilson, 1991; Zhu et al., 2009c). The extensive covalent crosslinking of lignin with other polysaccharides limits cellulose accessibility to the cellulose polymer (Vidal et al., 2011).

2.1.1 Cellulose

Cellulose is the most abundant biosynthesized material on earth. It is produced by plants, algae, as well as bacteria and fungi (Saxena and Brown, 2005; Tomme et al., 1995), and is comprised of β-1,4-linked glucose units ranging from 100 to more than 10,000 (Tomme et al., 1995). Cellulose in higher plants is organized into microfibrils measuring about 2 to 6 nm in diameter (Pingali et al., 2010). These microfibrils are aggregate of 36 β-1,4-glucan chains stack on top of each other, held together via strong intra- and intermolecular hydrogen bonds and van der Waals forces (Jarvis, 2003; Saxena and Brown, 2005). The resulting microfibril scaffolds act as tendons to build up the mechanical strength in primary cell walls (Vidal et al., 2011). Another important feature of the microfibrils is their component molecules can be packed sufficiently tight to prevent enzyme penetration (Chundawat et al., 2011a), creating a crystalline morphology that is thought to be responsible for the low cellulose saccharification rate (Tonukari, 2003; Walton, 1994). In addition to the crystalline regions, amorphous regions containing various types of twists of the microfibrils also exist in cellulose (Esquerre-Tugaye et al., 2000; Sun, 2005; Tomme et al., 1995). This structural heterogeneity makes it possible for fibers to be partially hydrated by water when immersed in aqueous solution, leaving open the possibility for large molecules (chemicals and enzymes) to penetrate into micropores or capillaries formed in cellulose (Lynd et al., 2002a).

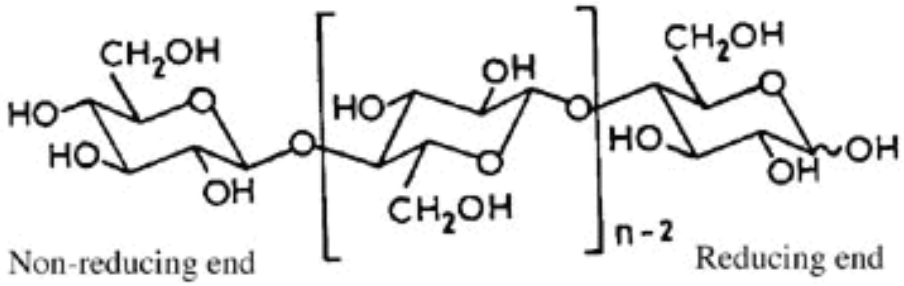

Figure 2.1. Schematic diagram of cellulose structure

The morphology of cellulose is responsible for the macroscopic properties of the polymer, and has a complex influence on its chemical properties. Different cellulose morphologies (I, II, III) have different hydroxyl group distributions and network of hydrogen bonds along the macromolecular chains. These networks generate a structure involving different interactions between the chains. The diversity of cellulose structures may, to a certain degree, account for the difference of biodegradability for different cellulosic biomass (Ciolacu et al., 2012). As shown in Figure 2.2, these structures are characterized by the arrangement of the cellulose chain sheets and the organization of the hydrogen bonds between these sheets.

Cellulose I is the form of cellulose found in nature (Ciolacu et al., 2012). The polymer chains in cellulose I are arranged parallel to each other along the long axis of the microfibril (Saxena and Brown, 2005; Tomme et al., 1995). Cellulose I is further characterized as either cellulose I_α or I_β. Cellulose I_α is mainly crystallized along the edges of the ribbon where shear stress is maximal. Cellulose I_β is crystallized in the central core region of the ribbons where shear stress is less (Langan et al., 2001). Besides, their molecular conformation and hydrogen bonding are also different (Lennholm et al., 1994; O'Sullivan, 1997).

Cellulose microfibrils can contain both cellulose I_α and I_β and the physical properties of

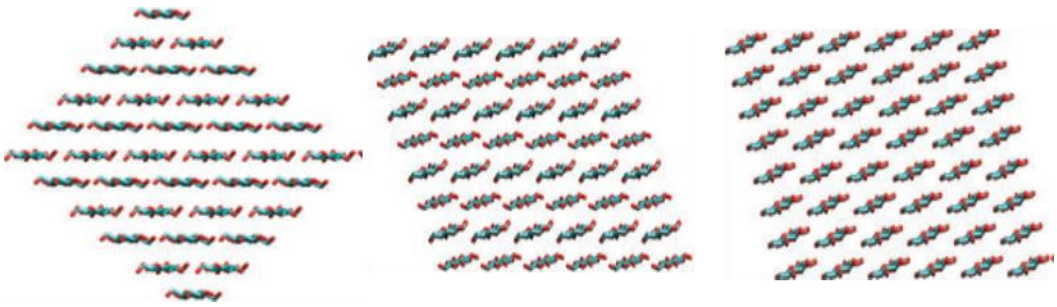

Cellulose I Cellulose II Cellulose III

Figure 2.2. Native (I) and synthetic (II, IIII) cellulose polymorph crystals (Chundawat et al., 2011a)

the cellulose fibers is dependent on the ratio of the two (Jarvis, 2003). For example, algal cellulose has both I_α and I_β alternating along the length of the microfibril. However, Cellulose I_α is the predominate form of cellulose in the cell wall produced by bacteria, while cellulose I_β predominates in the cell walls of plants (Tomme et al., 1995). Cellulose I_β is described to be more recalcitrant to conversion as it constitutes the metastable form of native cellulose (Coughlan, 1985; Ladisch et al., 1983). Previous studies using fungal enzyme systems proved it by showing a preferential degradation of the I_α phase (Hayashi et al., 1997). Similar results were observed in Cel9A for which enrichment in the I_β allomorph was observed thus indicating preferential conversion of the I_α allomorph (Corgié et al., 2011).

Crystalline cellulose can also occur as cellulose II, produced naturally by a few organisms, or by converting cellulose I via alkali treatment (Saxena and Brown, 2005; Tomme et al., 1995). Cellulose II is the crystalline form that emerges after regeneration from different media or mercerization with aqueous sodium hydroxide (Langan et al., 2001). Cellulose chains in cellulose II are anti-parallel and have an additional hydrogen bond per glucose residue, making cellulose II a very thermodynamically stable form (Tomme et al., 1995).

Cellulose III is considered as the most accessible organization form, followed by

cellulose II and cellulose I. Cellulose III has demonstrated a up to four fold higher saccharification rate than cellulose I_β (Ciolacu et al., 2012). The enhancement in cellulase activity was attributed to the amorphous cellulose III fibril that facilitated easier cellulase penetration (Atalla and Vanderhart, 1984; Saxena and Brown, 2005). The gap between cellulose I and cellulose III are not impassible. Ammonia pretreatment has been shown to decrease the number of cellulose intrasheet hydrogen bonds and increase the number of inter-sheet hydrogen bonds during the transformation process from cellulose I_β to cellulose III. This rearrangement increased the number of solvent exposed hydrogen bonds in cellulose chain by about 50% (Chundawat et al., 2011b).

2.1.2 Hemicellulose

Hemicellulose is composed of heterogeneous polysaccharides of five carbon residues, (xylose and arabinose), six carbon residues (glucose, galactose and mannose) and glucuronic acid, as shown in Figure 2.3 (Somerville et al., 2004). Hemicellulose backbone can form hydrogen bonds with lignin and cellulose chains in the plant cell wall. Sometimes a complex with pectins can be interlinked by covalent bonds to increase the flexibility of plant cell wall (Cosgrove, 2005). Together with the decoration of acetyl groups, hemicellulose generally shows as a highly branched polymer (Kim and Lee, 2002; Viamajala et al., 2006). This character drastically reduces the possibility for hemicelluloses to form a crystal structure as cellulose, which makes it easier to

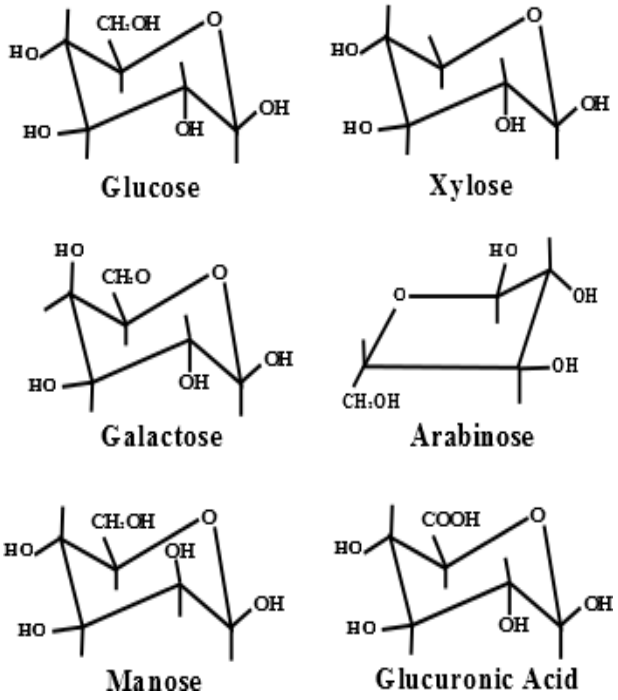

Figure 2.3. Structures of six monomers in hemicellulose

biologically degraded (Vidal et al., 2011). As a result, it is difficult to isolate pure hemicellulose from biomass without altering its original structure (Cosgrove, 2005; Gilbert, 2010). Besides, the exact composition and function of hemicellulose depends on plant species and environmental conditions. All these factors together with other lignocellulosic components in its vicinity, especially lignin linkages, make it extremely hard to study and differentiate the function of hemicelluloses in biomass.

2.1.3 Lignin

As the most abundant non-polysaccharide component in lignocellulosic biomass, lignin enables plant cell walls to cement all the packed cellulose fiber together and provides mechanical support for plant vascular tissues (Vidal et al., 2011). It also serves the principle shield to protect the plant from microbial and chemical degradation (Mooney et al., 1998). It is perceived that three monolignols are acting as source materials for biosynthesis of lignin: p-coumaryl, coniferyl, and sinapyl alcohols (Sarkanen and Hergert, 1971). However, the mechanism for the assembling of the monomers into lignin composition in higher plants is much more complex and is not well understood (Hatfield and Vermerris, 2001).

Whetten and Sederoff (1995) proposed a mechanism which involved peroxidase linking p-coumaryl, coniferyl, and sinapyl alcohols to lignocellulosic polymer, forming lignin

residue named p-hydroxyphenyl, guaiacyl (G) and syringyl (S). It has been reported that softwoods have predominantly guaiacyl lignin while hardwoods have a mix of guaiacyl and syringyl lignin residues (Viamajala et al., 2010; Zhu et al., 2009c). Different residues have been implicated responsible for different recalcitrance degrees (Ramos et al., 1992). Research manipulating S/G ratios found a stronger influence in biomass conversion rate. It has been suggested that guaiacyl lignin was more pretreatment resistant than syringyl lignin (Ramos et al., 1992). One point worth noting is that similar to hemicelluloses, the isolation of lignin cannot be achieved without altering its structure, which makes it extremely hard to determine its original ultra-state in biomass.

2.1.4 Cell wall structure

Plants cells have cell walls ranging from 0.1 to 10 μm that provides physical supports for themselves and inhibits insect and microbial pathogens (Chundawat et al., 2011a). A better understanding of plant cell-wall structure and function may help the optimization of bioconversion process (Nakashima et al., 1997). Plants generally have two types of cell walls, primary and secondary (Zeng et al., 2007; Zeng et al., 2012b). The inner most secondary wall contains mainly parallel cellulose microfibrils embedded with lignin. The outer primary wall has cellulose microfibrils organized in a meshwork. The outmost granular matrix enriched in pectin is formed by two adjacent plant cells (Grimson et al., 1996; Lacayo et al., 2010).

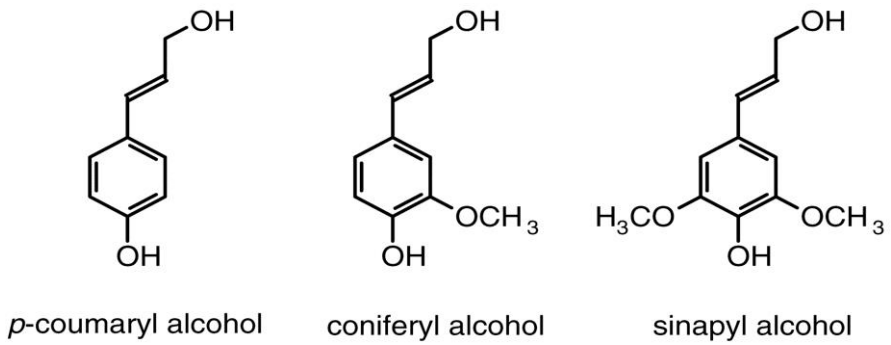

Figure 2.4. Structures of the three monolignols (Hatfield and Vermerris, 2001)

Primary cell walls consist of hydrogen bonded chains of cellulose microfibrils, hemicellulose and other materials which are woven into a meshwork. A microfibril's crystalline and amorphous cellulose core is surrounded by hemicellulose (Hill et al., 2005). The cellulose microfibrils in primary cell walls form a web-like matrix, that are separated by hemicellulose and pectins that control the overall wall porosity (<10-nm pore size) (Carpita et al., 1979; Chundawat et al., 2011a). Direct visualization of cross-links in the primary cell wall indicates the removal of some hemicelluloses allows lateral association of cellulose microfibrils in bundles of 2 to more than 20 fibers (McCANN et al., 1990).

Cell walls, especially those in vascular tissues, develop secondary walls inside the primary wall after the cell stopped growing. Secondary cell walls have extra rigidity and more recalcitrant to biological degradation than primary cell walls (Himmel et al., 2007). Cellulose microfibrils in secondary cell walls are more closely associated with each other and are oriented in parallel directions. One significant difference between primary and secondary cell wall is the universal presence of thickening lignin. Lignin in secondary cell walls form covalent associations with hemicelluloses creating enzyme impenetrable crosslink, which excludes water and prevent enzymatic degradation of cell walls (Kramer et al., 2007; Proseus and Boyer, 2005; Singh et al., 2009). Lignin thickening process in

secondary cell wall of *Zinnia* has been observed by a freeze-etch replica technique. Originally, microfibrils in the secondary wall are highly organized and oriented with a slightly irregular or wavy structure. As the active accumulation of lignin proceeded, spherical structures formed around the microfibrils. Finally, the cellulose microfibrils in the secondary wall were completely coated by lignin (Nakashima et al., 1997). Table 2.1 summarizes the typical values of cellulose, hemicellulose and lignin in some cellulosic materials. It is noticed that the compositions vary significantly among species of potential biofuel production biomass. The interlinkages among cellulose, hemicellulose and lignin components further complicate the biomass wall structures, making them recalcitrant to enzyme degradation.

2.2. Cellulase saccharification

2.2.1 Cellulases structures

Cellulases are enzymes that catalyze the hydrolysis of β-1,4-glycosidic linkage between two carbohydrates in cellulose. They are part of an enzyme group known as glycoside hydrolases which catalyze the glycosidic bonds during the hydrolysis process (Wilson, 2008).

Cellulases of all types are generally comprised of the carbohydrate binding module (CBM) and the catalytic domain (CD). These two domains are connected by a linker

Table 2.1. Typical values of biomass composition of certain cellulosic materials

Biomass	Cellulose (% dry weight)	Hemi-cellulose (% dry weight)	Lignin (% dry weight)	References
Corn stover	38	26	19	(Wiselogel et al., 1996)
Wheat straw	38	29	15	(Mani et al., 2006)
Switchgrass	37	29	19	(Sun and Cheng, 2002)
Sweet sorghum	23	14	11	(DOE, 2006)
Aspen	46	26	18	(Gong et al., 1999)
Spruce	43	26	29	(Gong et al., 1999)

region, though CBMs may exist as single, double, or triple domain in one enzyme (Gilkes et al., 1988; Tomme et al., 1988). The CD has an active site where a single cellulose chain is lined and liberated. The tunnels in the CDs can provide a large number of interactions with loose cellulose chain ends on the surface during enzymatic action, provided a plausible explanation for the specific binding of CDs to the cellulose surface (Divne et al., 1998). According to the similarity of amino acid sequence alignment and basic three dimensional structure of the CDs, cellulases have been classified into families.

Despite the many different families, generally two reaction mechanisms were proposed for CDs' hydrolysis reactions on cellulose: retaining or inverting (Davies and Henrissat, 1995; Koshland, 1953). Carboxyl side chain plays a crucial rule in both mechanisms. The inverting mechanism is a one-step reaction with the assistance of two amino acid side chains. One carboxyl side chain gets protonated and donate proton to the glycosidic oxygen of the leaving group. The other side chain removes the H-atom from the water molecule attaching the C1 carbon, which invert the linkage. The distance between the two side chains during reaction is about 10Å. The retaining mechanism is a two steps reaction in which β-1,4-glycosidic bond is severed and inverted twice with the help of two amino acid side chains located about 5.5 Å apart (Koshland, 1953). Generally the amino acids making up the side chains are glutamic or aspartic acid. The inverting and retaining mechanism for one β-glucosidic bond is shown in Figure 2.5 (Ikuta et al., 2008).

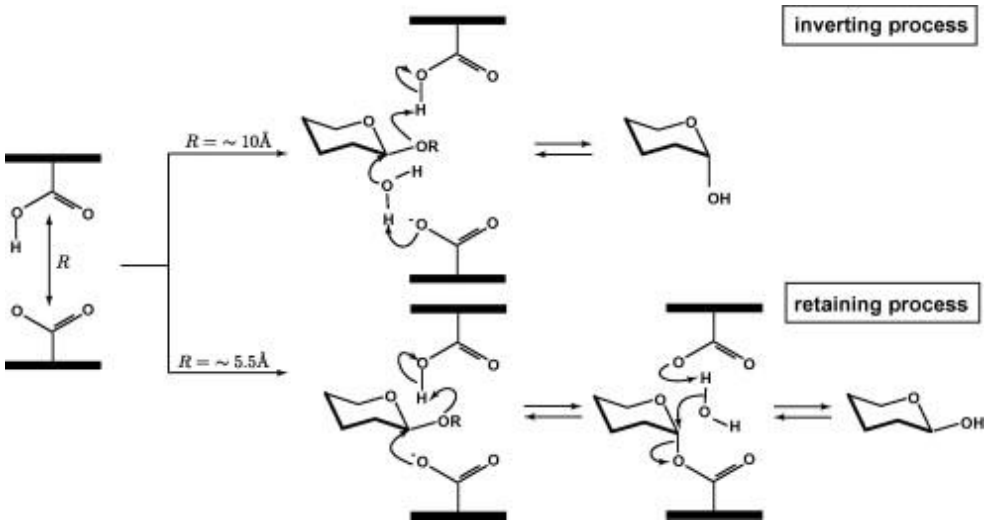

Figure 2.5. Diagram of the inverting and retaining mechanism of hydrolysis for cellulases (Ikuta et al., 2008)

The CBMs have stronger ability to bind carbohydrates than the CDs (Bothwell et al., 1997a; Jung et al., 2003). All CBMs are made of β-sheets with several aromatic residues on a flat face. It is believed that its binding capacity comes from this hydrophobic surface structured by several aromatic residues near the cleft (Shoseyov et al., 2006). The CBMs bind to accessible sites on cellulosic substrate by non-covalent and thermodynamically stable bonds, allowing the CDs to come into the vicinity of cellulose polymer and initiate one of the two hydrolysis mechanisms described above (Boraston et al., 2004). CBMs are classified into 64 families based on their structures (Cantarel et al., 2009).

Various researchers have shown that removal of the cellulase CBM reduces binding and hydrolysis yield on both pure cellulose and lignocellulosic biomass when compared to the intact cellulase with both CBM and CD (Shoseyov et al., 2006). It has been proposed that this action is either the result of a high local concentration of the cellulases on the cellulose surface due to higher affinity of the CBM, or higher accessibility of cellulose microfibrils by the disruption effects of crystalline substrate by the CBM (Shoseyov et al., 2006). While the first reason is obvious and has been proved experimentally, the latter is of particular interest. CBMs are assumed to act like expansins to intrude into and zipper open the crosslinking of cellulose microfibrils and consequently enhances cellulose accessibility and digestibility (Sampedro and Cosgrove, 2005).

Specific activities of some cellulases on various cellulosic substrates are presented in Table 2.2. The data show substantial variability for different substrate. Most of the cellulases exhibit low activity on insoluble substrates such as BMCC and filter paper, but much higher on soluble substrates such as carboxymethyl cellulose (CMC). Cel61 by itself show extremely low activity on both soluble and insoluble cellulosic substrates.

The molecular weights of cellulase (CD and CBM) are generally between 20 and 100 kDa. Three dimensional structures of some cellulases have been identified by X-ray diffraction and can be retrieved from the protein data bank (PDB) (Becker, 2001; Larsson et al., 2005; Varrot et al., 2003; Zou et al., 1999). By measuring the sizes of some cellulases and their catalytic domains stored in PDB using swiss PDBviewer (DeepView v4.04, SIB, Switzerland), the three dimensional size parameters were retrieved and listed in Table 2.3. Since most of cellulases are not perfectly spherical, size parameters in three perpendicular directions were measured and the longest axis of the cellulases are generally between 5 and 10 nm.

2.2.2 Cellulases classification

Cellulases can be classified by the location of the glycosidic bond cleavage (middle or end) and the way they act on cellulose (processive or non-processive). Endocellulases attach at random locations along a cellulose microfibril and cleave bonds from the middle

Table 2.2. Summary of some cellulases' specific activities on different substrates

Cellulases	Substrates	Specific activity (μmol cellubiose /min/μmol cellulase)	References
T. fusca Cel5A	BMCC	15.0	(Jeoh et al., 2002a)
T. fusca Cel5A	FP	0.8	(Wilson, 2004)
T. fusca Cel5A	CMC	2840	(Wilson, 2004)
T. fusca Cel6B	BMCC	2.0	(Jeoh et al., 2002a)
T. fusca Cel6B	FP	0.1	(Wilson, 2004)
T. fusca Cel9A	BMCC	19.1	(Jeoh et al., 2002a)
T. fusca Cel9A	FP	1.0	(Wilson, 2004)
T. reesei Cel7A	AC	2.4	(Tomme et al., 1988)
T. reesei Cel7A	FP	13.2	(Nidetzky et al., 1994)
T. reesei Cel7A	Avicel	3.9	(Baker et al., 1998)
T. reesei Cel6A	FP	19.8	(Nidetzky et al., 1994)
T. reesei Cel6A	AC	3.1	(Tomme et al., 1988)
T. reesei Cel6A	Avicel	3.6	(Baker et al., 1998)
T. reesei Cel7B	FP	60.0	(Nidetzky et al., 1994)
T. reesei Cel7B	Avicel	5.8	(Karlsson et al., 2001)
T. reesei Cel61A	CMC	0.04	(Karlsson et al., 2001)
T. terrestris Cel61B	FP	<0.01	(Harris et al., 2010)
T. viride Cel7A	AC	1.8	(Beldman et al., 1987)
T. viride Cel7B	Avicel	6.5	(Shoemaker et al., 1983)

Table 2.3. Three dimensional parameters of cellulases and their catalytic domains

Cellulases	Strains	PDB ID	MW (kDa)	Size parameters (nm)	References
Cel5A CD	*T. fusca*	2CKS	34	5.2×4.3×4.3	(Berglund, et al 2007)
Cel6A CD	*T. fusca*	2BOD	30	5.4×4.3×4.2	(Larsson et al., 2005)
Cel6A	*T. reesei*	1QK2	55	6×5.6×5.2	(Zou et al., 1999)
Cel6A	*H. insolens*	1OC6	55	5.8×5.4×5.2	(Varrot et al., 2003)
Cel7A	*T. reesei*	1EGN	60-65	6.8×5.5×4	(Becker, 2001)
Cel7B	*H. insolens*	2A39	50	6.6×5.5×5.3	(MacKenzie et al., 1998)
Cel9A	*T. fusca*	4TF4	90	10.1×5.7×4.3	(Li et al., 2007)
Cel61B	*H. jecorina*	2VTC	25-30	4.8×4.7×3.9	(Karkehabadi et al., 2008)
Cel61	*N. crassa*	4EIR	25-30	4.8×4.2×3.5	(Li et al., 2012)

of the chain, liberating oligosaccharides (Walker and Wilson, 1991). This open cleft structure allows the endocellulases to attack in the middle of cellulose chains. Endocellulases are thus identified by their ability to reduce cellulose chain length. *T. reesei* Cel7B and Cel5A and *T. fusca* Cel5A are among the most studied endocellulases. Processive endocellulases randomly attack in the middle of the cellulose polymers and release sugars as they move along the microfibril (Coughlan, 1985; Warren, 1996; Wilson and Irwin, 1999). They exhibit both endo- and exocellulase features with CBMs essential to the enzyme activity (Moran-Mirabal et al., 2008). The most studied processive endocellulases is *T. fusca* Cel9A. It is believed that its CBM3c disrupts the crystalline surface and is responsible for the processivity of Cel9A (Kostylev and Wilson, 2011).

Exocellulases bind to the ends and process along the cellulose polymers to release cellobiose. Some of the exocellulases can attack the cellulose chains from the reducing ends while others exocellulases can attack the nonreducing ends processively (Cantarel et al., 2009; Coughlan, 1985; Walker and Wilson, 1991). The CD containing the tunnel like catalytic site, in which cellulose chain is lined and liberated, is linked to a CBM by a flexible linker peptide. *T. reesei* Cel7A and Cel6A and *T. fusca* Cel6B are among those of most studied exocellulases.

Cellobiose is the major product of exocellulases, and is inhibitory to their activity

(Duff and Murray, 1996; Wen et al., 2004). β-glucosidase not only produce glucose that can be more easily metabolized, but also reduce cellobiose inhibition (Wilson, 2008). Many aerobic fungal organisms including *Trichoderma reesei* produce β-glucosidases.

Disruptive enzymes, such as family 61 glycoside hydrolases (GH61), exhibit strong synergistic effects working with *Trichoderma reesei* cellulases to enhance cellulose hydrolysis. For instance, *Trichoderma reesei* expressed GH61 can reduce the total protein loading of 1.4-2 folds but still reach 90% conversion of the cellulose in steam pretreated corn stover (Harris et al., 2010). Table 2.4 summarizes the enhanced hydrolysis effect on cellulosic materials by Cel61 working with other cellulases. However, the exact reaction mechanism of Cel61 proteins has not been fully understood (Arantes and Saddler, 2010). The structure of *Trichoderma reesei* Cel61B is devoid of any conventional glycoside hydrolase active site (Quinlan et al., 2011). However, a possible catalytic role has been speculated for the bound metal ion. Recent research showed the removal of the bound metal ions in GH61 drastically reduced the activity of enzyme mixture on biomass. Two structurally homologous sites are found on chitin binding protein-21 (CBP21), a non-catalytic carbohydrate binding protein shown to degrade chitin to oxidized chitin oligomers with the presence of O_2 and reducing agent (Vaaje-Kolstad et al., 2005a; Vaaje-Kolstad et al., 2005b); and CelS2, a protein cleaves cellulose into reducing-end oxidized cellodextrin (Forsberg et al., 2011).

Table 2.4. Enhanced hydrolysis effect on cellulosic materials by Cel61

Substrate	Cel61 sources and types except cellulases cocktail	Hydrolysis time (h)	Reducing sugar yield increase (%)	References
Pretreated corn stover	*Thermoascus aurantiacus Cel61A, Cel61E*	24,48,96	15-25	(Harris et al., 2010)
Microcrystalline cellulose	*Tribulus terrestris* Cel61E and CDH	72	110	(Langston et al., 2011)
Microcrystalline cellulose	*Thermoascus aurantiacus* Cel61A and *Humicola insolens* CDH	72	100	(Langston et al., 2011)
Pretreated wheat straw	*Sporotrichum thermophile* Cell61A	24	10-15	(Dimarogona et al., 2012)
Pretreated spruce	*Sporotrichum thermophile* Cell61A	24	10-40	(Dimarogona et al., 2012)

Given their structural similarity, a similar oxygenase mechanism has been proposed for cellulose attacked by GH61 (Langston et al., 2011; Vaaje-Kolstad et al., 2010). In essence, oxidized products have been detected for GH61(Vaaje-Kolstad et al., 2010). More recently, researchers incubated GH61 and cellobiose dehydrogenase (CDH) isolated from *Neurospora crassa* with cellulose and proposed a mechanism with oxidized cellodextrins modifications at the reducing or non-reducing ends. Isotope labeling experiments provided further evidence for the oxygen insertion and bond breakage process (Beeson et al., 2011; Phillips et al., 2011). While the exact mechanism of GH61 is still uncertain, it is generally accepted that GH61 causes a oxido-reductive cleavage in the cellulose crystalline region (Kostylev and Wilson, 2011).

2.2.3 Binding

Both cellulase CBMs and CDs exhibit high binding affinity to cellulose. Binding reversibility at different temperatures was investigated extensively and researchers showed quite divergent opinions on reversibility (Jervis et al., 1997). More recently, Fluorescence recovery after photobleaching (FRAP) experiments were performed on *T. fusca* cellulases Cel5A, Cel6B, and Cel9A bound onto BMCC fibrils and mats. The results showed that cellulase adsorption was only partially reversible and strongly depends on the type of cellulase and temperature, with more than 70% of bound molecules exhibiting mobility on the cellulose surface (Moran-Mirabal et al., 2011).

Formation of enzyme-cellulose complexes (ES, μmol/g) is a prerequisite for cellulose hydrolysis, and quantifying the formation of these complexes is essential for the development of models describing enzyme binding (Beldman et al., 1987; Fan et al., 1980; Mandels et al., 1971).

$$E(t) + S(t) \rightleftarrows ES(t) \tag{2.1}$$

Where S(t) is the concentration of available surface binding sites (μmol/g), E(t) is the free enzyme concentration in solution (μmol/L). The rate of change in the enzyme-substrate complex concentration over time can be described by

$$\frac{d[ES(t)]}{dt} = k_1[E(t)][S(t)] - k_{-1}[ES(t)] \tag{2.2}$$

Where k_1 is the binding reaction rate constant (L/(μmol·s)), k_{-1} is the unbinding reaction rate constant (s^{-1}). In addition to this rate equation the following mass balance defines the reaction system:

$$[E_{b,max}] = [ES(t)] + [S(t)] \tag{2.3}$$

Where $E_{b,max}$ is the maximum concentration of available binding sites on the cellulosic

substrate (μmol/g). Rearranging equation 2.3 to define [S(t)] and substituting this expression into equation 2.3 yields,

$$\frac{d[ES(t)]}{dt} = k_1[E(t)]\left[E_{b,max}\right] - (k_1[E(t)] + k_{-1})[ES(t)] \qquad (2.4)$$

Assuming that [E(t)] >> [ES(t)] one can get a constant free enzyme concentration, [E]. Meanwhile, [ES] is constant when equilibrium is reached, thus equation 2.4 can be to zero. Substituting [E] for [E(t)] and [ES] for [ES(t)] into equation 2.4 yields the following solution:

$$[ES] = \frac{k_1[E]\left[E_{b,max}\right]}{k_1[E] + k_{-1}} \qquad (2.5)$$

Let $\frac{k_1}{k_{-1}} = K_a$, the association constant (L/μmol). The reciprocal of K_a gives [E] to reach half of $[E_{b,max}]$. This results in the Langmuir binding isotherm (Zhu et al., 2011; Bothwell et al., 1995).

$$[ES] = \frac{K_a[E]\left[E_{b,max}\right]}{1 + K_a[E]} \qquad (2.6)$$

The Langmuir adsorption model was initially developed to model the amount of an ideal gas adsorbed on a surface as a function of free gas concentration (Adamson, 1983). It has been found feasible to be applied to adsorption in dilute solution. However, these following assumptions should be satisfied: the rates of adsorption and desorption are in equilibrium; a monolayer adsorption is present; this is no difference among all surface binding sites; only one type of adsorption molecule exists in the system and no interactions between them on adjacent binding sites. All these assumptions hold well for simplified cellulase binding kinetics.

Table 2.5 shows the Langmuir adsorption parameters for different cellulase on different substrates. A wide variations are observed in the parameter values for different cellulases, substrate, and temperature. Especially, it is noticed that same cellulases show very different $E_{b,max}$ on different substrates (i.e. Cel5A, Cel6A, Cel7A on BMCC and Avicel). This would suggest that the structural features of substrates are very different and can strongly influence the extent of binding. This issue is discussed in details in the session of "limiting factors for saccharification".

A temporal Langmuir binding saturation model was developed and described by Moran-Mirabal et al. (Moran-Mirabal et al., 2008). In this model, the rate of adsorption is proportional to the limited number of free binding sites on the cellulose surface and the amount of cellulases in solution. The model is described by the differential equation:

Table 2.5. Langmuir adsorption parameters for cellulases on different substrates

Cellulase	Strains	Substrates	Temperature (°C)	$E_{b,max}$ µmol/g or (mg/g)	K_a l/µmol or (ml/mg)	References
Cel5A	*T. fusca*	Avicel	50	0.67	0.22	(Bothwell et al., 1997a)
Cel5A	*T. fusca*	BMCC	50	12	0.13	(Bothwell et al., 1997a)
Cel5A	*T. viride*	Avicel	30	(90)	(0.28)	(Beldman et al., 1987)
Cel6A	*T. reesei*	Avicel	25	1.1	0.01	(Tomme et al., 1990)
Cel6A	*T. reesei*	FP	50	0.26	0.95	(Nidetzky and Claeyssens, 1994)
Cel6B	*T. fusca*	Avicel	50	0.4	0.2	(Bothwell et al., 1997a)
Cel6B	*T. fusca*	BMCC	50	11.4	0.1	(Bothwell et al., 1997a)
Cel7A	*T. reesei*	Avicel	50	0.48	0.09	(Bothwell et al., 1997a)
Cel7A	*T. reesei*	BMCC	50	4.6	0.28	(Bothwell et al., 1997a)
Cel7A	*T. reesei*	BMCC	40	4.2	0.43	(Srisodsuk et al., 1993)
Cel7A	*T. reesei*	Avicel	25	1.1	0.28	(Stahlberg et al., 1991)
Cel7B	*T. reesei*	FP	50	0.17	0.56	(Nidetzky and Claeyssens, 1994)
Cel7B	*T. viride*	Avicel	30	(126)	(0.88)	(Beldman et al., 1987)
Cel9A	*T. fusca*	Avicel	50	0.34	0.08	(Bothwell et al., 1997a)
Cel9A	*T. fusca*	BMCC	50	9.7	0.04	(Bothwell et al., 1997a)
Cel12	*T. reesei*	FP	50	0.31	0.91	Nidetzky & Claeyssens, 1994)

$$\frac{dC_b}{dt} = k_a C_s S \tag{2.7}$$

Where C_b is the concentration of enzyme bound on the substrate (nmol/g), k_a is the binding rate (L/nmol/min), C_s is the concentration of enzyme in free solution (nmol/L), and S is the number of available sites on biomass (nmol/g).

The authors define S as the difference between the maximum possible concentration of bound enzymes, C_m, and C_b, which generates:

$$\frac{dC_b}{dt} = k_a C_s (C_m - C_b) \tag{2.8}$$

The concentration of bound enzyme is proportional to the fluorescence with the assumption that the distance between the fluorophores does not permit quenching. In this case, the differential equation to describe binding in terms of fluorescence intensity is given by:

$$\frac{dI_b}{dt} = k_a C_s (I_m - I_b) \tag{2.9}$$

With the initial condition that $I_b(0)=0$, the solution for this temporal saturation binding process is:

$$I_b(t) = I_m(1 - e^{-C_s k_a t}) \tag{2.10}$$

With two known parameters, the concentration of enzymes applied in the free solution (C_s) and the observed saturation binding intensity (I_{max}), binding rate k_a is expected by fitting the experimental data into this theoretical model. This Langmuir binding model is simple and effective to extract temporal binding information from images. However, it does not consider the influences of enzyme desorption from substrate and diffusion retardation, which may cause discrepancies on interpreting the imaging data. To address these two issues, the authors developed a fluorescence recovery to study the reversibility and binding kinetics, this new study is discussed in the session "confocal imaging methods ".

2.2.4 Synergy

Individual enzymes exhibit very low activities on insoluble cellulose substrates. A cocktail of cellulases and other enzymes with different modes of catalysis is required for effectively hydrolyze both pure and in lignocellulosic biomass better than would be expected of each component working individually (Irwin et al., 1993; Santhanam and Walker, 2008; Walker et al., 1993; Watson et al., 2002). One assumed scenario is that endocellulases can create more available sites for exocellulases to act; β-glucosidases can reduce the end product inhibition and GH61s can make oxidized modifications for cellulose to be easier degraded (Wilson, 2012). Besides, several non-cellulase proteins exist that can enhance enzymatic hydrolysis of cellulose by cellulases. They include

expansins and swollenin from fungi (Bansal et al., 2009; Vaaje-Kolstad et al., 2010). Indeed, an expansin like protein produced by the bacteria *Bacillus subtilis* has been proven to stimulate the hydrolysis of corn stover (Kim et al., 2009). The overall activity of the mixture is generally greater than the sum of the activities of the individual enzymes. This enhanced activity is called synergism. In reality, cellulose degrading organisms such as plant pathogenic fungi, produce a cocktail of enzymes, including cellulases with varying modes of action and accessory enzymes for biomass hydrolysis (King et al., 2009; Paper et al., 2007; Phalip et al., 2005).

Synergism is most often observed between endo-exo, exo-exo and exo-β-glucosidases (Wood and McCrae, 1986; Woodward et al., 1988a). Recently, disruptive enzymes as family 61 glycoside hydrolases (GH61) have shown strong synergistic effects working with *T. reesei* cellulases to enhance cellulose hydrolysis. It is generally accepted that GH61 makes oxido-reductive cleavages in the cellulose crystalline region, creating new chain ends that are accessible to exocellulases (Kostylev and Wilson, 2011).

Synergism is measured as the degree of synergistic effect (DSE), which is a general concept not limited to cellulases but all enzymes catalyzing cellulose degradation. It is expressed by the following equation.

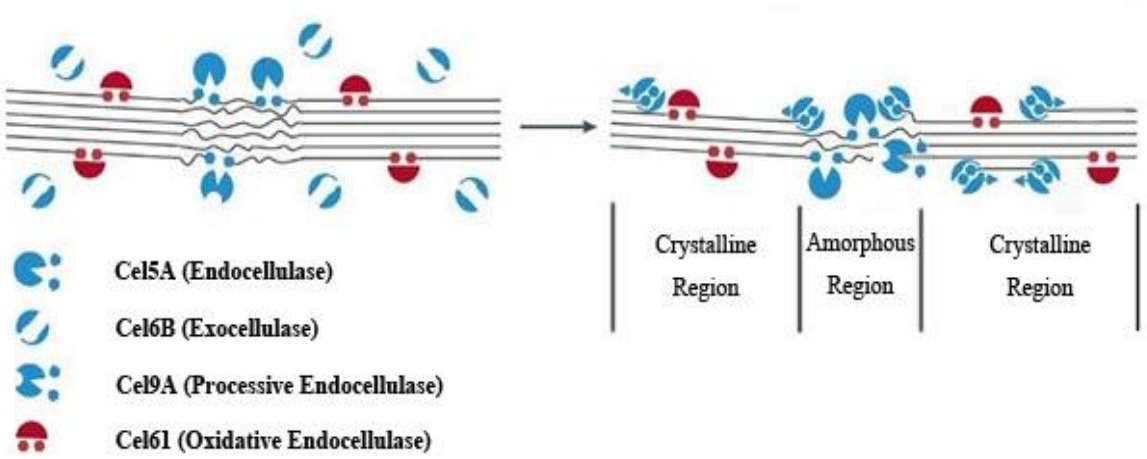

Figure 2.6. Schematic figure of a proposed enzyme cocktail on cellulose

$$DSE = \frac{X_{mix}}{\sum_{i=1}^{2} X_i} \qquad (2.11)$$

Where X_{mix} is the activity or extent of a synergistic mixture and X_i is the activity or extent of the individual enzymes in that mixture(Beldman et al., 1988). The DSE is the ratio of the activity of a cellulase mixture to the sum of the activities of the individual components of the mixture (Jeoh et al., 2002a; Santhanam and Walker, 2008).

Jeoh et al. observed cellulase binding on BMCC using mixtures of *T. fusca* cellulases Cel5A, Cel6B and Cel9A, representing a classical endocellulase, an exocellulase and a processive endocellulase respectively, at 5 and 50°C (Jeoh et al., 2002a). They found DSE was < 1 at 5°C and attributed to the competition for a limited number of available binding sites (Jeoh et al., 2002a; Jung et al., 2003). At 50°C, up to 120% DSE was observed for cellulase mixture compared to the activity of the individual cellulases. She concluded this increase was due to an increase in the number of available binding sites. In addition, the DSE was found to be sensitive to the molar fraction of each enzyme(Jeoh et al., 2002a). In another research, binding time course data were collected for BMCC and pre-hydrolyzed BMCC (PHBMCC), which represent the easily hydrolysable and the more recalcitrant fractions of cellulose, respectively (Jeoh et al., 2006). Samples of either BMCC or PHBMCC were incubated with binary mixtures of *T. fusca* cellulases Cel5A,

Cel6B and Cel9A. The degree of synergistic binding (DSB) was proposed to reflect the concentration of bound cellulases mixture compared to single cellulase. Its expression is as follows:

$$DSB = \frac{E_{b,mix}}{\sum_{i=1}^{2}\left(E_{b,single}\right)_i} \quad (2.12)$$

Where $E_{b,mix}$ is the concentration of bound enzyme in the mixture and $E_{b,single}$ is the concentration of bound cellulases in a single component reaction. Observing the DSB throughout a time course allowed us to know whether cellulases exhibited increased binding due to synergism. At least one of the cellulases in the mixture exhibited a DSB >1 on BMCC, while the temporal binding trends showed little evidence of enhanced binding effects on the PHBMCC. Jeoh et al. concluded that synergism decreases as the cellulose substrate becomes more recalcitrant (Jeoh et al., 2006).

Santhanam and Walker developed a high-throughput assay to measure binding and synergism in ternary mixtures of cellulases on BMCC using *T. fusca* cellulases Cel5A, Cel6B and Cel9A, which are closer to what is observed in nature than binary system (Santhanam and Walker, 2008). The maximum extent of hydrolysis was observed when exocellulases were 90% of the bound enzymes. It also agreed with the previous results

from Jeoh et al, 2002, showing that 10% of the loaded mixture needed to be endocellulase Cel5A. Values of DSE and DSB for enzymes on different substrates are summarized in Table 2.6.

Langmuir based models for synergistic interactions can help us understand the mechanisms of binding and hydrolysis. Since binding is prerequisite for hydrolysis to start, to study the temporal change of bound enzymes concentration is important to reveal their implications and the mechanisms behind synergism (Bansal et al., 2009). A multiple component Langmuir kinetics has been proposed with similar format to Equation 2.12.

$$ES_i = \frac{K_{a,i}E_i(\sum_{i=1}^{n} E_{b,max,i})}{1 + \sum_{i=1}^{n} K_{a,i}E_i} \quad (2.13)$$

In which, ES_i is the of bound enzyme i (μmol/g), $K_{a,i}$ is the association constant of enzyme i (ml/μmol), E_i is the concentration of enzyme i in free solution (μmol/ml), $E_{b,max,i}$ is the maximum binding capacities of enzyme i (μmol/g).

The assumptions include: equilibrium system with equal adsorption and desorption rate; equivalent binding sites; up to one bound enzyme to each site; and no interactions between enzymes on adjacent sites.

Table 2.6. Synergistic effects of enzyme mixtures on different substrates

Substrate	*Enzyme Mixture*	*Cellulase molar fraction*	*DSE*	*DSB*	*References*
Avicel 105	*T. reesei* Endo:Exo	0.5:0.5	1.2	--	(Woodward et al., 1988b)
Avicel	*T. viride* Endo:Exo	0.5:0.5	2.1	--	(Beldman et al., 1988)
Avicel	*T. reesei* Endo:Exo	0.25:0.75	2.03	--	(Converse and Optekar, 1993)
Cellulose CF1	*C. stercorarium* Avicelase I:Avicelase II	0.17:0.83	2.5	--	(Riedel et al., 1997)
Avicel 105	*C. stercorarium* Avicelase I:Avicelase II	0.17:0.83	1.8	--	(Riedel et al., 1997)
Filter paper	*T. reesei* Endo:Exo	0.5:0.5	3	--	(Henrissat et al., 1985)
Acid treated cotton	*T. reesei* Endo:Exo	0.5:0.5	2	--	(Srisodsuk et al., 1998)
Avicel	*T. fusca* Cel6B:Cel9A	0.2:0.8	3.7	--	(Watson et al., 2002)
BMCC	*T. fusca* Cel5A:Cel6B	0.5:0.5	1.9	1.44	(Jeoh et al., 2002a)
BMCC	*T. fusca* Cel5A:Cel9A	0.5:0.5	1.18	1.36	(Jeoh et al., 2002a)
BMCC	*T. fusca* Cel6B:Cel9A	0.5:0.5	1.87	1.11	(Jeoh et al., 2002a)
PHBMCC	*T. fusca* Cel5A:Cel6B	0.5:0.5	0.9	0.95	(Jeoh et al., 2006)
PHBMCC	*T. fusca* Cel5A:Cel9A	0.5:0.5	0.8	1	(Jeoh et al., 2006)
PHBMCC	*T. fusca* Cel6B:Cel9A	0.5:0.5	0.8	0.75	(Jeoh et al., 2006)
BMCC	*T. fusca* Cel5A:Cel6B:Cel9A	0.1:0.75:0.15	3.3	1.1	(Santhanam and Walker, 2008)

Converse and Optekar developed a model for the synergistic interaction of endo and exo cellulases based on the assumption that endocellulases break internal glycosidic bonds and exocellulases and release cellobiose from cellulose chain ends with competitive adsorption between the two on the same binding sites (Converse and Optekar, 1993). The model is based on the following reaction mechanisms:

$$EG_s + S_{1,f} \leftrightarrow EG_a \quad (2.14)$$

$$CBH_s + S_{1,f} \leftrightarrow CBH_a \quad (2.15)$$

$$EG_a \rightarrow S_2(+S_{1f}) + EG_s \quad (2.16)$$

$$S_2 + CBH_a \rightarrow G(+S_2) \quad (2.17)$$

Where EG is the endocellulase, S is the substrate, CBH is the exocellulase. In this model, EG in solution, EG_s, is adsorbed reversibly on unoccupied intermonomer bonds on the surface of the substrate, $S_{1,f}$ to form EG_a, adsorbed endocellulase. The adsorbed EG_a acts as an enzyme-substrate complex and breaks the bond, forming cellulose polymer ends, S_2. This action does not necessarily reduce $S_{1,f,}$ since an intermonomer bond below the surface may be exposed. This is represented by the term $+S_{1,f}$. The adsorbed exocellulase reacts with the polymer ends, S_2 to produce glucose, G, with the help of β-glucosidase. For simplification the authors integrated the function of β-glucosidase into exocellulase. The kinetic model described by this reaction mechanism is shown below.

The binding of EG is governed by:

$$\frac{dEG_a}{dt} = k_{aEG}(S_1 - CBH_a - EG_a)(EG_T - EG_aC_0) - k_{dEG}EG_a \qquad (2.18)$$

Where EG_T is the total amount of endocellulase, C_0 is the initial concentration of cellulose, k_{aEG} is the adsorption rate constant and k_{dEG} is the desorption rate constant for EG.

The binding equation for CBH is:

$$\frac{dCBH_a}{dt} = k_{aCBH}(S_1 - CBH_a - EG_a)(CBH_T - CBH_aC_0) - k_{dCBH}CBH_a \qquad (2.19)$$

Similarly, CBH_T is the total amount of exocellulase, k_{aCBH} is the adsorption rate constant and k_{dCBH} is the desorption rate constant for CBH.

The concentration of substrate is modeled by:

$$\frac{dS_1}{dt} = -P_f(k_1EG_a + k_2CBH_aS_2C_0) \qquad (2.20)$$

The factor P_f is the fraction of accessible intermonomer cellulosic bonds. The generation of polymer chain ends is described by:

$$\frac{dS_2}{dt} = k_1 EG_a - k_2 S_2 CBH_a C_0 / DP \qquad (2.21)$$

where DP is the degree of polymerization. The second term on the right side of the equation is divided by the DP to account for the fact that chain end disappears after a cellulose chain is hydrolyzed. The formation of glucose is given by:

$$\frac{dG}{dt} = k_2 CBH_a S_2 C_0 \qquad (2.22)$$

The model was fit to experimental data from Woodward et al. for verification (Woodward et al., 1988b). The five equations give a good fit to the experimental data but not for the saturation phase in the curve. The authors attribute the decline in DSE at high total enzyme loading to competitive adsorption. In essence, by setting $k_{dCBH} < k_{dEG}$ at higher enzyme concentration, the model predicted less chain ends production (S_2), therefore, lower glucose production due to less preferential endocellulase binding to cellulose than exocellulasae. However, in the case of biomass hydrolysis by a mixture of endocellulases and exocellulase, the enzymes should not be competing for the same sites, but may encounter the steric hindrance within pore structure, which is the main factor limiting their accessibility to reactive cellulose surface and hydrolysis rates and extents. This is because synergistic degradation can only occur when the synergistic enzymes occupy the same reaction space. Given the difference in enzymes molecular weights, it is possible

that pore size and steric hindrance act as a sieving mechanism that limits synergistic activities. Therefore, a new model should be proposed to address these concerns while studying enzyme synergistic binding and hydrolysis behaviors.

2.2.5 Inhibition

A typical phenomenon of cellulose hydrolysis by cellulases is the declining hydrolysis rate over reaction time, resulting in the incomplete degradation of the substrates (Eriksson et al., 2002; Herr, 1980; Ooshima et al., 1991) (Santhanam, 2009). This inhibition can be cause by a number of chemical mechanisms. Enzyme can be inhibited by end products such as cellobiose and glucose by competitive inhibition or noncompetitive inhibition (Dekker, 1986; Ferchak and Pye, 1983; Holtzapple et al., 1990; Jung et al., 2002a; Murray, 1987). Another possibility is enzyme deactivation caused by reactor operation such as high fluid shear stress and bubbling that degrade enzymes (Converse et al., 1988; San and Stephanopoulos, 1983; Zhang et al., 2010). In addition, chemical and physical changes of substrate occurring during hydrolysis can slow enzyme activity down. These substrate changes include cellulose morphology crystallinity, non-cellulose components and pore size distribution, which are discussed in details in next session (Corgié et al., 2011; Igarashi et al., 2009; Jeoh et al., 2007; Park et al., 2010; Zhu et al., 2008).

2.3. Limiting factors for saccharification

In a typical enzymatic hydrolysis process, conversion usually starts with the rapid cellulases binding and fast hydrolysis on the easily accessible cellulose (Arantes and Saddler, 2010; Ooshima et al., 1991). After an intermediate phase where most of the accessible portion has been hydrolyzed and rapid decline in cellulose hydrolysis rate were observed, a third phase with decreasing reaction rate results in very limited increase in cellulose hydrolysis (Arantes and Saddler, 2011; Converse et al., 1988). Generally high enzyme loadings are required to achieve a near-complete conversion of cellulose (Watson et al., 2002; Zhang and Lynd, 2004).

Various substrate- and enzyme-related factors have been suggested to explain the slowdown in the rate of hydrolysis and the incomplete hydrolysis of cellulosic biomass (Himmel et al., 2007). However, hydrolysis experiments with almost no enzyme inactivation or product inhibition show that a significant part of the slow-down effect could be attributed to cellulosic biomass itself (Jeoh et al., 2006; Jung et al., 2002b; Väljamäe et al., 1998; Zhang et al., 1999). Valjamae et al. (1998) tried to explain the rate decline in terms of hindrance due to nonproductive cellulase adsorption. Zhang et al. (1999) explained the declining reactivity effect by substrate heterogeneity, whereby more easily degradable substrate was depleted at a faster rate early during hydrolysis. Jung et al. (2002) attributed the declining of the bound CD to the loss of binding sites due to BMCC

hydrolysis. This conclusion was supported by prehydrolysis experiments where the easily hydrolysable BMCC fraction was removed. These experiments measured the binding of three CDs to the recalcitrant fraction and native BMCC and indicated no desorption with prehydrolyzed BMCC. Jeoh et al. (2006) observed a 10% to 30% decreasing synergism effect on the more recalcitrant cellulose, which is the remaining BMCC after prehydrolyzed by CD_{Cel5A}.

Although there have been considerable debates about the contributions of each of substrate-related factors, what governs this result is still not clear (Tanaka et al., 1988; Zhou et al., 2009). It may depend on a number of factors, such as surface area, degree of polymerization, crystallinity, biomass moisture content, the presence of lignin and other carboxylic acid groups and cellulose molecular structure, as well as their interactions. Those interactions are influenced by the weighted roles of the inner surface, the supramolecular organization, the fibrillar architecture, etc.

2.3.1 Degree of polymerization

Decrease in cellulose degree of polymerization (DP) was observed when cellulosic materials were subjected to physical or chemical treatment. For instance, the DP of cotton is reduced to 3,000 or less from 15,000 after treatment involving dewaxing and milling (Ryu et al., 1982). After partial acid hydrolysis, the DP of Avicel is decreased to around

300 from 1500 for wood pulp (Hoshino et al., 1997). Research carried out to determine the cellulose structure change presented contradictory conclusions regarding to the role of DP (Mansfield et al., 1999).

Early researchers have used crude cellulases mixture on pure cellulose showing that the DP of the residual material following hydrolysis was very similar to that of the unhydrolyzed sample (Walseth, 1952). In another research, DSE of more than 2 was observed by *T. reesei* Cel6A and Cel6B on cotton cellulose but no synergistic effect of decreasing DP (Kleman-Leyer et al., 1996). Stalbrand et al,1998 reported *Cellulomonas fimi* endocellulase decreased the DP of PASC from 100 to 40 after 96h hydrolysis. On the other hand, the DP kept stable when it was attacked by exocellulases (Stålbrand et al., 1998). They attributed it to the different reaction mechanisms the endo- and exocellulases have. Exocellulases act on cellulose ends and can only slightly decrease DP. Endocellulases cut glucosidic bonds in the middle of the cellulose chain to rapidly decrease DP (Figure 2.7). Stalbrand et al,1998 also reported no significant difference was observed when bacterial cellulose was attacked by both endo- and exocellulases, attributing the reason to much higher crystallinity in BMCC than in PASC (Stålbrand et al., 1998). In another research, initial DP reducing followed by leveling off of depolymerization for pretreated wood-derived cellulose has been observed (Wood and McCrae, 1979). It is postulated to be the increasing recalcitrance effect of the residual

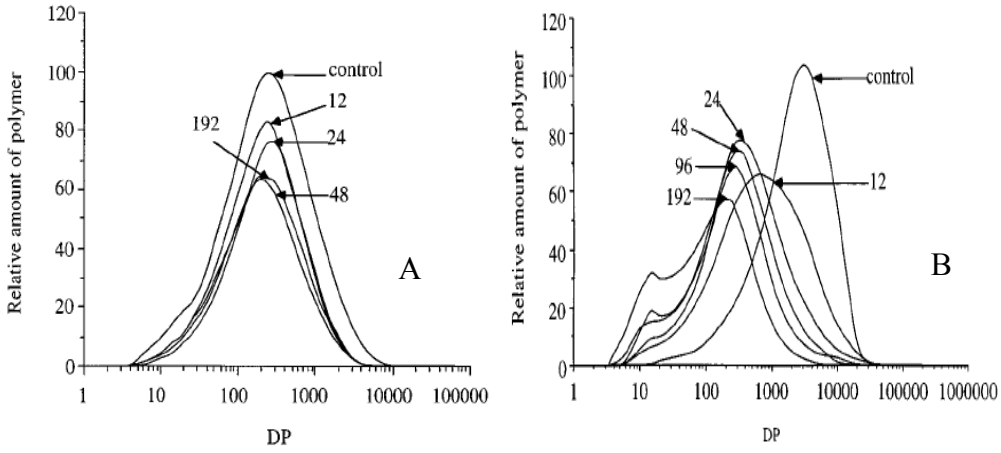

Figure 2.7. DP distribution of BMCC after it was hydrolyzed by exocellulase Cel6A (A) and endocellulase Cel6B (B). Numbers represent hydrolysis hours. It showed a stable DP in A and a declining DP in B as hydrolysis proceeded (Kleman-Leyer et al., 1996)

cellulose (Kleman-Leyer et al., 1994). Therefore, the involvement of substrate characteristics makes it further uncertain to say cellulose DP along is a limiting factor (Srisodsuk et al., 1998).

Since the data collected by various researchers regarding degree of polymerization is often contradictory, it remains unclear as to whether cellulose DP along is a limiting factor, or it is associated with other factors such as crystallinity and available surface area to influence hydrolysis. This is not hard to understand since the length of cellulose is related to its size and morphology. Thus, DP partially decides the structure and orientation of the cellulose. Table 2.7 shows the DP of some cellulosic biomass (Zhang and Lynd, 2004).

2.3.2 Crystallinity

Cellulose crystallinity is another factor in determining cellulose's susceptibility to enzyme hydrolysis (Coughlan, 1985; Ladisch et al., 1983; Walker et al., 1993). Natural cellulose is often considered as a combination of amorphous and crystalline (Jeoh et al., 2006; Jung et al., 2002a). Amorphous cellulose has disturbed hydrogen bonding interactions resulting from imperfections in the chain packing or chemical/mechanical treatments (Tomme et al., 1995). In crystalline cellulose, the hydroxyl groups are forced into radial orientation by the chair conformation of the glucose residues. Consequently,

Table 2.7. DP of some cellulosic biomass

Substrate	Avicel	Bacterial Cellulose	PASC	Cotton	Filter paper	Wood pulp
DP	130-800	2000	100	1000-3000	750	500-1500

strong inter-chain hydrogen bonding in a cellulose sheet makes crystalline cellulose resistant to enzymatic hydrolysis (Park et al., 2010).

The crystallinity of cellulose has been considered an important structural feature because most cellulases only penetrate and locate in the more accessible amorphous regions, leaving the bulk of the crystalline cellulose unaffected (Ciolacu et al., 2012). As the crystallinity increases, cellulose becomes increasingly resistant to further hydrolysis (Fan et al., 1981). Results show up to 30 times faster cellulose hydrolysis rate for amorphous cellulose compared to crystalline cellulose by fungal cellulases (Lynd et al., 2002b). The initial degree of crystallinity of cellulose is an important factor in determining the rate of a hydrolysis reaction (Hall et al., 2010). This agrees with our previous statement that more amorphous Cellulose III has much faster hydrolysis rate than cellulose I_{β}. Another research showed 72h reducing sugar yield from a poplar wood dropped from 40% to 10% when the degree of crystallinity increased from 30% to 55% (Chang and Holtzapple, 2000).

Crystallinity index (CrI) defines the percentage of total cellulose that is crystalline in a given material (Fan et al., 1981; Walker et al., 1993). X-ray diffraction is most commonly employed to determine the CrI (Park et al., 2010; Thygesen et al., 2005). CrI is determined by a plot of intensity versus diffraction angle, 2θ, generated by X-ray

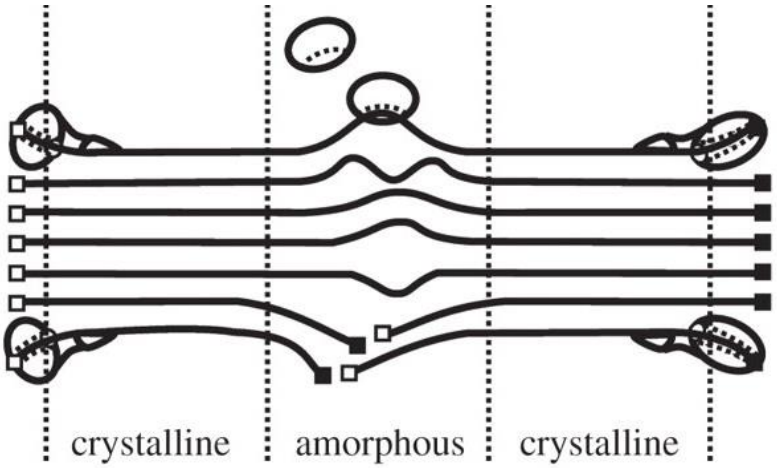

Figure 2.8. Schematic diagram of the amorphous and crystalline cellulose during hydrolysis. Filled squares represent reducing ends and the open squares represent non-reducing ends. Cellulases are indicated (circles with dots inside) (Gilbert,2010).

diffraction measurements. The angle θ is the angle of incidence of X-ray beam. The intensity of the peak at 2θ = 22° corresponds to the crystalline contribution, and the amorphous contribution is the intensity at 2θ= 18°. CrI was calculated from the ratio of the area corresponding to the crystalline region to that of both crystalline and amorphous regions (Corner, 2003; Kawakubo et al., 2010).

$$\mathrm{CrI} = \frac{\mathrm{F_c} - \mathrm{F_a}}{\mathrm{F_c}} \qquad (2.23)$$

where F_c is the intensity of the peak corresponds to the crystalline region, F_a is the intensity of the peak corresponds amorphous region.

Crystallinity influences hydrolysis at the cellulose microfibril level. This is directly related to the fact that cellulases can access the surfaces of amorphous microfibrils without any interruption from lignin and hemicellulose. However, when these elementary microfibrils are associated into the cell walls, the accessibility of the cellulose chains is dramatically reduced. In lignocellulosic biomass, factors such as accessible surface area and lignin content are considered more influential than crystallinity, polymorph crystals and DP of the cellulose in determining the rate and extent of hydrolysis (Mansfield et al., 1999).

Table 2.8. Crystallinity index of some cellulosic biomass.

Substrate	Crystallinity Index	References
Avicel PH102	0.81	(Walker and Wilson, 1991)
Bacterial cellulose	0.76	(Zhang and Lynd, 2004)
Sigmacell 50	0.87	(Carrasco et al., 1994)
PASC	0-0.04	(Park et al., 2010)
Solka Floc	0.74	(Fan et al., 1980)
Ball milled Solka Floc	0.05-0.66	(Fan et al., 1980)
Filter paper	0.45	(Zhang and Lynd, 2004)
Cotton	0.81-0.95	(Ryu et al., 1982)
Poplar wood	0.54	(Chang and Holtzapple, 2000)
Wood pulp	0.5-0.7	(Carrasco et al., 1994)
Bagasse	0.55-0.6	(Rivers and Emert, 1988)
Rice straw	0.56	(Rivers and Emert, 1988)

2.3.3 Particle size

Previous studies provide a contradictory picture of the effect that substrate size has on the rate and extent of cellulose enzymatic hydrolysis. Several studies reported no significant correlation and suggest that particle size was a weak predictor of susceptibility to enzymatic hydrolysis (Del Rio et al., 2011; Rivers and Emert, 1987; Vidal et al., 2011). For instance, Rivers and Emert concluded that particle size of substrates after ball milling had no effect on hydrolysis in the size range of 0.25–0.47mm (Rivers and Emert, 1987). Del Rio et al. found no significant increase in hydrolysis yields after mill refining treatment of the organosolv treated substrates, even though decreases in particle size and crystallinity were observed (Del Rio et al., 2011). Arantes and Saddler found that the minimum enzyme requirement for efficient hydrolysis had no correlation with the average particle size (Arantes and Saddler, 2011).

Others reported a modest influence in biomass digestibility due to physical size reduction (Zhu et al., 2009a). Mooney et al. indicated that hydrolysis rate of pulp wood was significantly affected by particle size (Mooney et al., 1998). Elshafei et al. reported hydrolysis extent of 45 and 35 percent after 72hr of hydrolysis for 0.15mm and 2mm untreated corn stover particles (Elshafei et al., 1991). Zeng et al. showed that smaller 53–75 mm corn stover particles were 50% more susceptible to hydrolysis than 425–710 mm particles (Zeng et al., 2007). Dasari and Berson chose oak saw dust to study the effect of

particle size and found that glucose conversion rate almost doubled when particle size was reduced from 590 to 33 μm (Dasari and Eric Berson, 2007). Fan et al. proposed that the overall increase in digestibility after size reduction is a result of increased available surface area (micrometer level change) rather than reduced crystallinity (nanometer level change) (Fan et al., 1980).

Higher surface area-to-weight ratio generated by size reduction should mean more available adsorption sites (Viamajala et al., 2010). However, external surface area, which is closely related to the shape and size of the cellulose particles, does not necessarily reflect the overall cellulose surface area available to the cellulase enzymes (Wang et al., 2012). Researchers reported that the values of the external specific surface area of unbeaten wood pulp fibers range from 0.6 to 1.5 m^2/g by microscopic observation (Fan et al., 1980; Fan et al., 1981). In contrast, pretreated hardwood showed 37-140 m^2/g surface area measured by solute exclusion, about 100 times of the reported external surface area above (Grethlein, 1985). This suggests that the substrate external surface plays a minor role contributing to cellulose accessibility. This is especially true for pretreated biomass with extensive capillary pores and consequently more accessible internal surface area.

Influences of particle size on diffusivity should also be considered while evaluating the necessity of size reduction. Research showed that it took three times longer for sulfuric

acid to diffuse into bagasse with 10-20mm length than 0.8-1.4mm (Kim and Lee, 2002). In a proposed pore hindered diffusion and reaction model, diffusion was found not a rate-limiting factor for particles smaller than 50μm, compared hydrolysis reaction (Luterbacher et al, 2013). In another research where filter paper was modeled as a 20×20×200μm rectangular cuboid, almost instant pore accessibility by cellulase-size dextran probes confirmed that diffusion is not a restricting factor for substrate reaction at this dimension (Yang et al., 2013). Vidal et al.2011 summarized the "cut-off" sizes of pretreated biomass to indicate a norm below which particle sizes show no increase in biomass digestibility in terms of the enzymatic conversion result after pretreatment. They found a smaller cut-off size for dilute acid and base pretreated biomass (2-3mm) than steam explosion pretreated biomass (10-50mm). They also found the cut-off sizes were dependent on feedstock, with woody biomass showing higher cut-off sizes (>3 mm) than grassy biomass (<3 mm). This phenomenon is quite possibly related to macroscopic transportation in biomass, since size reduction can hardly modify microfibril pore structures deeply buried in biomass (Hui et al., 2009).

Those dependence together with the intensive energy requirement of size reduction processes, can provide more information to assess the feasibility of different bioconversion techniques (Vidal et al., 2011). The influences of size reduction on hydrolysis extent are summarized in Table 2.9.

Table 2.9. Size reduction effects on hydrolysis extent of different biomass

Biomass type	Biomass original sizes (mm)	Sizes after reduction (mm)	Sugar yield before and after 72h hydrolysis (%)	References
Non-pretreated biomass				
Hammer milled wood chip	>1.27	<0.318	4.5 → 13	(Zhu et al., 2009a)
Disk milled wood chip	>1.8	0.25-0.53	14 → 20	(Zhu et al., 2009a)
Corn stover	1.7-2.0	0.08-0.15	35→45	(Elshafei et al., 1991)
Corn stover	2-10	0.17	25→40	(Chundawat et al., 2007)
Red oak sawdust	0.59-0.85	0.033-0.075	15→23.2	(Dasari and Eric Berson, 2007)
Bagasse	0.443	0.224	6.1, No difference	(Rivers and Emert, 1988)
Rice straw	0.465	0.107	21, No difference	(Rivers and Emert, 1988)
Corn stover	0.43-0.71	0.053-0.075	14.6→25.9	(Zeng et al., 2007)
Pretreated biomass				
Kraft pulped Dougfir	1.20	0.15	70→90	(Mooney et al., 1999)
Hot water pretreated corn stover	0.43-0.71	0.053-0.075	64.2→69.6	(Zeng et al., 2007)
Hot water treated poplar	12-15	2-5	No difference	(Negro et al., 2003)
Steam treated herbaceous feedstock	8-12	2-5,5-8	85→100	(Ballesteros et al., 2002)
Lime pretreated switchgrass	0.841	0.420,0.177	No difference	(Chang et al., 1997)
AFEX pretreated corn stover	2-10	0.85,0.5,0.43,0.15	83, No difference	(Chundawat et al., 2007)
Acid pretreated switchgrass	10	3	60→80	(Hsu et al., 1996)

2.3.4 Lignin hindrance and binding

Lignin sheath can restrict the swelling of cellulose and consequently limits cellulose accessible surface area to cellulases (Jeoh et al., 2007; Mooney et al., 1998; Wong et al., 1988). Because lignin is structurally intertwined with cellulose, its removal can heavily affect depolymerization process of the neighboring polysaccharides. The breakage of this closely association of lignin with the cellulose is essential to achieving efficient cellulose hydrolysis (Arantes and Saddler, 2010). Besides, lignin reduces the effectiveness of enzymatic hydrolysis by unproductively adsorbing cellulases, thereby reducing the availability of the enzymes (Berlin et al., 2005; Kumar et al., 2012). This has been observed numerous times in the literature (Kumar et al., 2012; Mansfield et al., 1999; Zeng et al., 2012b). A positive relationship between adsorption capacity and initial hydrolysis rates was revealed for substrates containing little or no lignin, while substrates with high lignin contents demonstrated a poor correlation (Lee et al., 1994). Other researchers have shown that cell wall with twice specific surface area exhibited comparable hydrolysis rate as pure cellulose - Avicel. The authors attributed that 50% of the cellulases bound to cellulose surface area and the rest went to noncellulose structure including lignin in cell wall (Piccolo et al., 2010; Tanaka et al., 1990). Piccolo et al. found lower protein adsorption per gram wheat straw than spruce. One factor they indicated is the lower lignin content in wheat straw “shunt” less unproductive cellulases (Piccolo et al., 2010).

Though the lignin content in biomass creates hydrolysis hindrance and unproductive enzyme binding, it is not economically feasible to completely remove it (Palmqvist and Hahn-Hagerdal, 2000; Wyman et al., 2005). Among all leading pretreatment methods, alkaline pretreatment is known for its capacity to partially dissolve lignin and hemicelluloses. Consequently, the swelling of the cellulose fibers help cellulases gain better access to its binding sites (Hendriks and Zeeman, 2009). During dilute acid pretreatments, lignin goes through physical and chemical changes that may influence downstream enzymatic hydrolysis. However, its removal is minimal (Viamajala et al., 2010). Relationship between lignin removal and biomass hydrolysis extent for different pretreated biomass are summarized in Figure 2.9, where most of the data fell above the diagonal line. It indicates that the increase of biomass hydrolysis extent is not linearly related to lignin removal. That is to say, complete lignin removal is not required to reach high hydrolysis extent.

Rather than complete delignification, it is possible to improve the overall biomass hydrolysis rate by modification of the lignin. These modifications may range from covalent bond breakage to structure reorganization (Hu et al., 2011; Ooshima et al., 1990). For example, research has shown aside from delignification, the improvements in hydrolysis were caused by reduced non-specific binding of the cellulases to the lignin after organosolv pretreatment (sulfonation). The authors attributed it to electrostatic

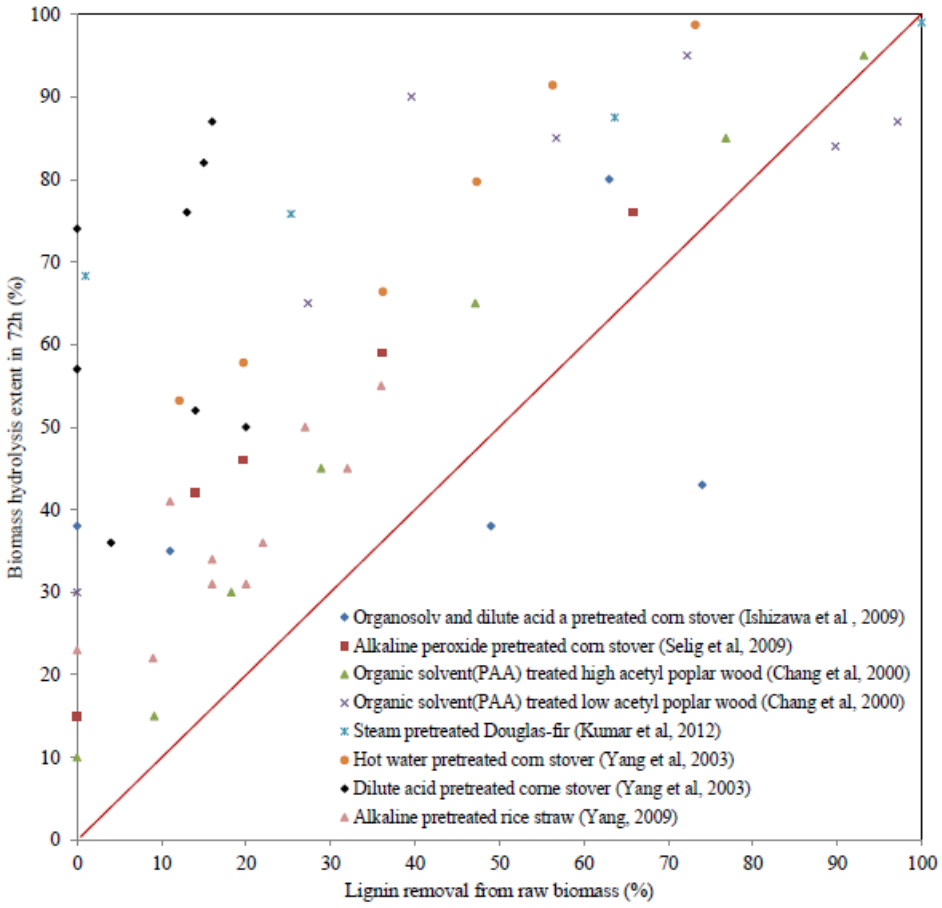

Figure 2.9. Relationship between lignin removal and biomass hydrolysis extent for different pretreated biomass

repulsion from increased anionic charges in the residual lignin (Del Rio et al., 2011). Kumar and Wyman showed that residual lignin from acid pretreatments had a significantly lower inhibitory effect than residual lignin from alkaline pretreatments. They postulated that alkaline pretreatment caused a change of lignin chemistry, resulting in a lignin surface that was more prone to adsorb protein (Kumar and Wyman, 2009; Pavlostathis and Gossett, 1985). After dilute acid or hot water hydrolysis, SEM images showed that the lignin squeezed out of the concrete cellulose matrix redeposited onto cellulose surfaces, forming spherical droplets ranging from 40 nm to 2 μm. This reorganization dramatically opened up the structure of the cell wall matrix without being removed from the biomass altogether (Donohoe et al., 2008; Zeng et al., 2007). Reducing sugar yield increased from 15% to 75% while the lignin content was almost the same as in corn stover without pretreatment (Zeng et al., 2012a). Plant biology research was also conducted to redirect lignin synthesis to maximize enhanced hydrolysis. After different steps in the lignin biosynthesis process was down regulated in alfalfa, a two fold increase in the yield of fermentable sugars was observed. These experiments provided evidence for lignin modification to enhance enzymatic hydrolysis (Chen and Dixon, 2007)

It has been reported that higher delignification after organosolv and dilute-acid pretreatment reduce cellulose conversion and accessibility (Ishizawa et al., 2009). One possible reason is the aggregation of the cellulose microfibrils resulting in decreased

cellulase accessibility (Delgenès et al., 2002; Pingali et al., 2010). Rolin et al. showed that despite the high level of delignification reached by aqueous ammonia treatment, the lignin remaining after had a significant negative effect on cellulase performance (Rollin et al., 2011). Zhu et al. suggested that lignin removal higher than 50% could result in cellulose pore collapse and declining cellulose accessibility (Zhu et al., 2008). This agreed with results from Ishizawa et al., who argued that the redeposit residual lignin acted as spacers between cellulose microfibrils, preventing neighboring cellulose fibrils to aggregate (Ishizawa et al., 2009).

2.4. Accessible surface area and diffusivity

2.4.1 Internal and external surface area

An important variable to consider in enzymatic cellulose hydrolysis is the surface area available to the cellulases that are involved in cell-wall deconstruction. Cellulosic feedstocks are complex physical materials that have micro and macro pore structure that play an active role in defining reactive surface area. The external surface area depends on the size and shape of the cellulose particle, while the internal surface area is determined by the pore structure of the cellulose particle and the size of the enzyme relative to the pore diameter of the particles (Grethlein, 1985; Walker et al., 1993). Internal area can only be accessed by cellulases that penetrate the interstice space of the cellulose particle; thus, the maximum amount of bound cellulase is very much depend on the pore structure

of the interstice space and the dimensions of the enzyme (Jung et al., 2003).

It has been reported that the external surface area is much smaller than the internal surface area of cellulose (Park et al., 2007; Walker et al., 1992). For pretreated biomass, the differences can be higher than two orders of magnitude (Grethlein, 1985; Weimer et al., 1990). Therefore, it seems logical that the inner structure of cellulose has a major influence on enzymes diffusing into the cellulose network (Arantes and Saddler, 2011). Because of the disaggregation and fragmentation of the cellulose particle size during enzyme hydrolysis (Ladisch et al., 1983), it has been postulated that enzymatic hydrolysis of the microcrystalline cellulose is dominated by a process where cellulases attack the cellulose by penetrating into the accessible interior of the particle (Walker et al., 1990).

Cellulosic particle undergoes a fragmentation process where large particles are fragmented into smaller ones when exposed to enzyme cocktails and with some individual cellulase (Fan et al., 1980; Walker et al., 1992; Walker et al., 1990). Fan et al. observed up to 300% increase in the specific surface due to cellulose fragmentation. Walker et al. observed that the rate of fragmentation was linearly dependent on the amount of bound cellulase from *Thermobifida fusca* (Walker et al., 1990). It has been reported that both endocellulases and exocellulases are capable of fragmenting cellulose, but that the bulk of the fragmentation activity is associated with endocellulase (Walker

and Wilson, 1991). Thygesen et al. also observed significant decrease in cellulose fiber length during enzymatic hydrolysis and they concluded that cleavage in the fiber axial direction was not likely (Thygesen et al., 2011).

2.4.2 Accessible surface area is essential for high hydrolysis rate and extent

There has been long debate about the dominant factors in enzymatic cellulose hydrolysis process with some researchers underscoring the difficulties of decoupling the effect of accessibility with the other factors such as crystallinity index. For example, Fan et al. developed an empirical hydrolysis expression suggested that the hydrolysis rate was more sensitive to crystallinity than surface area for Solka Floc (Fan et al., 1980; Fan et al., 1981). However, crystallinity and accessibility effects can be interconnected to each other (Lynd et al., 2002a).

A set of experiments included column solute exclusion, particle size analysis, X-ray diffraction, fourier transform infrared spectroscopy and solid state ^{13}C nuclear magnetic resonance was performed to apply partial least squares (PLS) method seeking the key factors limiting cellulose digestion. It showed the most important factor for cellulose digestion was accessible surface area, followed by delignification and the destruction of the hydrogen bonds (Huang et al., 2010). Other research studies have also suggested that biomass accessible surface area is the most important factor influencing biomass

hydrolysis (Bothwell, 1994; Bothwell et al., 1993; Donohoe et al., 2009; Focher et al., 1981; Grethlein, 1985; Jeoh et al., 2007; Jeoh et al., 2002a; Zhang and Lynd, 2004). More importantly, several groups have shown a good correlation between the determined pore volume and the enzymatic digestibility of lignocellulosic substrates (Figure 2.10) (Arantes and Saddler, 2011; Grethlein, 1985; Mooney et al., 1998; Piccolo et al., 2010; Stone et al., 1969; Weimer et al., 1990; Zeng et al., 2007). For example, enzymatic hydrolysis of sulphonated Douglas-fir pulp showed that the proportion of lignin did not affect enzyme adsorption when cellulose fibers were sufficiently swollen (Mooney et al., 1998).

Stone and Scallan reported a linear relationship between the initial cellulase reaction rate and the surface area inside the cellulose that was accessible to a molecule with 40Å in diameter (Stone et al., 1969). The assumed pores in the cell wall are parallel slots between multiple lameallae. Therefore, the surface area could be calculated by

$$\Delta A = \frac{2\Delta V}{w} \qquad (2.24)$$

Where ΔA is the incremental surface area (nm^2), ΔV is the volume increment (nm^3), and w is the average pore width (nm).

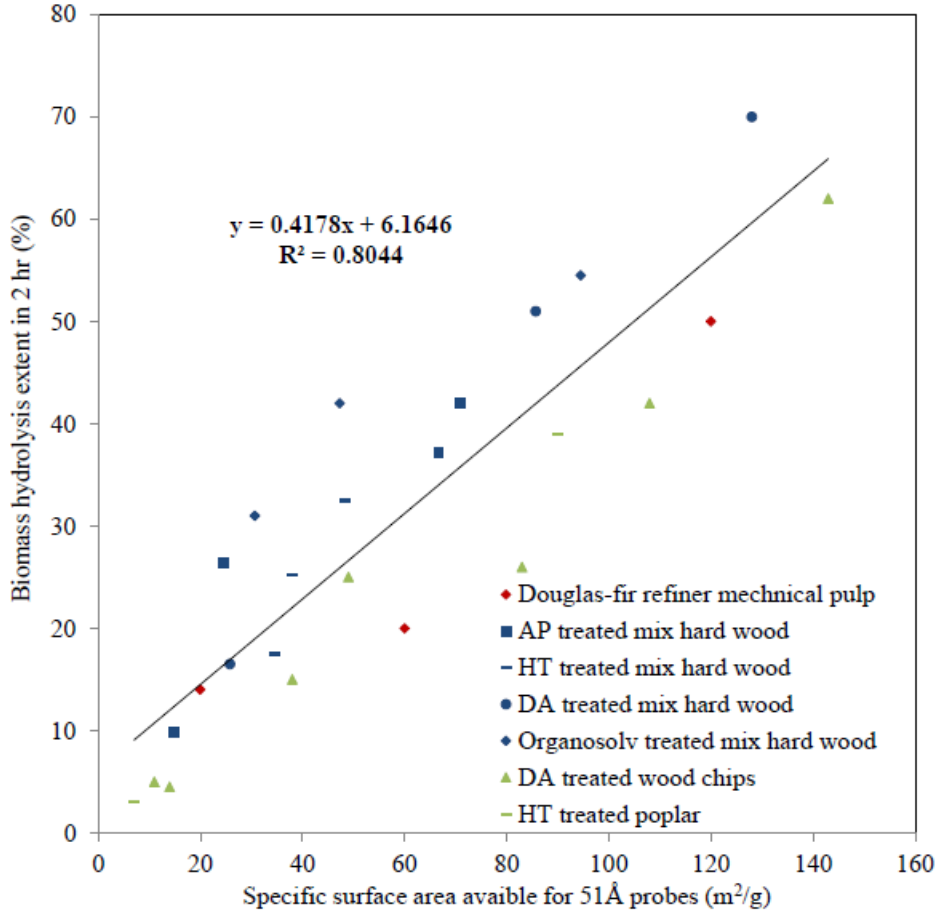

Figure 2.10. Relationship between biomass hydrolysis extent and available surface area to 51Å probes on different pretreated lignocellulosic biomass. Different color of the dots represent different source of data (Grethlein, 1985; Mooney et al., 1998; Thompson et al., 1992). Data points in red are from Mooney et al, 1998. Data points in blue are from Thompson et a, 1992. Data points in green are from Grethlein, 1985. AP: Alkaline peroxide; HT: Hydrothermal treatment; DA: Dilute acid.

Grethlein obtained an excellent linear correlation between available surface area to probes with molecular diameter of 51Å and the initial glucose yield for acid pretreated mixed hardwood. He observed that 80% or more of the pore volume of untreated substrates is inaccessible to solutes of 51Å or larger (Grethlein, 1985; Grethlein et al., 1984). Other studies where the initial rate of hydrolysis and binding shows a positive correlation to the available specific area include steam exploded pine (Wong et al., 1988) , acid/alkali/oxidative pretreated sugar cane bagasse (Sinitsyn et al., 1991), SO_2/steam pretreated wheat and spruce (Piccolo et al., 2010) and organosolv pretreated cedar (Kawakubo et al., 2010). This strong correlation between accessible surface area and the rate or extent of hydrolysis has been documented for a wide range of substrates, pretreatment technologies, enzymes and their loadings. These studies suggest that the rate-limiting factor in enzymatic hydrolysis is the limited accessibility of the enzymes to the cellulose chains due to the physical structure of the cellulosic biomass. These results are not hard to interpret since in a surface-dominated process, such as cellulase-cellulose reaction, a physical complex between enzymes and substrate must form before hydrolysis initiates (Arantes and Saddler, 2011; Zeng et al., 2007).

2.4.3 Pore size measurements

Internal pore surfaces have been measured using sub-micron imaging (Chundawat et al., 2011c; Himmel et al., 2007; Zhu et al., 2009a), NMR (Jackson and McKenna, 1990),

water retention value(Hui et al., 2009; Topgaard and Söderman, 2001), solute exclusion (Corner, 2003; Grethlein, 1985; Ishizawa et al., 2007; Lin et al., 1987; Neuman and Walker, 1992a) and from smaller molecule or enzyme adsorption data (Chesson et al., 1997; Kumar et al., 2012; Mansfield et al., 1999; Zhu et al., 2009b). Several of this methods require sample drying. However, biomass sample drying is generally understood to negatively affect the pore accessibility of the cellulose fraction in biomass by limiting enzyme accessibility (Weise, 1998). Another research revealed that enzymatic hydrolysis efficiency could be reduced by approximately 94% compared to its never dry state (Topgaard and Söderman, 2001). Results from a competitive dye adsorption experiment (Simons' stain) revealed that drying significantly reduced the population of larger pores and created a large number of smaller pores that are not accessible to the larger dye due to partial closure of larger pores (Esteghlalian et al., 2001). Consequently, pore size measurement with prerequisite of drying generate misleading information about pore size (Wang et al., 2012).

2.4.3.1 SEM observation

Scanning electron microscope (SEM) has been used to measure the radius and length of wood chip fiber by direct observation (Zhu et al., 2009a). Wood chips were milled and allowed to pass through 0.1mm mesh. The measured dimensions of individual fibers were used to estimate the substrate external surface, assuming the wood fiber a perfect

cylinder. Cellulose conversion was reported by Zhu, et al to increases with specific surface area. Biomass density was report to be $1g/cm^3$ and specific surface area was reported to be $0.1m^2/g$, which is one-tenth of the values reported by solute exclusion method. Therefore, the problem with this method is obvious, since the authors neglected the internal surface area when calculating specific surface area, especially when internal porous surface contributed to over 90% of the total surface of their microcrystalline cellulose (Zhu et al., 2009a).

2.4.3.2 Three dimensional – TEM

Transmission electron microscopy (TEM) has also been used to measure cellulose particle size. It is a technique that uses a beam of transmitted electrons to interact with a cellulose sample and the image is detected and magnified by a sensor. Since multiple views can be obtained by rotating the sample, a 3D specimen reconstruction can be generated after multiple images at differing angles are taken (Hoppe, 1974).

Three dimensional TEM tomograms were applied to model the porous regions within AFEX pretreated cell wall. Biomass was stained with 2% aqueous uranyl acetate and 1% $KMnO_4$. Porous regions (red spot areas in Figure 2.11) were not stained and could be distinguished by 3D-TEM tomograms. Total porosity (unstained regions) was estimated by computing the fractional surface area contributed by each region within the cell wall

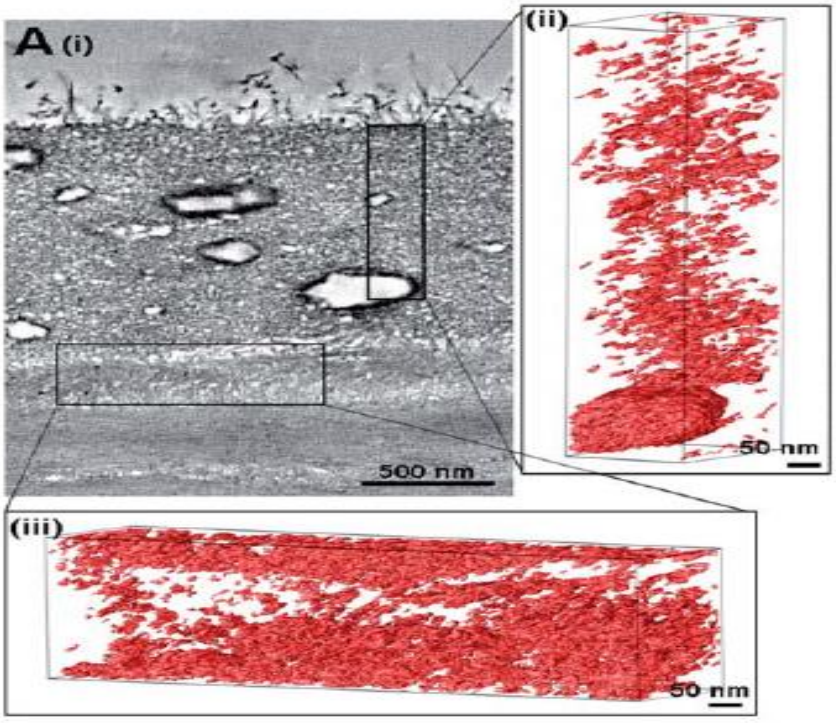

Figure 2.11. Modeling porous regions within AFEX pretreated cell wall using 3D-TEM tomograms. Red spots in reconstructed 3D figure (ii and iii) stand for pore regions in the cell wall (Chundawat et al., 2011c).

tomogram. Authors determined the porous area to be 23 m^2 per g cell wall for AFEX pretreated corn stover. The TEM tomography can help reconstruct the 3D porous structure. The limitations are also very noticeable. First, TEM based pore analysis is limited by the staining ability of the chemicals to visually differentiate pores from the cell wall background. Second, since the resolution in vertical direction is 5 nm compared to 1-2 nm in horizontal direction, three dimensional reconstruction may encounter resolution limitations, consequently influencing the accuracy of pore size estimation especially for pore width smaller than 5 nm (Chundawat et al., 2011c).

2.4.3.3 ^{1}H NMR thermoporometry

^{1}H nuclear magnetic resonance (NMR) uses melting point depression of water to estimate pore size when it is confined within small spaces (Topgaard and Söderman, 2001). The amount of unfrozen liquid at a specific temperature is directly related to the pore volume of a defined size. According to a simplified Gibbs-Thompson equation (Jackson and McKenna, 1990),

$$\Delta T = T_b - T_p = \frac{K}{w} \qquad (2.25)$$

The melting point of the water in pores, T_p, decreased with decreasing pore diameter, w. T_b is the constant melting point of bulk water and K is a constant depending on the

characteristics of the material. This linear correlation between the melting point depression (ΔT) and the reciprocal diameter can be utilized to investigate pore size distribution. About 40m^2/g surface area in pores large than 2nm was observed for acid treated corn stover (Ishizawa et al., 2007). The drawback of this method is that it cannot reflect the presence of restricted pore openings as narrow bottle shaped pores.

2.4.3.4 Water retention value (WRV)

The Water Retention Value (WRV) is often used to quantify the fiber swelling behavior as water absorbency is a key quality in textile fibers (Hui et al., 2009). It directly measures the accessible volume using water molecule (Kumar et al., 2012). After soaking for two hours, the wrapped suspension was centrifuged. WRV of the substrate is simply the amount of water retained after centrifuging as a percentage of the substrate dry weight. Researchers have showed that WRV was not limited only to the pores in fibers, but also on the surface of fiber microstructures (Hill et al., 2005). Hui et al argued that WRV represents the sum of bound water, both in pores and on the fiber surface (Hui et al., 2009). The disadvantage of this method is the huge variations due to centrifugation operation. Besides, the fact that water molecule size is much smaller compared to cellulases generally leads to overestimation of the enzyme accessible pore surface (Luo and Zhu, 2011; Wang et al., 2012). Assuming pores in the cell wall are parallel slots, about 300 m^2/g surface area for wood pulp was obtained.

2.4.3.5 Simons' stain adsorption

Simons' stain is a semi-quantitative method based on the competitive adsorption of two dyes in an aqueous environment and can provide useful information about both internal and external accessible surface area of a porous substrate. The large orange dye molecules have greater affinity to the cellulose hydroxyl groups. They can replace the small blue dye molecules in pores where they can penetrate (Chesson et al., 1997). Thus, the proportion of blue and orange dye absorbed to the substrate indicates of the distribution of "small" and "large" pores according to their dye sizes. Using this method Esteghlalian et al. demonstrated that drying accounted for the partial closure of larger pores and creation a large number of smaller pores (Esteghlalian et al., 2001). Apparently the problem with this method is that it cannot provide quantitative measurement of pore size distribution. Furthermore, the cellulose accessibility based on dye adsorption is different from those determined using enzymes because the molecular sizes of the dyes (less than 1 kDa) are often significantly smaller than those of enzymes (Wang et al., 2012).

2.4.3.6 Nitrogen and water vapor adsorption

Nitrogen adsorption has been used broadly to estimate specific surface area for cellulosic substrates such as BMCC, Sigmacel, Solka Floc and biomss. In this method, the Bennet-Emmit-Teller (BET) adsorption equation is used to measures the surface area available to nitrogen molecule:

$$\frac{1}{v\,(\frac{P_0}{P}-1)} = \frac{c-1}{V_m c}\left(\frac{P}{P_0}\right) + \frac{1}{V_m c} \qquad (2.26)$$

where v is the adsorbed gas volume, P and P_0 are the equilibrium and the saturation pressure of gas at the temperature of adsorption, V_m is the monolayer adsorbed gas volume and c is the BET constant. V_m and c can be found by plotting $\frac{1}{v\,(\frac{P_0}{P}-1)} \sim \left(\frac{P}{P_0}\right)$ (BET plot). The specific area by gas adsorption is then generated by the following equation.

$$S = \left(\frac{V_m}{V}\right)\frac{Na}{m} \qquad (2.27)$$

In which S is the specific surface area (m^2/g), V_m is the adsorbed gas volume (m^3),V is the molar volume of adsorbed gas (m^3/mole), N is the Avogadro's number (6.02×10^{-23} $mole^{-1}$), a is the projection region of a adsorbed gas molecule (m^2), and m is the mass of absorbent (g).

In practice, the specific surface area of each sample is measured using a sorptometer by placing dried biomass in a U-tube. Nitrogen is most commonly used as the adsorbate gas and helium is used as the carrier gas. Desorption at several different nitrogen partial pressures are generally performed to find the slope and intercept of a BET plot. The specific surface area is then calculated. Specific surface areas ranging from 1 to 200 m^2

per g dry cellulose have been reported (Bothwell et al., 1997a; Chesson et al., 1997; Fan et al., 1980; Zhang and Lynd, 2004).

As this technique involves drying the substrate, it does not give a measurement that is comparable to the swollen substrate in aqueous solution. Another problem with this technique is the difference in size between the nitrogen molecule and that of an enzyme. Since the nitrogen molecule is 3200 times smaller than average size of cellulase, it has access to pores that the cellulase enzyme cannot enter (Neuman and Walker, 1992a). As it is the surface area accessible to the cellulases matters, this method can distort useful pore size information (Mansfield et al., 1999). This is especially a problem if the mouth of the pore is much smaller than the bulk of the pore volume (Chundawat et al., 2011c). Nitrogen could penetrate in the bulk pore body from the narrow mouth or congregate to block the mouth, whichever way results in distortion of the accessible porosity to enzyme.

2.4.3.7 Solute exclusion

Solute exclusion is one of the methods for estimating pore volume and subsequently pore surface area that overcomes the limitations of nitrogen and water adsorption methods. The solute exclusion technique measures capillaries between microfibrils rather than macropores such as the cell lumen and pit apertures (Grethlein, 1985; Lin et al., 1987). It is more representative of the actual surface area accessible to the enzyme molecule in

solution because it does not require drying (Ishizawa et al., 2007; Mansfield et al., 1999). The pore volume per gram of substrate accessible to each solute decreases as the diameter of the solute increase.

Early efforts to use solute exclusion to measure pore size distribution and to estimate specific surface area were done in batch mode. Wet cellulose samples were immersed in solutions of known concentration of probes (i.e. PEG, dextran, etc.) until equilibrium was reached. Probe concentration of the supernatant was measured. Based on this concentration and using a mass balance, the accessible pore volume could be calculated. Using this method, Grethlein observed less than 20% of the pore volume is accessible to a 51Å solute and less than 7% is accessible to a 90Å solute for diluted acid pretreated poplar wood (Grethlein, 1985). In addition, an excellent correlation was observed between available surface areas of 51 Å dextran and initial phase digestibility of cellulosic substrates. These results suggested that cellulase had a molecular diameter of approximated 5nm and this was confirmed by small-angle scattering measurement with cellulases (Dmitri and Michel, 2003). The problem with this technique is that only very small changes in concentration could be measured, resulting in low precision and large measurement variance (Neuman and Walker, 1992a; Tanaka et al., 1988).

Another more precise way to measure pore volume distribution employs measuring the

elution profile from a packed column to obtain a more accurate probe concentration (Corner, 2003; Neuman and Walker, 1992a; Neuman and Walker, 1992b). Using a series of inert poly-ethylene glycol (PEG) probes, a solution containing probe solute is loaded onto a packed column of cellulosic particles. Since the solute can diffuse into some of the cellulose pores, its travelling pathway is elongated and travelling time through the column is retarded (Neuman and Walker, 1992a). Figure 2.12 shows a typical elution curve with PEG 1000 probes in Avicel PH 102 column.

Analysis of elution profile can generate the accessible pore volume. In essence, assuming same solute concentration in column, the total solute mass consists of the mass of solute in the cellulose pore volume (V_p) and the mass of solute in the external void volume (V_e). Mathematically this is represented as

$$M = C_0 \left(V_p + V_e\right) = C_0 V_{total} \tag{2.28}$$

Thus, the total available void volume (V_{total}) for a certain solute is

$$V_{total} = \frac{M}{C_0} = \frac{\int_0^\infty C\, dv}{C_0} = \sum_{n=1}^{m} \frac{C_n}{C_0} V_n \tag{2.29}$$

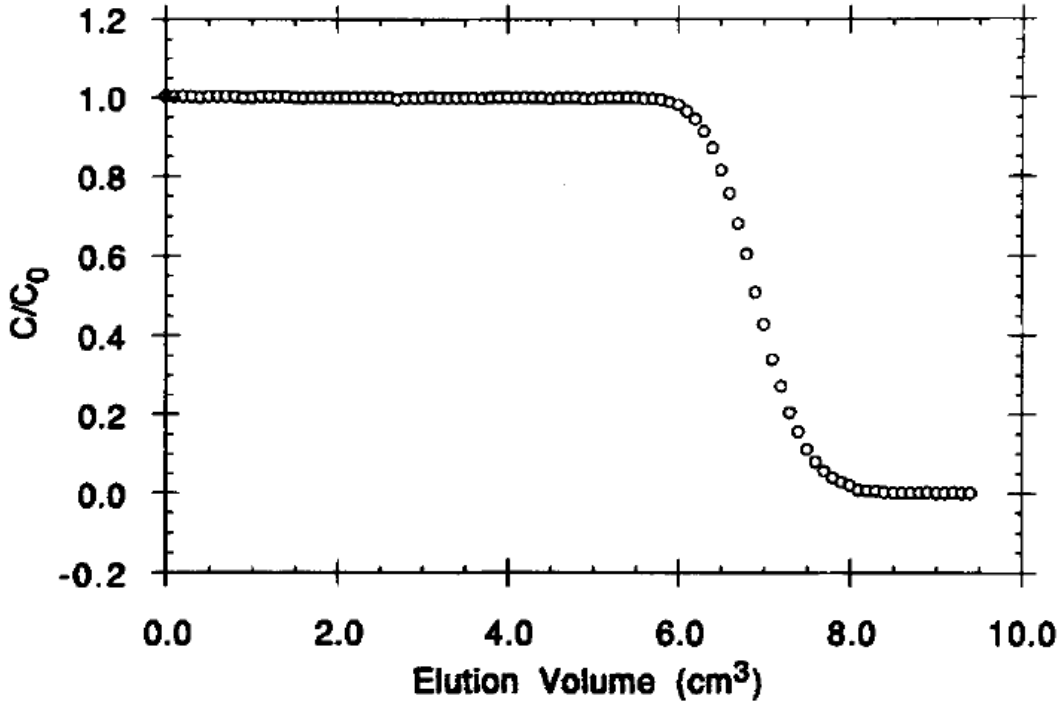

Figure 2.12. Typical elution curve with PEG 1000 probes in Avicel PH 102 column (Neuman and Walker, 1992a).

C_n and V_n are the concentration and volume of each solute sample from elution profiles. Therefore, V_e can be measured from large dextran (i.e. 2MDa) elution curves with the assumption that no V_p is accessible to such a large probe. Meanwhile, V_{total} generated by smaller probes consists of both V_p and V_e. Since all measurements include the dead volume of the column fittings and tubing, a simple subtraction can generate the pore volume accessible to the smaller probe. The effect of dispersion, mass transfer and pore diffusion could also be modeled by a combined mass transfer and pore diffusion model (Neuman and Walker, 1992a; Neuman and Walker, 1992b).

Another packed column size-exclusion chromatography was developed to characterize the cellulose matrix of Avicel PH 102 and observe the movement of cellulase catalytic domains within the matrix. The PEGs exhibited concise size-based trends with accessible volume and the accessible surface area was determined at 31 m^2/g cellulose. Size exclusion velocity with catalytic domains were retarded because of weak binding activities with cellulose (Corner, 2003).

2.4.3.8 Measurements of bound cellulases to estimate available surface area

Indirect measurements of bound cellulases to estimate available surface area involve the following steps: Firstly substrate and enzyme are incubated at a temperature at which hydrolysis was minimal. After incubated for a certain time, they are separated by

microfiltration/centrifugation. The absorbance of the supernatant was read at 280 nm by an OD reader. Beer–Lambert law was applied to back calculate the protein concentration in supernatant with known extinction coefficient. The bound fraction can be determined based on the difference between the known total enzyme input and the measured enzyme in free solution (Stahlberg et al., 1991). With known surface area for each bound cellulase, the available binding surface in biomass can be estimated.

Several researchers have used this method to estimate bound cellulases (Beldman et al., 1987; Bothwell et al., 1997a; Lee et al., 1982; Ryu et al., 1984; Stahlberg et al., 1991). Some research showed the maximum adsorption levels (μmol cellulase/g cellulose) of 46.3 kDa Cel5A on Avicel was 74% greater than that of 59.6 kDa Cel6B, while they were approximately the same on BMCC. The authors attributed this to the diffusion hindrance from the more restrictive pore structure of Avicel than BMCC (Bothwell et al., 1997a). Langmuir binding model has been applied to describe the binding activities. Maximum binding capacity has been determined at 12, 23 and 10 μmol/g cellulose for Cel5A, Cel6B and Cel9A at 5 °C, respectively (Jung et al., 2003). The irreversible binding was assumed to be caused by interstice entrapment of cellulases (Bothwell et al., 1997b; Jung et al., 2002a; Jung et al., 2002b).

Bothwell et al quantified the accessible surface area of cellulosic biomass by enzyme

binding capacity. Assuming certain geometry based on a solved cellulase structure, they calculated the volume per mole of *T. reesei* Cel7A to be 5.8×10^{4} cm^3 (Bothwell, 1994). By multiplying maximum binding capacity derived from experimental data, she estimated the *T. reesei* Cel7A accessible pore volume to be 0.03 cm^3/g Avicel, which is comparative to the 0.04 cm^3/g pore volume measured by size-exclusion chromatography (Neuman and Walker, 1992a). A family 2a cellulose-specific carbohydrate binding module (CBM2a, 15.2kDa) from *Cellulomonas fimi* (Xu et al., 1995) was used in an adsorption experiment as an indicator of the total available cellulose surface area (McLean et al., 2002; McLean et al., 2000). The concentration of CBM2a in the supernatant was determined by measuring the absorbance of the solution at 280 nm after the mixture of BMCC and CBM2a were incubated and centrifuged (Kumar et al., 2012). Given the area of 1.32×10^{-13} cm^2 shadowed by a bound CBM2a molecule, they calculated the maximum binding capacity to be 13 μmol/g BMCC, which is consistent with the capacity of 11.7 μmol/g BMCC generated by Langmuir binding model (McLean et al., 2000). These are very meaningful endeavors to explain and validate the maximum binding capacity from molecular level. They also demonstrated that a simple geometry assumption of the cellulase size can, to some extent, help determine the accessible volume/surface.

Hong et al. (2007) elucidated the cellulose accessible surface area by defining cellulose

accessibility to cellulase (CAC), which is a function of the indirect measured binding capacity of TGC fusion protein (62 kDa):

$$\mathrm{CAC} = \alpha A_{max} N_A A_{G2} \qquad (2.30)$$

Where α is 21.2 cellobiose lattices occupied by a TGC molecule, A_{max} is the maximum protein adsorption capacity (mole cellulase/g cellulose), N_A is the Avogadro's constant (6.023×10^{23} molecules/mol), and A_{G2} is the area of the cellobiose lattice in the 110 face ($5.5\times10^{-19}m^2$).

Assuming monolayer adsorption, CAC value of BMCC was found to be 14-fold larger than that of crystalline celluloses Avicel (Hong et al., 2007). Zhu et al. further improved the method by constructing a nonhydrolytic recombinant protein TGC containing a cellulose-binding module and a green fluorescence protein. With BSA to block the unspecific binding sites (i.e. lignin), cellulose accessibility to cellulase in pretreated biomass was acquired. These results showed that COSLIF-pretreated corn stover had a CAC of 11.57 m^2/g, nearly twice that of the DA-pretreated biomass (Zhu et al., 2009c). The application of this method allow for the robust correlation of binding curves and estimated surface areas. However, the authors assumed that the BSA bound to nonspecific binding sites can not be substituted by enzyme. In reality, enzyme binding

should be a dynamic exchange process between the bound and unbound (Bothwell et al., 1997b; Jung et al., 2003). So the conclusion that the non-specific binding could be blocked by BSA is unsubstantiated. The values of the specific surface area using methods described above for pure cellulose and lignocellulosic biomass are summarized in Table 2.10.

2.4.4 Enzyme accessibility is influenced by steric hindrance

Micro- and mesoporous materials contain pores with diameters less than 50 nm (Rouquerol et al., 1994). At the ultra-structural scale of plant cell walls, cellulases may initially penetrate into the structure of the cellulose that are large enough to accommodate them, and then, in a process limited by diffusion, bind to sites located within the particle (Arantes and Saddler, 2011). Therefore, simple measurement of surface area is not sufficient to characterize cellulose accessibility. The mass transport into the micro- and mesoporous region of the material is defined by the molecular diffusion of the enzyme, pore size distribution, binding affinity of the enzyme and other chemical and physical factors. The porosity of the cellulosic particle creates small diffusion space and pathway. The pore volume accessibility of cellulases is limited by the effective cross-sectional area available for diffusion (Carpita et al., 1979). In addition, transport may be limited by a tortuous pathway, which increases the collision times of enzymes on their diffusion pathway (Almeida and Huber, 1999). Second, the excluded volume may include some

Table 2.10. Values of the specific surface area for pure cellulose substrates

Substrate	Specific Surface Area (m^2/g)	Measuring technique	References
Solka Floc	2.13	Nitrogen adsorption	(Fan et al., 1980; Fan et al., 1981)
Sigmacell	1.84	Nitrogen adsorption	(Fan et al., 1980)
Avicel PH101	3	Nitrogen adsorption	(Gama et al., 1994)
Whatman filter paper	2.07	Nitrogen adsorption	(Gama et al., 1994)
Phosphoric acid swollen cellulose	240	Nitrogen adsorption	(Zhang and Lynd, 2004)
BMCC	200	Nitrogen adsorption	(Bothwell et al., 1997a)
Avicel PH101	19	Protein adsorption	(Stahlberg et al., 1991)
Sigmacell 100	0.61	Protein adsorption	(Gama et al., 1994)
BMCC	120	Protein adsorption	(McLean et al., 2000)
Filter paper	10	Protein adsorption	(Hong et al., 2007)
Aspen high yield pulp	300	WRV	(Hui et al., 2009)
Difibered pulp	2.6	Solute exclusion	(Tanaka et al., 1988)
Solka Floc BW 300	11.6	Solute exclusion	(Neuman and Walker, 1992a)
Avicel PH102	10.5	Solute exclusion	(Neuman and Walker, 1992a)
Avicel PH102	31	Solute exclusion	(Corner, 2003)

Table 2.10. Values of the specific surface area for lignocellulosic biomass (continued)

Substrate	Specific Surface Area (m^2/g)	Measuring technique	References
Wheat straw internode	3.3	Nitrogen adsorption	(Chesson et al., 1997)
Tulip poplar	0.6	Nitrogen adsorption	(Koo et al., 2012)
Organosolv pretreated tulip poplar	1.8	Nitrogen adsorption	(Koo et al., 2012)
Acid treated corn stover	40	^{1}H NMR	(Ishizawa et al., 2007)
COSLIF treated corn stover	14.44	Protein adsorption	(Zhu et al., 2009c)
Acid treated corn stover	7.66	Protein adsorption	(Zhu et al., 2009c)
AFEX treated corn stover	23	3D-TEM	(Chundawat et al., 2011c)
Lignin removed corn cob (60um)	7.2	Solute exclusion	(Neuman and Walker, 1992a)
Lignin removed corn cob (300um)	9.9	Solute exclusion	(Neuman and Walker, 1992a)
Untreated hardwood	10.5	Solute exclusion	(Grethlein, 1985)
Pretreated hardwood	37-140	Solute exclusion	(Grethlein, 1985)
Acid swollen cotton	10-100	Solute exclusion	(Stone et al., 1969)
Steam treated wood pulp	55-61	Solute exclusion	(Carrasco et al., 1994)
Alkaline peroxide treated mixed hardwood	66-71	Solute exclusion	(Thompson et al., 1992)
Dilute acid treated mixed hardwood	86-128	Solute exclusion	(Thompson et al., 1992)

water molecules that are strongly bound to cell wall polymers, forming a hydration layer inaccessible to a diffusing solute (Mercado et al., 2004). Third, large number of fixed negative charges may present in the cell wall, largely in the form of ionized carboxyl groups. These are expected to repel negatively charged solute molecules (Kramer et al., 2007). Fourth, synergism effect can be affected since only the smaller components of the cellulase complex can enter some pores due to sieving mechanism. This tends to segregate the cellulase components to reduce the overall hydrolysis rate because the synergistic action of the cellulase complex is reduced. This is especially true when small pores dominate, only the smaller enzyme components diffuse into the pores and synergism with the larger components is impossible. When larger pores dominate, the cocktail can diffuse in and synergism can deploy (Tanaka et al., 1988).

Diffusion of a solute into a pore is influenced by the pore size even if this pore is considerably larger than the particle. Due to steric hindrance, the pore diffusion rate of a solute in a pore space or gel network is frequently less than its value in the bulk solution. This phenomenon is characterized as hindered diffusion and reflects the degree of interaction between the diffusion molecule and the matrix (Lawrence et al., 1994). Several correlations have been reported that provides very good estimate of pore diffusion including the following by Harriott (Harriott, 2002):

$$\frac{D_{pore}}{D_{bulk}} = \left(1 - \frac{d_{solute}}{d_{pore}}\right)^4 \quad (2.31)$$

Where d_{solute} is the hydrodynamic radii of solute (i.e. enzyme)(nm), d_{pore} is the average pore width (nm), D_{bulk} is the solute diffusion coefficient in bulk solution (cm^2/s), and D_{pore} is the solute diffusion coefficient inside pores (cm^2/s).

Another way to describe the hindered pore diffusion is through effective diffusion coefficient (D_e). It consider influences from porosity (V_f) and tortuosity (τ). These two factors are used to introduce structural factors such as the extended diffusion pathway due to sinuosity in the pores and continuity of the pores. If other factors such as the solute physical interaction with the pore surface, the tortuosity is defined as the apparent tortuosity, τ. Apparent tortuosity can be used to calculate pore diffusion coefficient as follows (Takahashi et al., 2002):

$$D_e = \frac{V_f}{\tau} D_{pore} \quad (2.32)$$

Sometimes the entrance to the pore is much smaller than the bulk of the pore volume. This could result in condensation of cellulases at the pore mouth without much penetration into the pore, which would result in an underestimation of the total porosity

(Srebotnik et al., 1988). Three dimensional - TEM tomography confirmed this type of narrow mouth is quite common within pretreated cell walls and could explain the discrepancy seen in the results from BET analysis compared to TEM based porosity (Chundawat et al., 2011c).

2.4.5 Enzyme transportation process

Previous discussions demonstrate that simple measurement of surface area is not sufficient to characterize cellulose accessibility. In fact, the mass transfer study of enzymes from bulk to binding sites inside biomass can provide direct insights on how enzymes overcome steric hindrance and gain access to accessible surface area. This mass transfer process is mainly comprised of three processes: macroscopic diffusion, microscopic diffusion and binding to available sites.

2.4.5.1 Macroscopic transport

Bulk fluids can travel to cells and cell surfaces by the same macroscopic routes (>50nm) that were evolved for liquid transport in the living plant (Viamajala et al., 2006). Specifically, bulk liquids navigate the vascular tissues such as xylem and phloem which are the primary routes for transport of water and nutrients along the length of the plant stem and leaves. Additional transport between adjacent cells is carried out through the pits, the intercellular void space of cell junctions and cell corners. For instance, it was

observed that the pits disintegrated and opened up during pretreatment allowing fluid flow (Donohoe et al., 2008). However, these gross capillaries in the size of 0.02–10 mm in a fiber only constitute a small fraction of total available surface area (Zeng et al., 2007).

The rate of bulk transport of liquids through pretreated biomass differs from native plant material because of the absence of transpiration pulling force through the vascular system (Donohoe et al., 2009). Size reduction can facilitate macroscopic transport in harvested biomass to a certain degree (Himmel et al., 2007). Kim and Lee demonstrated that acid took three times longer to reach 70% penetration of biomass cut randomly to 1 to 2 cm compared to powdered samples of about 1mm sieve size (Kim and Lee, 2002). On the other hand, considering the high energetic costs of grinding, bioprocessing industry would ideally be capable of using feedstocks in the 1-10 centimeter fragment range (Torget et al., 1991). As noted earlier, critical balancing must be chosen between increasing the accessibility of the substrate and the energy cost to achieve the desired size reduction (Vidal et al., 2011).

Air entrained or entrapment in the cell lumen can also be a major barrier to fluid transport into dry plant materials. Aqueous pretreatment before hydrolysis can help overcome the macroscopic transport hindrance caused by trapped air. Researchers reported poor treatability of corn stover during steam explosion if materials were not pre-wetted with

dilute acid. They attributed this result to mass transport limitation caused by trapped air (Tucker et al., 2003). One option for overcoming this problem is to immerse biomass in liquids to help compel entrapped air out. Another option for removing trapped air is vacuum removal (Gardner et al., 1999; Viamajala et al., 2010; Viamajala et al., 2006).

2.4.5.2 Microscopic transport

Mesopores and micropores with diameter less than 50 nm are ubiquitously distributed around plant cell walls (Chesson et al., 1997; Esteghlalian et al., 2001; Grethlein, 1985; Ishizawa et al., 2007; McCANN et al., 1990; Munoz et al., 2003; Nakashima et al., 1997). These pores behave like capillaries, which are different from artery-like macropores. For the purpose of improving biomass deconstruction, the nanoscale spaces among the cellulose microfibrils are the most important routes for cellulase penetration (Donohoe et al., 2008). One of the most commonly used cellulase Cel7A, has dimensions about 5 nm. However, several researchers have observed that Cel7A had limited accessibility to cellulose in lignocellulosic biomass (Divne et al., 1998; Torquato and Avellaneda, 1991; Viamajala et al., 2010). Moran-Mirabal et al. 2011 observed different FRAP recovery curve between BMCC fibrils and mats. For cellulose fibrils, all surface area available was equally accessible and no diffusion hindrance was observed, leading to similar FRAP recovery curves from different-size bleached areas. In the case of porous structure such as mats, cellulose in deep layers was not as accessible for enzyme to reach as that on the

external surface. This was deduced from the observed temporal recovery of florescence with mats (Moran-Mirabal et al., 2011; Moran-Mirabal et al., 2008).

To enhance cellulases access to lignocellulosic biomass, thermochemical pretreatments have been performed to disrupt covalent linkages between lignin and cellulose and to increase the inter microfibrillar cavities at a submicron level (Donohoe et al., 2008; Zeng et al., 2007). For example, SEM micrographs and FTIR analysis of ionic liquid pretreated switchgrass suggested increased porosity and weaken covalent linkages between lignin and cellulose (Singh et al., 2009). A recent study using nano-gold labeled antibodies to cellulases shows that enzyme penetration into mildly pretreated cell walls is minimal. In moderately and severely pretreated cell walls, cellulases are able to partially or thoroughly penetrate the entire cell wall, consequently increasing reducing sugar yield. These results suggest that pretreatment significantly opens up the pore structure on plant biomass materials. The newly created micropores can work together with macroscopic transport pathways to better overcome mass transfer hindrance in biomass (Donohoe et al., 2009).

With modifications created by pretreatment, macroscopic transport can be converted or at least partially resemble microscopic transport. Pits and cell corners are known to be important for transport among adjacent cells and tissues. After dilute aid pretreatment,

three macropore ultra-structural regions: pits, cell corners, and delamination layers all accumulated a high concentration of lignin droplets. Results from SEM and TEM showed a pit partly occluded by a cluster of droplets, and single droplets nearly large enough to block the pit channel was also observed (Donohoe et al., 2008). These regions are important for transport of enzymes through the biomass structure. The obstruction would likely decrease the width of macropores and create barriers limiting access through these originally macroscopic pathways. On the other hand, lignin coalescing to a more localized, concentrated distribution from homogenous distribution is expected to generate new microscopic pathways and increase the accessibility of cellulose microfibrils buried deep within the cell wall.

2.4.5.3 Binding sites

Even if cellulases successfully diffused to the vicinity of cellulose fibril this does not guarantee full saccharification. A study showed that cell wall structure was significantly loosened by thermochemical pretreatment to allow cellulase enzymes to penetrate completely into cellulose particles (Donohoe et al., 2009). However, this full penetration did not yield 100% saccharification. One explanation was that cellulases still do not have access to all the binding surfaces on the microfibril that they need to proceed effectively in depolymerize the cellulose fiber, even when they have access to the fibers. The binding sites are still partially unsheathed by coalesced lignin (Donohoe et al., 2009).

Therefore, a third limitation to cellulose digestibility is cellulases gaining access to cellulose binding and reactive sites. Once the enzymes transport through the plant tissue and penetrate the pore structure of the cell wall matrix, they must locate an accessible binding site to anchor itself, through the cellulose binding module, and form a complex between the cellulose polymer chain and the catalytic domain of the enzyme. This means that a region of cellulose microfibril must be sufficiently unsheathed from lignin and hemicellulose to expose the cellulose.

Though it is hard to separate the contribution from diffusion and binding, it is still valuable to know which one is the dominant or rate limiting factor. Similar work has been conducted to put weight on the influence from reaction and diffusion in a pretreatment process. Kim and Lee chose to use Thiele modulus (Kim and Lee, 2002), Ø, to evaluate the process

$$\text{Thiele modulus} = \emptyset = \mathrm{L}\left(\frac{\mathrm{k}}{\mathrm{D_e}}\right)^{0.5} \qquad (2.33)$$

Where L is the size of biomass (cm), k is the first-order rate constant of the pretreatment process (s^{-1}), and D_e is the effective diffusion coefficient (cm^2/s).

Assuming an average diffusion coefficient, Theile number was found much smaller than 1 by fitting all the experimental based L, k, D_e into equation 2.33. This means the acid diffusion process was not likely to affect the overall process because most of the reaction occurred after acid fully saturated the biomass (Kim and Lee, 2002).

2.4.6 Confocal imaging methods for diffusion measurement

Confocal laser scanning microscopy (CLSM) provides high spatial and temporal resolution for measuring the emission light of fluorescence labeled biomolecules (Bancel and Hu, 1996). Cellulases and other biomolecules can be labeled with a variety of fluorescent tags, which can be illuminated through an objective with light of a wavelength specific to their excitation spectrums. The tag then emits light of a longer wavelength than that of the excitation light, which can be collected by the imaging system. In this section, different methods utilizing CLSM to study the diffusion behaviors of inert probes and cellulases in cellulose matrix are reviewed.

2.4.6.1 Confocal laser scanning microscopy (CLSM) observation of inert probes diffusion

CLSM has been used to explore the diffusion behaviors of different fluorescence labeled probes through cellulose particle (Zhu et al., 2011). Fluoresceinisothiocyanato (FITC)-dextran are some of the most widely used probes for such studies and they have been shown no interaction with plant cell walls (Lawrence et al., 1994; Waharte et al., 2010;

Wang et al., 2008). In a study by Proseus and Boyer, *Chara corallina* primary cell walls were attached to one end of a glass capillary. Solutions of different size FITC-dextran or suspensions of gold colloids were pushed from the capillary into the cell walls using different pressures. The authors defined the pressure applied against the inner wall face as P, the turgor pressure, and monitored probe movement and distribution through the cell wall by CLSM (Proseus and Boyer, 2005). Figure 2.13 shows the experimental setup (A) and proposed probe movements into cell wall matrix (B).

The authors observed that small solute (0.8 nm) moved freely through these interstices unaffected by P, while larger molecules were obstructed as their Stokes' diameters approached the size of wall interstices. In addition, the authors showed that dextrans of 3.5 nm diameter moved faster at higher P, while dextran of 9 nm scarcely entered unless high P was present. The interpretation of these results is illustrated in Figure 2.13, B. They did not quantify polymer movement distance over time. Therefore, no diffusivity was reported even though it could have been.

2.4.6.2 FRAP measurement of inert probes diffusion

Fluorescence recovery after photobleaching (FRAP) is an optical technique capable of quantifying the diffusion of fluorescently labeled probes across the surface of a molecularly thin film (Zhang et al., 2011). Through photobleaching, the fluorophores in

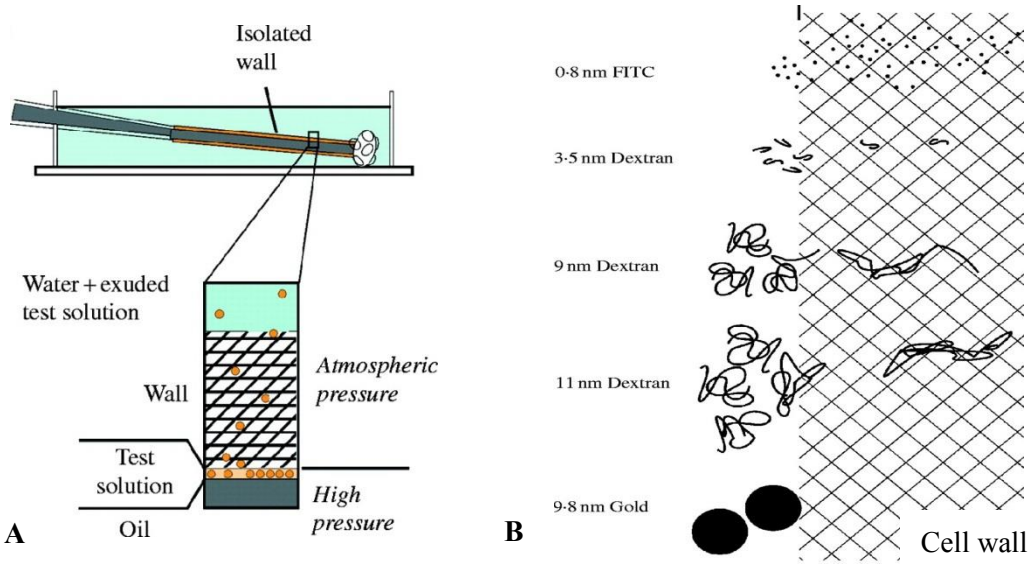

Figure 2.13. Schematic diagram of experimental setup(A) and probe movements into cell wall matrix(B) (Proseus and Boyer, 2005).

this region receive high intensity illumination, which causes their fluorescence lifetime to quickly diminish (Moran-Mirabal et al., 2008). Diffusion rate is a dominate factor in the recovery of fluorescence recovery. The rate of labeled enzyme diffusing into the bleached area and the rate of bleached proteins unbinding from their sites are two factors influencing fluorescence recovery rate (Soumpasis, 1983; Sprague and McNally, 2005; Sprague et al., 2004). To simplify this problem, previous researchers generally categorized FRAP experiments into two processes respectively limited by isotropic diffusion and unbinding.

Axelrod et al. derived the mathematical foundation to extract diffusion coefficient from FRAP experiments (Axelrod et al., 1976). They considered that diffusion of the probe mainly occurs in a two-dimension surface with no binding interaction between the probes and the porous structure. Assuming circular bleach area, they proposed a radial diffusion equation to correlate fluorescence signal to time. Recovery time constant, τ, can be found by fitting experimental data.

$$F(t) = e^{-2\tau/t}(I_0(2\tau/t) + I_1(2\tau/t)) \qquad (2.34)$$

Where F(t) is the normalized fluorescence, t is the recovery time (s), I_0 and I_1 are modified Bessel functions, and τ is the recovery time constant, the time required for the

bleach spot to recover half of its initial integrated intensity (s).

Assuming Gaussian intensity distribution, diffusion coefficient can be derived by

$$D = r^2/4\tau \qquad (2.35)$$

where r is the radius of the bleach spot (Axelrod et al., 1976)

Since the model was developed, FRAP has been broadly applied for the measurement of diffusion activities in different materials (Blonk et al., 1993). For example, FITC-Dextran have been used to study diffusion in biofilm with pore size larger than 50 nm by FRAP (Waharte et al., 2010). FRAP has also been applied to quantify the translational diffusion of FITC-dextrans in the cytoplasm and nucleus of epithelial cells. It was found that FITC-dextran diffusion coefficient decreased from 75 to 8.4×10^{-7} cm^2/s when dextran size increased from 4 to 2000 kDa (Seksek et al., 1997). Other researchers have devised gel systems to simulate the secondary cell wall, in which the mobility of FITC-dextrans was studied by FRAP. Diffusion coefficient dropped from 5 to 1×10^{-7} cm^2/s when the average size of the FITC dextran increases from 10 to 250 kDa. However, the pore size in this artificial gel is too large (220-320nm) to resemble the actual pore sizes, which are generally below 20 nm (Paës and Chabbert, 2011).

In addition, FRAP has been used to record fluorescence from carboxyfluorescein (CF, 376Da) in the root cell wall of Arabidopsis thaliana. Roots were immersed in a solution of the fluorescent dye and viewed through a confocal fluorescence microscope. The diffusion coefficient of CF in the cell wall was probed using fluorescence recovery after photobleaching technique (Kramer et al., 2007). Diffusion coefficient in the cell wall of mature cortex and mature epidermis were 3.2×10^{-7} cm^2/s, and 2.5×10^{-8} cm^2/s, respectively, compared to bulk diffusion coefficient of 4.9×10^{-6} cm^2/s. This study provided a quantitative estimate of the permeability of plant cell walls to small molecules. One problem with this method is the size of the probes is much smaller (376Da) comparing to cellulase (>20kDa). Besides, the CF in the apoplast was predominantly in charged forms (Kramer et al., 2007), which could increase the possibility of interactions with plant cell wall.

2.4.6.3 FRAP measurement of fluorescently labeled cellulases

Using fluorescently labeled enzymes makes it possible to measure the bound cellulase concentration directly, therefore reducing the error associated with the estimated kinetic parameters. Jeoh. et al demonstrated that cellulases can be labeled with fluorophores without inhibiting activities. In addition, using fluorescent labeled cellulases to estimate bound cellulases results in greater sensitivity, and the many fluorescent tags and dyes available make it possible to simultaneously measure multiple types of cellulases acting

synergistically in a solution (Jeoh et al., 2002a).

When the FRAP recovery experiment is performed using enzyme instead of inert probes, enzyme-substrate interactions like binding/unbinding cannot be ignored during recovery process. Thus, the Axelrod et al. equation cannot be directly applied to fit the experimental data. Moran-Mirabal et al. proposed a model for a FRAP recovery process which is enzyme binding/unbinding limited.

$$\frac{dI_B}{dt} = k_{on} S C_F \alpha - k_{off} I_B \qquad (2.36)$$

In this model, I_B is the fluorescence intensity from cellulase, k_{on} and k_{off} are the binding and unbinding rate constant, S is the concentration of available binding sites on the cellulose surface, C_F is the cellulase concentration in solution, and α is the fluorescence intensity of unit bound cellulase. Assuming equilibrium between bound and unbound molecules, an exponential decay equation has also been developed to fit fluorescence recovery after integration of the equation above (Moran-Mirabal et al., 2011).

$$I_B(t) = F_M(1 - e^{-k_{off}t}) \qquad (2.37)$$

Where F_M is the mobile fraction, dimensionless, k_{off} is the unbinding rate constant (s^{-1}),

and t is the recovery time (s).

The authors reported up to 6 times faster recovery rates on fibrils than the recovery on mats (Moran-Mirabal et al., 2011). They attributed the differences to cellulose accessibility and hindered diffusion. In the case of cellulose fibrils, all surface area available is equally accessible and no diffusion hindrance is expected, leading to absolute binding/unbinding dominant recovery process. On the other hand, mats have a porous structure where cellulose in deep layers is not as accessible as that on the external surface. This leads to longer recovery time because steric hindrance through the interstitial spaces within the mats makes hindered diffusion another important factor besides binding/unbinding (Moran-Mirabal et al., 2011).

2.5. Summary of literature review

Enzymatic saccharification of lignocellulosic biomass has been identified as one of the most costly steps during ethanol production process (Luterbacher et al., 2010; Lynd et al., 2008; Wang et al., 2012). This is partially due to the comparatively high protein loadings required to degrade the structurally complex lignocellulosic substrates. In this section, the structures of lignocellulosic substrate and enzymatic saccharification process have been reviewed. The effects of cellulose structure features (i.e. degree of polymerization, crystallinity, particle size, lignin content and accessible surface area) on enzymatic

saccharification have been discussed. Work described in this section demonstrates that accessible surface area is essential for high saccharification rate and extent (Bothwell et al., 1997a; Grethlein, 1985). Enzyme accessibility to surface area is influenced by steric hindrance during the transportation process (Arantes and Saddler, 2011; Kramer et al., 2007). The different methods measuring the pore sizes and diffusivity reviewed in this section provide tools to analyze the experimental results and extract substrate/process parameters.

2.6. References

Adamson AW. 1983. Physical chemistry of surface. New York: Wiley.

Almeida DPF, Huber DJ. 1999. Apoplastic pH and inorganic ion levels in tomato fruit: A potential means for regulation of cell wall metabolism during ripening. Physiologia Plantarum 105(3):506-512.

Annis SL, Goodwin PH. 1997. Recent advances in the molecular genetics of plant cell wall-degrading enzymes produced by plant pathogenic fungi. European Journal of Plant Pathology 103:1-14.

Arantes V, Saddler J. 2010. Access to cellulose limits the efficiency of enzymatic hydrolysis: the role of amorphogenesis. Biotechnology for Biofuels 3(1):4.

Arantes V, Saddler J. 2011. Cellulose accessibility limits the effectiveness of minimum cellulase loading on the efficient hydrolysis of pretreated lignocellulosic substrates. Biotechnology for Biofuels 4(1):3.

Aro N, Pakula T, Penttila M. 2005. Transcriptional regulation of plant cell wall degradation by filamentous fungi. FEMS Microbiology Reviews 29:719-739.

Atalla RH, Hackney JM, Uhlin I, Thompson NS. 1993. Hemicelluloses as structure regulators in the aggregation of native cellulose. International Journal of Biological Macromolecules 15(2):109-112.

Atalla RH, Vanderhart DL. 1984. Native cellulose: A composite of two distinct crystalline forms. Science 223(4633):283-285.

Axelrod D, Koppel DE, Schlessinger J, Elson E, Webb WW. 1976. Mobility measurement by analysis of fluorescence photobleaching recovery kinetics. Biophysical Journal 16(9):1055-1069.

Baker J, Ehrman C, Adney W, Thomas S, Himmel M. 1998. Hydrolysis of cellulose using ternary mixtures of purified celluloses. Applied Biochemistry and Biotechnology 70-72(1):395-403.

Ballesteros I, Oliva JM, Negro MJ, Manzanares P, Ballesteros M. 2002. Enzymic hydrolysis of steam exploded herbaceous agricultural waste (Brassica carinata) at different particule sizes. Process Biochemistry 38(2):187-192.

Bancel S, Hu W-S. 1996. Confocal laser scanning microscopy examination of cell distribution in macroporous microcarriers. Biotechnology Progress 12(3):398-402.

Bansal P, Hall M, Realff MJ, Lee JH, Bommarius AS. 2009. Modeling cellulase kinetics on lignocellulosic substrates. Biotechnology Advances Volume 27(Issue 6):833-848.

Becker DB, C H Brumer , 3rd, M Claeyssens, C Divne, B R Fagerström, M Harris, T A Jones, G J Kleywegt, A Koivula, S Mahdi, K Piens, M L Sinnott, J Ståhlberg, T T Teeri, M Underwood, and G Wohlfahrt. 2001. Engineering of a glycosidase Family 7 cellobiohydrolase to more alkaline pH optimum: the pH behaviour of

Trichoderma reesei Cel7A and its E223S/ A224H/L225V/T226A/D262G mutant. Biochemistry Journal 356:19-30.
Beeson WT, Phillips CM, Cate JHD, Marletta MA. 2011. Oxidative Cleavage of Cellulose by Fungal Copper-Dependent Polysaccharide Monooxygenases. Journal of the American Chemical Society 134(2):890-892.
Beldman G, Voragen AGJ, Rombouts FM, Pilnik W. 1988. Synergism in cellulose hydrolysis by endoglucanases and exoglucanases purified from *Trichoderma viride*. Biotechnology and Bioengineering 31:173-178.
Beldman G, Voragen AGJ, Rombouts FM, Searle-van Leeuwen MF, Pilnik W. 1987. Adsorption and kinetic behavior of purified endoglucanases and exoglucanases from Trichoderma viride. Biotechnology and Bioengineering 30(2):251-257.
Berlin A, Gilkes N, Kurabi A, Bura R, Tu M, Kilburn D, Saddler J. 2005. Weak lignin-binding enzymes. Applied Biochemistry and Biotechnology 121(1):163-170.
Blonk JCG, Don A, Van Aalst H, Birmingham JJ. 1993. Fluorescence photobleaching recovery in the confocal scanning light microscope. Journal of Microscopy 169(3):363-374.
Bond JQ, Alonso DM, Wang D, West RM, Dumesic JA. 2010. Integrated catalytic conversion of γ-Valerolactone to liquid alkenes for transportation fuels. Science 327(5969):1110-1114.
Boraston AB, Bolam DN, Gilbert HJ, Davies GJ. 2004. Carbohydrate-binding modules: fine-tuning polysaccharide recognition. Biochemical Journal 382(3):769-781.
Bothwell MK. 1994. Binding kinetics of Thermomonospora Fusca E3 and E5, and Trichoderma Reesei CBHI. Ph.D. Dissertation, Cornell University, Ithaca.
Bothwell MK, Daughhetee SD, Chaua GY, Wilson DB, Walker LP. 1997a. Binding capacities for Thermomonospora fusca E3, E4 and E5, the E3 binding domain, and Trichoderma reesei CBHI on Avicel and bacterial microcrystalline cellulose. Bioresource Technology 60(2):169-178.
Bothwell MK, Walker LP, Wilson DB, Irwin DC, Price M. 1993. Synergism between pure Thermomonospora fusca and Trichoderma reesei cellulases. Biomass and Bioenergy 4(4):293-299.
Bothwell MK, Wilson DB, Irwin DC, Walker LP. 1997b. Binding reversibility and surface exchange of Thermomonospora fusca E3 and E5 and Trichoderma reesei CBHI. Enzyme and Microbial Technology 20(6):411-417.
Cantarel BL, Coutinho PM, Rancurel C, Bernard T, Lombard V, Henrissat B. 2009. The Carbohydrate-Active EnZymes database (CAZy): an expert resource for Glycogenomics. Nucl. Acids Res. 37(suppl_1):D233-238.
Carpita N, Sabularse D, Montezinos D, Delmer DP. 1979. Determination of the pore size of cell walls of living plant cells. Science 205(4411):1144-1147.
Carrasco JE, Sáiz MC, Navarro A, Soriano P, Sáez F, Martinez JM. 1994. Effects of dilute acid and steam explosion pretreatments on the cellulose structure and

kinetics of cellulosic fraction hydrolysis by dilute acids in lignocellulosic materials Applied Biochemistry and Biotechnology 45/46(1):23-34.
Chang VS, Burr B, Holtzapple MT. 1997. Lime pretreatment of switchgrass. Applied Biochemistry and Biotechnology 63-5:3-19.
Chang VS, Holtzapple MT. 2000. Fundamental factors affecting biomass enzymatic reactivity Applied Biochemistry and Biotechnology 84-86(1-9):5-37.
Chanzy H, Henrissat B, Vuong R. 1984. Colloidal gold labelling of l,4-β-D-glucan cellobiohydrolase adsorbed on cellulose substrates. FEBS Letters 172(2):193-197.
Chen F, Dixon RA. 2007. Lignin modification improves fermentable sugar yields for biofuel production. Nat Biotech 25(7):759-761.
Chesson A, Gardner PT, Wood TJ. 1997. Cell wall porosity and available surface area of wheat straw and wheat grain fractions. Journal of the Science of Food and Agriculture 75(3):289-295.
Chundawat SPS, Beckham GT, Himmel ME, Dale BE. 2011a. Deconstruction of lignocellulosic biomass to fuels and chemicals. Annual Review of Chemical and Biomolecular Engineering 2(1):121-145.
Chundawat SPS, Bellesia G, Uppugundla N, da Costa Sousa L, Gao D, Cheh AM, Agarwal UP, Bianchetti CM, Phillips GN, Langan P and others. 2011b. Restructuring the crystalline cellulose hydrogen bond network enhances its depolymerization rate. Journal of the American Chemical Society 133(29):11163-11174.
Chundawat SPS, Donohoe BS, da Costa Sousa L, Elder T, Agarwal UP, Lu F, Ralph J, Himmel ME, Balan V, Dale BE. 2011c. Multi-scale visualization and characterization of lignocellulosic plant cell wall deconstruction during thermochemical pretreatment. Energy & Environmental Science 4(3):973-984.
Chundawat SPS, Venkatesh B, Dale BE. 2007. Effect of particle size based separation of milled corn stover on AFEX pretreatment and enzymatic digestibility. Biotechnology and Bioengineering 96(2):219-231.
Ciolacu D, Pitol-Filho L, Ciolacu F. 2012. Studies concerning the accessibility of different allomorphic forms of cellulose. Cellulose:1-14.
Converse AO, Matsuno R, Tanaka M, Taniguchi M. 1988. A model of enzyme adsorption and hydrolysis of microcrystalline cellulose with slow deactivation of the adsorbed enzyme. Biotechnology and Bioengineering 32(1):38-45.
Converse AO, Optekar JD. 1993. A synergistic kinetics model for enzymatic cellulose hydrolysis compared to degree-of-synergism experimental results. Biotechnology and Bioengineering 42(1):145-148.
Corgié SC, Smith HM, Walker LP. 2011. Enzymatic transformations of cellulose assessed by quantitative high-throughput fourier transform infrared spectroscopy (QHT-FTIR). Biotechnology and Bioengineering 108(7):1509-1520.
Corner CV. 2003. A size-exclusion chromatography system for observing the transport

and weak binding of Thermobifida Fusca catalytic domains: Experiemntal and theoretical investigation. Ph.D. Dissertation, Cornell University, Ithaca.
Cosgrove DJ. 2005. Growth of the plant cell wall. Nature Reviews Molecular Cell Biology 6(11):850-861.
Coughlan M. 1985. The properties of fungal and bacterial cellulases with comment on their production and application. Biotechnology and Genetic Engineering Reviews 3:39-109.
Dasari R, Eric Berson R. 2007. The effect of particle size on hydrolysis reaction rates and rheological properties in cellulosic slurries. Applied Biochemistry and Biotechnology 137-140(1):289-299.
Davies G, Henrissat B. 1995. Structures and mechanisms of glycosyl hydrolases. Structure 3(9):853-859.
Dekker RFH. 1986. Kinetic, inhibition, and stability properties of a commercial β-D-glucosidase (cellobiase) preparation from aspergillus niger and its suitability in the hydrolysis of lignocellulose. Biotechnology and Bioengineering 28(9):1438-1442.
Del Rio LF, Chandra RP, Saddler JN. 2011. The effects of increasing swelling and anionic charges on the enzymatic hydrolysis of organosolv-pretreated softwoods at low enzyme loadings. Biotechnology and Bioengineering 108(7):1549-1558.
Delgenès JP, Penaud V, Moletta R. 2002. Pretreatments for the Enhancement of Anaerobic Digestion of Solid Wastes. In: Mata-Alvarez J, editor. Biomethanization of the organic fraction of municipal solid waste. Cornwall, U.K.: IWA.
Dimarogona M, Topakas E, Olsson L, Christakopoulos P. 2012. Lignin boosts the cellulase performance of a GH-61 enzyme from Sporotrichum thermophile. Bioresource Technology 110(0):480-487.
Divne C, Ståhlberg J, Teeri TT, Jones TA. 1998. High-resolution crystal structures reveal how a cellulose chain is bound in the 50 Å long tunnel of cellobiohydrolase I from Trichoderma reesei. Journal of Molecular Biology 275(2):309-325.
Dmitri IS, Michel HJK. 2003. Small-angle scattering studies of biological macromolecules in solution. Reports on Progress in Physics 66(10):1735.
DOE. 2006. Biomass feedstock composition and property database.
Donohoe BS, Decker SR, Tucker MP, Himmel ME, Vinzant TB. 2008. Visualizing lignin coalescence and migration through maize cell walls following thermochemical pretreatment. Biotechnology and Bioengineering 101(5):913-925.
Donohoe BS, Selig MJ, Viamajala S, Vinzant TB, Adney WS, Himmel ME. 2009. Detecting cellulase penetration into corn stover cell walls by immuno-electron microscopy. Biotechnology and Bioengineering 103(3):480-489.
Duff SJB, Murray WD. 1996. Bioconversion of forest products industry waste cellulosics to fuel ethanol: A review. Bioresource Technology 55(1):1-33.

Elshafei AM, Vega JL, Klasson KT, Clausen EC, Gaddy JL. 1991. The saccharification of corn stover by cellulase from Penicillium funiculosum. Bioresource Technology 35(1):73-80.

Eriksson T, Karlsson J, Tjerneld F. 2002. A model explaining declining rate in hydrolysis of lignocellulose substrates with cellobiohydrolase I (Cel7A) and endoglucanase I (Cel7B) of Trichoderma reesei. Applied Biochemistry and Biotechnology 101(1):41-60.

Esquerre-Tugaye M-T, Boudart G, Dumas B. 2000. Cell wall degrading enzymes, inhibitory proteins, and oligosaccharides participate in the molecular dialogue between plants and pathogens. Plant Physiology and Biochemistry 38:157-163.

Esteghlalian AR, Bilodeau M, Mansfield SD, Saddler JN. 2001. Do enzymatic hydrolyzability and simons' stain reflect the changes in the accessibility of lignocellulosic substrates to cellulase enzymes? Biotechnology Progress 17(6):1049-1054.

Fan LT, Lee Y-H, Beardmore DH. 1980. Mechanism of the enzymatic hydrolysis of cellulose: Effects of major structural features of cellulose on enzymatic hydrolysis. Biotechnology and Bioengineering 22(1):177-199.

Fan LT, Lee YH, Beardmore DR. 1981. The influence of major structural features of cellulose on rate of enzymatic hydrolysis. Biotechnology and Bioengineering 23(2):419-424.

Ferchak JD, Pye EK. 1983. Effect of cellobiose, glucose, ethanol, and metal ions on the cellulase enzyme complex of Thermomonospora fusca. Biotechnology and Bioengineering 25(12):2865-2872.

Focher B, Marzetti A, Cattaneo M, Beltrame PL, Carniti P. 1981. Effects of structural features of cotton cellulose on enzymatic hydrolysis. Journal of Applied Polymer Science 26(6):1989-1999.

Forsberg Z, Vaaje-Kolstad G, Westereng B, Bunæs AC, Stenstrøm Y, MacKenzie A, Sørlie M, Horn SJ, Eijsink VGH. 2011. Cleavage of cellulose by a CBM33 protein. Protein Science 20(9):1479-1483.

Gallezot P. 2012. Conversion of biomass to selected chemical products. Chemical Society Reviews.

Gama FM, Teixeira JA, Mota M. 1994. Cellulose morphology and enzymatic reactivity: A modified solute exclusion technique. Biotechnology and Bioengineering 43(5):381-387.

Gardner PT, Wood TJ, Chesson A, Stuchbury T. 1999. Effect of degradation on the porosity and surface area of forage cell walls of differing lignin content. Journal of the Science of Food and Agriculture 79(1):11-18.

Gilbert HJ. 2010. The biochemistry and structural biology of plant cell wall deconstruction. Plant Physiology 153(2):444-455.

Gilkes NR, Warren RA, Miller RC, Kilburn DG. 1988. Precise excision of the cellulose

binding domains from two Cellulomonas fimi cellulases by a homologous protease and the effect on catalysis. Journal of Biological Chemistry 263(21):10401-10407.
Gong CS, Cao NJ, Du J, Tsao GT. 1999. Ethanol production from renewable resources. Adv Biochem Eng Biotechnol 65:207-41.
Grethlein HE. 1985. The effect of pore size distribution on the rate of enzymatic hydrolysis of cellulosic substrates. Nat Biotech 3(2):155-160.
Grethlein HE, Allen DC, Converse AO. 1984. A comparative study of the enzymatic hydrolysis of acid-pretreated white pine and mixed hardwood. Biotechnology and Bioengineering 26(12):1498-1505.
Grimson MJ, Haigler CH, Blanton RL. 1996. Cellulose microfibrils, cell motility, and plasma membrane protein organization change in parallel during culmination in Dictyostelium discoideum. Journal of Cell Science 109:3079-3087.
Gusakov AV, Sinitsyn AP, Salanovich TN, Bukhtojarov FE, Markov AV, Ustinov BB, Zeijl Cv, Punt P, Burlingame R. 2005. Purification, cloning and characterisation of two forms of thermostable and highly active cellobiohydrolase I (Cel7A) produced by the industrial strain of *Chrysosporium lucknowense*. Enzyme and Microbial Technology 36(1):57-69.
Hall M, Bansal P, Lee JH, Realff MJ, Bommarius AS. 2010. Cellulose crystallinity - a key predictor of the enzymatic hydrolysis rate. FEBS Journal 277(6):1571-1582.
Harriott P. 2002. Chemical reactor design. Marcel Dekker:142-143.
Harris PV, Welner D, McFarland KC, Re E, Navarro Poulsen J-C, Brown K, Salbo R, Ding H, Vlasenko E, Merino S and others. 2010. Stimulation of Lignocellulosic Biomass Hydrolysis by Proteins of Glycoside Hydrolase Family 61: Structure and Function of a Large, Enigmatic Family. Biochemistry 49(15):3305-3316.
Hatfield R, Vermerris W. 2001. Lignin formation in plants. the dilemma of linkage specificity. Plant Physiology 126(4):1351-1357.
Hayashi N, Sugiyama J, Okano T, Ishihara M. 1997. Selective degradation of the cellulose Ia component in Cladophora cellulose with Trichoderma viride cellulase. Carbnhydrate research 305(1):109-116.
Hendriks ATWM, Zeeman G. 2009. Pretreatments to enhance the digestibility of lignocellulosic biomass. Bioresource Technology 100(1):10-18.
Henrissat B, Driguez H, Viet C, Schulein M. 1985. Synergism of Cellulases from Trichoderma reesei in the Degradation of Cellulose. Nat Biotech 3(8):722-726.
Herr D. 1980. Conversion of cellulose to glucose with cellulase of Trichoderma viride ITCC-1433. Biotechnology and Bioengineering 22(8):1601-1612.
Hill CAS, Forster SC, Farahani MRM, Hale MDC, Ormondroyd GA, Williams GR. 2005. An investigation of cell wall micropore blocking as a possible mechanism for the decay resistance of anhydride modified wood. International Biodeterioration & Biodegradation 55(1):69-76.

Himmel ME, Ding S-Y, Johnson DK, Adney WS, Nimlos MR, Brady JW, Foust TD. 2007. Biomass recalcitrance: engineering plants and enzymes for biofuels production. Science 315(5813):804-807.

Holtzapple M, Cognata M, Shu Y, Hendrickson C. 1990. Inhibition of Trichoderma reesei cellulase by sugars and solvents. Biotechnology and Bioengineering 36(3):275-287.

Hong J, Ye X, Zhang YHP. 2007. Quantitative determination of cellulose accessibility to cellulase based on adsorption of a nonhydrolytic fusion protein containing CBM and GFP with Its applications. Langmuir 23(25):12535-12540.

Hoppe W. 1974. Towards three-dimensional "electron microscopy" at atomic resolution. Naturwissenschaften 61(6):239-249.

Hoshino E, Shiroishi M, Amano Y, Nomura M, Kanda T. 1997. Synergistic actions of exo-type cellulases in the hydrolysis of cellulose with different crystallinities. Journal of Fermentation and Bioengineering 84(4):300-306.

Hsu T-A, Himmel M, Schell D, Farmer J, Berggren M. 1996. Design and initial operation of a high-solids, pilot-scale reactor for dilute-acid pretreatment of lignocellulosic biomass. Applied Biochemistry and Biotechnology 57-58(1):3-18.

Hu G, Cateto C, Pu Y, Samuel R, Ragauskas AJ. 2011. Structural Characterization of Switchgrass Lignin after Ethanol Organosolv Pretreatment. Energy & Fuels.

Huang R, Su R, Qi W, He Z. 2010. Understanding the key factors for enzymatic conversion of pretreated lignocellulose by partial least square analysis. Biotechnology Progress 26(2):384-392.

Huber GW, Chheda JN, Barrett CJ, Dumesic JA. 2005. Production of liquid alkanes by aqueous-phase processing of biomass-derived carbohydrates. Science 308(5727):1446-1450.

Hui L, Liu Z, Ni Y. 2009. Characterization of high-yield pulp (HYP) by the solute exclusion technique. Bioresource Technology 100(24):6630-6634.

Igarashi K, Koivula A, Wada M, Kimura S, PenttilÃ¤ M, Samejima M. 2009. High speed atomic force microscopy visualizes processive movement of Trichoderma reesei cellobiohydrolase I on crystalline cellulose. Journal of Biological Chemistry 284(52):36186-36190.

Ikuta Y, Karita S, Kitago Y, Watanabe N, Hirata F. 2008. A water molecule identified as a substrate of enzymatic hydrolysis of cellulose: A statistical-mechanics study. Chemical Physics Letters 465(4–6):279-284.

Irwin DC, Spezio M, Walker LP, Wilson DB. 1993. Activity studies of eight purified cellulases: Specificity, synergism, and binding domain effects. Biotechnol Bioeng 42(8):1002-13.

Ishizawa C, Jeoh T, Adney W, Himmel M, Johnson D, Davis M. 2009. Can delignification decrease cellulose digestibility in acid pretreated corn stover? Cellulose 16(4):677-686.

Ishizawa CI, Davis MF, Schell DF, Johnson DK. 2007. Porosity and its effect on the digestibility of dilute sulfuric acid pretreated corn stover. Journal of Agricultural and Food Chemistry 55(7):2575-2581.

Jackson CL, McKenna GB. 1990. The melting behavior of organic materials confined in porous solids The Journal of Chemical Physics 93(12):9002-9011.

Jarvis M. 2003. Chemistry: Cellulose stacks up. Nature 426(6967):611-612.

Jeoh T, Ishizawa CI, Davis MF, Himmel ME, Adney WS, Johnson DK. 2007. Cellulase digestibility of pretreated biomass is limited by cellulose accessibility. Biotechnology and Bioengineering 98(1):112-122.

Jeoh T, Wilson DB, Walker LP. 2002a. Cooperative and competitive binding in synergistic mixtures of *Thermobifida fusca* Cel5A, Cel6B and Cel9A. Biotechnology Progress 18(4):760-769.

Jeoh T, Wilson DB, Walker LP. 2002b. Cooperative and Competitive Binding in Synergistic Mixtures of Thermobifida fuscaCellulases Cel5A, Cel6B, and Cel9A. Biotechnology Progress 18(4):760-769.

Jeoh T, Wilson DB, Walker LP. 2006. Effect of cellulase mole fraction and cellulose recalcitrance on synergism in cellulose hydrolysis and binding. Biotechnol Prog 22(1):270-7.

Jervis EJ, Haynes CA, Kilburn DG. 1997. Surface diffusion of cellulases and their isolated binding domains on cellulose. Journal of Biological Chemistry 272(38):24016-24023.

Jung H, Wilson DB, Walker LP. 2002a. Binding mechanisms for Thermobifida fusca Cel5A, Cel6B, and Cel48A cellulose-binding modules on bacterial microcrystalline cellulose. Biotechnology and Bioengineering 80(4):380-392.

Jung H, Wilson DB, Walker LP. 2002b. Binding of Thermobifida fusca CDCel5A, CDCel6B and CDCel48A to easily hydrolysable and recalcitrant cellulose fractions on BMCC. Enzyme and Microbial Technology 31(7):941-948.

Jung H, Wilson DB, Walker LP. 2003. Binding and reversibility of Thermobifida fusca Cel5A, Cel6B, and Cel48A and their respective catalytic domains to bacterial microcrystalline cellulose. Biotechnology and Bioengineering 84(2):151-159.

Karkehabadi S, HANSSON H, KIM S, PIENS K, MITCHINSON C, SANDGREN M. 2008. The First Structure of a Glycoside Hydrolase Family 61 Member, Cel61 B from Hypocrea jecorina, at 1.6 A Resolution. Kidlington, ROYAUME-UNI: Elsevier. 11 p.

Karlsson J, Saloheimo M, Siika-aho M, Tenkanen M, Penttilä M, Tjerneld F. 2001. Homologous expression and characterization of Cel61A (EG IV) of Trichoderma reesei. European Journal of Biochemistry 268(24):6498-6507.

Kawakubo T, Karita S, Araki Y, Watanabe S, Oyadomari M, Takada R, Tanaka F, Abe K, Watanabe T, Honda Y and others. 2010. Analysis of exposed cellulose surfaces in pretreated wood biomass using carbohydrate-binding module (CBM)–cyan

fluorescent protein (CFP). Biotechnology and Bioengineering 105(3):499-508.
Kim ES, Lee HJ, Bang W-G, Choi I-G, Kim KH. 2009. Functional characterization of a bacterial expansin from Bacillus subtilis for enhanced enzymatic hydrolysis of cellulose. Biotechnology and Bioengineering 102(5):1342-1353.
Kim SB, Lee YY. 2002. Diffusion of sulfuric acid within lignocellulosic biomass particles and its impact on dilute-acid pretreatment. Bioresource Technology 83(2):165-171.
King BC, Donnelly MK, Bergstrom GC, Walker LP, Gibson DM. 2009. An optimized microplate assay system for quantitative evaluation of plant cell wall-degrading enzyme activity of fungal culture extracts. Biotechnology and Bioengineering 102(4):1033-1044.
Kleman-Leyer K, Gilkes N, Miller Jr R, Kirk T. 1994. Changes in the molecular-size distribution of insoluble celluloses by the action of recombinant Cellulomonas fimi cellulases. Biochemistry 302:463-469.
Kleman-Leyer KM, Siika-Aho M, Teeri TT, Kirk TK. 1996. The Cellulases Endoglucanase I and Cellobiohydrolase II of Trichoderma reesei Act Synergistically To Solubilize Native Cotton Cellulose but Not To Decrease Its Molecular Size. Applied and environmental microbiology 62(8):2883-7.
Koo B-W, Min B-C, Gwak K-S, Lee S-M, Choi J-W, Yeo H, Choi I-G. 2012. Structural changes in lignin during organosolv pretreatment of Liriodendron tulipifera and the effect on enzymatic hydrolysis. Biomass and Bioenergy 42(0):24-32.
Koshland DEJ. 1953. Stereochemistry and the mechanism of enzymatic reactions. Biological Reviews 28(4):416-436.
Kostylev M, Wilson D. 2011. Synergistic interactions in cellulose hydrolysis. Biofuels 3(1):61-70.
Kramer EM, Frazer NL, Baskin TI. 2007. Measurement of diffusion within the cell wall in living roots of Arabidopsis thaliana. Journal of Experimental Botany 58(11):3005-3015.
Kumar L, Arantes V, Chandra R, Saddler J. 2012. The lignin present in steam pretreated softwood binds enzymes and limits cellulose accessibility. Bioresource Technology 103(1):201-208.
Kumar R, Wyman CE. 2009. Access of cellulase to cellulose and lignin for poplar solids produced by leading pretreatment technologies. Biotechnology Progress 25(3):807-819.
Kunkes EL, Simonetti DA, West RM, Serrano-Ruiz JC, Gärtner CA, Dumesic JA. 2008. Catalytic conversion of biomass to monofunctional hydrocarbons and targeted liquid-fuel classes. Science 322(5900):417-421.
Lacayo CI, Malkin AJ, Holman H-YN, Chen L, Ding S-Y, Hwang MS, Thelen MP. 2010. Imaging cell wall architecture in single zinnia elegans tracheary elements. Plant Physiology 154(1):121-133.

Ladisch MR, Lin KW, Voloch M, Tsao GT. 1983. Process considerations in the enzymatic hydrolysis of biomass. Enzyme and Microbial Technology 5:82-102.
Langan P, Nishiyama Y, Chanzy H. 2001. X-ray Structure of Mercerized Cellulose II at 1 Å Resolution. Biomacromolecules 2(2):410-416.
Langston JA, Shaghasi T, Abbate E, Xu F, Vlasenko E, Sweeney MD. 2011. Oxidoreductive cellulose depolymerization by the enzymes cellobiose dehydrogenase and glycoside hydrolase 61. Applied and environmental microbiology 77(19):7007-7015.
Larsson AM, Bergfors T, Dultz E, Irwin DC, Roos A, Driguez H, Wilson DB, Jones TA. 2005. Crystal Structure of Thermobifida fusca Endoglucanase Cel6A in Complex with Substrate and Inhibitor: The Role of Tyrosine Y73 in Substrate Ring Distortion†,‡. Biochemistry 44(39):12915-12922.
Lawrence JR, Wolfaardt GM, Korber DR. 1994. Determination of diffusion coefficients in biofilms by confocal laser microscopy. Applied and Environmental Microbiology 60(4):1166-1173.
Lee D, Yu A, Wong K, Saddler J. 1994. Evaluation of the enzymatic susceptibility of cellulosic substrates using specific hydrolysis rates and enzyme adsorption. Applied Biochemistry and Biotechnology 45-46(1):407-415.
Lee SB, Shin HS, Ryu DDY, Mandels M. 1982. Adsorption of cellulase on cellulose: Effect of physicochemical properties of cellulose on adsorption and rate of hydrolysis. Biotechnology and Bioengineering 24(10):2137-2153.
Lennholm H, Larsson T, Iversen T. 1994. Determination of cellulose I[alpha] and I[beta] in lignocellulosic materials. Carbohydrate Research 261(1):119-131.
Li X, Beeson William T, Phillips Christopher M, Marletta Michael A, Cate Jamie HD. 2012. Structural Basis for Substrate Targeting and Catalysis by Fungal Polysaccharide Monooxygenases. Structure (London, England : 1993) 20(6):1051-1061.
Li Y, Irwin DC, Wilson DB. 2007. Processivity, Substrate Binding, and Mechanism of Cellulose Hydrolysis by Thermobifida fusca Cel9A. Appl. Environ. Microbiol. 73(10):3165-3172.
Lin JK, Ladisch MR, Patterson JA, Noller CH. 1987. Determining pore size distribution in wet cellulose by measuring solute exclusion using a differential refractometer. Biotechnology and Bioengineering 29(8):976-981.
Luo X, Zhu JY. 2011. Effects of drying-induced fiber hornification on enzymatic saccharification of lignocelluloses. Enzyme and Microbial Technology 48(1):92-99.
Luterbacher JS, Tester JW, Walker LP. 2010. High-solids biphasic CO2–H2O pretreatment of lignocellulosic biomass. Biotechnology and Bioengineering 107(3):451-460.
Lynd LR, Laser MS, Bransby D, Dale BE, Davison B, Hamilton R, Himmel M, Keller M,

McMillan JD, Sheehan J and others. 2008. How biotech can transform biofuels. Nat Biotech 26(2):169-172.

Lynd LR, Weimer PJ, van Zyl WH, Pretorius IS. 2002a. Microbial cellulose utilization: fundamentals and biotechnology. Microbiology and Molecular Biology Reviews 66(3):506-577.

Lynd LR, Weimer PJ, van Zyl WH, Pretorius IS. 2002b. Microbial Cellulose Utilization: Fundamentals and Biotechnology. Microbiol. Mol. Biol. Rev. 66(3):506-577.

MacKenzie LF, Sulzenbacher G, Divne C, Jones TA, Wöldike HF, Schülein M, Withers SG, Davies GJ. 1998. Crystal structure of the family 7 endoglucanase I (Cel7B) from Humicola insolens at 2.2 A resolution and identification of the catalytic nucleophile by trapping of the covalent glycosyl-enzyme intermediate. Biochem. J. 335(2):409-416.

Mandels M, Kostick J, Parizek R. 1971. The use of adsorbed cellulase in the continuous conversion of cellulose to glucose. Journal of Polymer Science C36:445-459.

Mani S, Tabil LG, Sokhansanj S. 2006. Effects of compressive force, particle size and moisture content on mechanical properties of biomass pellets from grasses. Biomass and Bioenergy 30(7):648-654.

Mansfield SD, Mooney C, Saddler JN. 1999. Substrate and enzyme characteristics that limit cellulose hydrolysis. Biotechnology Progress 15(5):804-816.

McCANN MC, Wells B, Roberts K. 1990. Direct visualization of cross-links in the primary plant cell wall. Journal of Cell Science 96(2):323-334.

McLean BW, Boraston AB, Brouwer D, Sanaie N, Fyfe CA, Warren RAJ, Kilburn DG, Haynes CA. 2002. Carbohydrate-binding Modules Recognize Fine Substructures of Cellulose. Journal of Biological Chemistry 277(52):50245-50254.

McLean BW, Bray MR, Boraston AB, Gilkes NR, Haynes CA, Kilburn DG. 2000. Analysis of binding of the family 2a carbohydrate-binding module from Cellulomonas fimi xylanase 10A to cellulose: specificity and identification of functionally important amino acid residues. Protein Engineering 13(11):801-809.

Mendgen K, Hahn M, Deising H. 1996. Morphogenesis and mechanisms of penetration by plant pathogenic fungi. Annual Review of Phytopathology 34:367-386.

Mercado JA, Matas AJ, Heredia A, Valpuesta V, Quesada MA. 2004. Changes in the water binding characteristics of the cell walls from transgenic Nicotiana tabacum leaves with enhanced levels of peroxidase activity. Physiologia Plantarum 122(4):504-512.

Mooney CA, Mansfield SD, Beatson RP, Saddler JN. 1999. The effect of fiber characteristics on hydrolysis and cellulase accessibility to softwood substrates. Enzyme and Microbial Technology 25(8–9):644-650.

Mooney CA, Mansfield SD, Touhy MG, Saddler JN. 1998. The effect of initial pore volume and lignin content on the enzymatic hydrolysis of softwoods. Bioresource Technology 64(2):113-119.

Moran-Mirabal JM, Bolewski JC, Walker LP. 2011. Reversibility and binding kinetics of Thermobifida fusca cellulases studied through fluorescence recovery after photobleaching microscopy. Biophysical Chemistry 155(1):20-28.

Moran-Mirabal JM, Corgie SC, Bolewski JC, Smith HM, Cipriany BR, Craighead HG, Walker LP. 2009. Labeling and purification of cellulose-binding proteins for high resolution fluorescence applications. Analytical Chemistry 81(19):7981-7987.

Moran-Mirabal JM, Santhanam N, Corgie SC, Craighead HG, Walker LP. 2008. Immobilization of cellulose fibrils on solid substrates for cellulase-binding studies through quantitative fluorescence microscopy. Biotechnology and Bioengineering 101(6):1129-1141.

Munoz IG, Mowbray SL, Stahlberg J. 2003. The catalytic module of Cel7D from Phanerochaete chrysosporium as a chiral selector: structural studies of its complex with the beta blocker (R)-propranolol. Acta Crystallographica Section D 59(4):637-643.

Murray WD. 1987. Effects of cellobiose and glucose on cellulose hydrolysis by both growing and resting cells of Bacteroides cellulosolvens. Biotechnology and Bioengineering 29(9):1151-1154.

Nakashima J, Mizuno T, Takabe K, Fujita M, Saiki H. 1997. Direct visualization of lignifying secondary wall thickenings in zinnia elegans cells in culture. Plant and Cell Physiology 38(7):818-827.

Negro M, Manzanares P, Ballesteros I, Oliva J, Cabañas A, Ballesteros M. 2003. Hydrothermal pretreatment conditions to enhance ethanol production from poplar biomass. Applied Biochemistry and Biotechnology 105(1):87-100.

Neuman RP, Walker LP. 1992a. Solute exclusion from cellulose in packed columns: Experimental investigation and pore volume measurements. Biotechnology and Bioengineering 40(2):218-225.

Neuman RP, Walker LP. 1992b. Solute exclusion from cellulose in packed columns: Process modeling and analysis. Biotechnology and Bioengineering 40(2):226-234.

Nidetzky B, Claeyssens M. 1994. Specific quantification of trichoderma reesei cellulases in reconstituted mixtures and its application to cellulase–cellulose binding studies. Biotechnology and Bioengineering 44(8):961-966.

Nidetzky B, Steiner W, Hayn M, Claeyssens M. 1994. Cellulose hydrolysis by the cellulases from *Trichderma reesei*: a newmodel for synergistic interaction. Biochemical Journal 298(3):705-710.

O'Sullivan AC. 1997. Cellulose: the structure slowly unravels. Cellulose 4(3):173-207.

Ooshima H, Burns DS, Converse AO. 1990. Adsorption of cellulase from Trichoderma reesei on cellulose and lignacious residue in wood pretreated by dilute sulfuric acid with explosive decompression. Biotechnology and Bioengineering 36(5):446-452.

Ooshima H, Kurakake M, Kato J, Harano Y. 1991. Enzymatic activity of cellulase adsorbed on cellulose and its change during hydrolysis. Applied Biochemistry and Biotechnology 31(3):253-266.

Paës G, Chabbert B. 2011. Characterization of arabinoxylan/cellulose nanocrystals gels to investigate fluorescent probes mobility in bioinspired models of plant secondary cell wall. Biomacromolecules.

Palmqvist E, Hahn-Hagerdal B. 2000. Fermentation of lignocellulosic hydrolysates. I: inhibition and detoxification. Bioresource Technology 74(1):17-24.

Paper JM, Scott-Craig JS, Adhikari ND, Cuomo CA, Walton JD. 2007. Comparative proteomics of extracellular proteins *in vitro* and *in planta* from the pathogenic fungus *Fusarium graminearum*. Proteomics 7:3171-3183.

Park S, Baker J, Himmel M, Parilla P, Johnson D. 2010. Cellulose crystallinity index: measurement techniques and their impact on interpreting cellulase performance. Biotechnology for Biofuels 3(1):10.

Park S, Venditti RA, Abrecht DG, Jameel H, Pawlak JJ, Lee JM. 2007. Surface and pore structure modification of cellulose fibers through cellulase treatment. Journal of Applied Polymer Science 103(6):3833-3839.

Pavlostathis SG, Gossett JM. 1985. Modeling Alkali Consumption and Digestibility Improvement from Alkaline Treatment of Wheat Straw. Biotechnology and Bioengineering 27(3):345-354.

Phalip V, Delalande F, Carapito C, Goubet F, Hatsch D, Leize-Wagner E, Dupree P, Dorsselaer A, Jeltsch J-M. 2005. Diversity of the exoproteome of *Fusarium graminearum* grown on plant cell wall. Current Genetics 48:366-379.

Phillips CM, Beeson WT, Cate JH, Marletta MA. 2011. Cellobiose Dehydrogenase and a Copper-Dependent Polysaccharide Monooxygenase Potentiate Cellulose Degradation by Neurospora crassa. ACS Chemical Biology 6(12):1399-1406.

Piccolo C, Wiman M, Bezzo F, Lidén G. 2010. Enzyme adsorption on SO2 catalyzed steam-pretreated wheat and spruce material. Enzyme and Microbial Technology 46(3–4):159-169.

Pingali SV, Urban VS, Heller WT, McGaughey J, O'Neill H, Foston M, Myles DA, Ragauskas A, Evans BR. 2010. Breakdown of cell wall nanostructure in dilute acid pretreated biomass. Biomacromolecules 11(9):2329-2335.

Proseus TE, Boyer JS. 2005. Turgor pressure moves polysaccharides into growing cell walls of chara corallina. Annals of Botany 95(6):967-979.

Quinlan RJ, Sweeney MD, Lo Leggio L, Otten H, Poulsen J-CN, Johansen KS, Krogh KBRM, Jørgensen CI, Tovborg M, Anthonsen A and others. 2011. Insights into the oxidative degradation of cellulose by a copper metalloenzyme that exploits biomass components. Proceedings of the National Academy of Sciences.

Riedel K, Ritter J, Bronnenmeier K. 1997. Synergistic interaction of the Clostridium stercorarium cellulases Avicelase I (CelZ) and Avicelase II (CelY) in the

degradation of microcrystalline cellulose. FEMS Microbiology Letters 147(2):239-244.
Rivers DB, Emert GH. 1987. Lignocellulose pretreatment: A comparison of wet and dry ball attrition. Biotechnology Letters 9(5):365-368.
Rivers DB, Emert GH. 1988. Factors affecting the enzymatic hydrolysis of bagasse and rice straw. Biological Wastes 26(2):85-95.
Rollin JA, Zhu Z, Sathitsuksanoh N, Zhang YHP. 2011. Increasing cellulose accessibility is more important than removing lignin: A comparison of cellulose solvent-based lignocellulose fractionation and soaking in aqueous ammonia. Biotechnology and Bioengineering 108(1):22-30.
Rouquerol J, Avnir D, Everett DH, Fairbridge C, Haynes M, Pernicone N, Ramsay JDF, Sing KSW, Unger KK. 1994. Guidelines for the Characterization of Porous Solids. In: J. Rouquerol FR-RKSWS, Unger KK, editors. Studies in Surface Science and Catalysis: Elsevier. p 1-9.
Ryu DDY, Kim C, Mandels M. 1984. Competitive adsorption of cellulase components and its significance in a synergistic mechanism. Biotechnology and Bioengineering 26(5):488-496.
Ryu DDY, Lee SB, Tassinari T, Macy C. 1982. Effect of compression milling on cellulose structure and on enzymatic hydrolysis kinetics. Biotechnology and Bioengineering 24(5):1047-1067.
Sampedro J, Cosgrove D. 2005. The expansin superfamily. Genome Biology 6(12):242.
San K-Y, Stephanopoulos G. 1983. Optimal control policy for substrate inhibited kinetics with enzyme deactivation in an isothermal CSTR. AIChE Journal 29(3):417-424.
Santhanam N. 2009. Investigating the enzymatic hydrolysis of crystalline cellulose using fluorescence based assays - implications of synergism, binding and product inhibition: Cornell University.
Santhanam N, Walker LP. 2008. A high throughput assay to measure cellulose binding and synergism in ternary mixtures. Biological Engineering 1(1):1-19.
Saxena IM, Brown RMJ. 2005. Cellulose biosynthesis: current views and evolving concepts. Ann Bot 96(1):9-21.
Seksek O, Biwersi J, Verkman AS. 1997. Translational diffusion of macromolecule-sized solutes in cytoplasm and nucleus. The Journal of Cell Biology 138(1):131-142.
Shoemaker S, Watt K, Tsitovsky G, Cox R. 1983. Characterization and Properties of Cellulases Purified from Trichoderma Reesei Strain L27. Nat Biotech 1(8):687-690.
Shoseyov O, Shani Z, Levy I. 2006. Carbohydrate binding modules: biochemical properties and novel applications. Microbiology and Molecular Biology Reviews 70(2):283-295.
Singh S, Simmons BA, Vogel KP. 2009. Visualization of biomass solubilization and cellulose regeneration during ionic liquid pretreatment of switchgrass.

Biotechnology and Bioengineering 104(1):68-75.
Sinitsyn A, Gusakov A, Vlasenko E. 1991. Effect of structural and physico-chemical features of cellulosic substrates on the efficiency of enzymatic hydrolysis. Applied Biochemistry and Biotechnology 30(1):43-59.
Snow P, O'Dea K. 1981. Factors affecting the rate of hydrolysis of starch in food. The American Journal of Clinical Nutrition 34(12):2721-7.
Somerville C, Bauer S, Brininstool G, Facette M, Hamann T, Milne J, Osborne E, Paredez A, Persson S, Raab T and others. 2004. Toward a systems approach to understanding plant cell walls. Science 306(5705):2206-2211.
Soumpasis DM. 1983. Theoretical analysis of fluorescence photobleaching recovery experiments. Biophysical Journal 41(1):95-97.
Sprague BL, McNally JG. 2005. FRAP analysis of binding: proper and fitting. Trends in Cell Biology 15(2):84-91.
Sprague BL, Pego RL, Stavreva DA, McNally JG. 2004. Analysis of Binding Reactions by Fluorescence Recovery after Photobleaching. Biophysical Journal 86(6):3473-3495.
Srebotnik E, Messner K, Foisner R. 1988. Penetrability of white rot-degraded pine wood by the lignin peroxidase of phanerochaete chrysosporium. Applied and environmental microbiology 54(11):2608-14.
Srisodsuk M, Kleman-Leyer K, Keränen S, Kirk TK, Teeri TT. 1998. Modes of action on cotton and bacterial cellulose of a homologous endoglucanase-exoglucanase pair from Trichoderma reesei. European Journal of Biochemistry 251(3):885-892.
Srisodsuk M, Reinikainen T, Penttilä M, Teeri TT. 1993. Role of the interdomain linker peptide of Trichoderma reesei cellobiohydrolase I in its interaction with crystalline cellulose. Journal of Biological Chemistry 268(28):20756-61.
Stahlberg J, Johansson G, Pettersson G. 1991. A new model for enzymatic hydrolysis of cellulose based on the two-domain structure of cellobiohydrolase I. Nat Biotech 9(3):286-290.
Stålbrand H, Mansfield SD, Saddler JN, Kilburn DG, Warren RAJ, Gilkes NR. 1998. Analysis of Molecular Size Distributions of Cellulose Molecules during Hydrolysis of Cellulose by Recombinant Cellulomonas fimiβ-1,4-Glucanases. Applied and environmental microbiology 64(7):2374-2379.
Stone JE, Scallan AM, Donefer E, Ahlgren E. 1969. Digestibility as a simple function of a molecule of similar size to a cellulase enzyme. Cellulases and Their Applications: AMERICAN CHEMICAL SOCIETY. p 219-241.
Sun C. 2005. True density of microcrystalline cellulose. Journal of Pharmaceutical Sciences 94(10):2132-2134.
Sun Y, Cheng J. 2002. Hydrolysis of lignocellulosic materials for ethanol production: a review. Bioresource Technology 83(1):1-11.
Takahashi R, Sato S, Sodesawa T, Nishida H. 2002. Effect of pore size on the liquid-

phase pore diffusion of nickel nitrate. Physical Chemistry Chemical Physics 4(15):3800-3805.
Tanaka M, Ikesaka M, Matsuno R, Converse AO. 1988. Effect of pore size in substrate and diffusion of enzyme on hydrolysis of cellulosic materials with cellulases. Biotechnology and Bioengineering 32(5):698-706.
Tanaka M, Matsuno R, Converse AO. 1990. n-butylamine and acid-steam explosion pretreatments of rice straw and hardwood: Effects on substrate structure and enzymatic hydrolysis. Enzyme and Microbial Technology 12(3):190-195.
Thompson DN, Chen H-C, Grethlein HE. 1992. Comparison of pretreatment methods on the basis of available surface area. Bioresource Technology 39(2):155-163.
Thygesen A, Oddershede J, Lilholt H, Thomsen AB, Ståhl K. 2005. On the determination of crystallinity and cellulose content in plant fibres. Cellulose 12(6):563-576.
Thygesen L, Hidayat B, Johansen K, Felby C. 2011. Role of supramolecular cellulose structures in enzymatic hydrolysis of plant cell walls. Journal of Industrial Microbiology & Biotechnology 38(8):975-983.
Tomme P, Heriban V, Claeyssens M. 1990. Adsorption of two cellobiohydrolases from<i>Trichoderma reesei</i> to Avicel: Evidence for “exo-exo” synergism and possible “loose complex” formation. Biotechnology Letters 12(7):525-530.
Tomme P, Tilbeurgh H, Pettersson G, Damme J, Vandekerckhove J, Knowles J, Teeri T, Claeyssens M. 1988. Studies of the cellulolytic system of *Trichoderma reesei* QM 9414. European Journal of Biochemistry 170(3):575-581.
Tomme P, Warren RA, Gilkes NR. 1995. Cellulose hydrolysis by bacteria and fungi. Advances in Microbial Physiology 37:2-81.
Tonukari NJ. 2003. Enzymes and fungal virulence. Journal of Applied Sciences & Environmental Management 7(1):5-8.
Topgaard D, Söderman O. 2001. Diffusion of water absorbed in cellulose fibers studied with 1H-NMR. Langmuir 17(9):2694-2702.
Torget R, Himmel ME, Grohmann K. 1991. Dilute sulfuric acid pretreatment of hardwood bark. Bioresource Technology 35(3):239-246.
Torquato S, Avellaneda M. 1991. Diffusion and reaction in heterogeneous media: Pore size distribution, relaxation times, and mean survival time The Journal of Chemical Physics 95(9):6477-6489.
Toth IK, Birch PRJ. 2005. Rotting softly and stealthily. Current Opinion in Plant Biology 8:424-429.
Tucker MP, Kim KH, Newman MM, Nguyen QA. 2003. Effects of temperature and moisture on dilute-acid steam explosion pretreatment of corn stover and cellulase enzyme digestibility. Applied Biochemistry and Biotechnology 105:165-177.
Vaaje-Kolstad G, Horn SJ, van Aalten DMF, Synstad B, Eijsink VGH. 2005a. The Non-catalytic Chitin-binding Protein CBP21 from Serratia marcescens Is Essential for

Chitin Degradation. Journal of Biological Chemistry 280(31):28492-28497.
Vaaje-Kolstad G, Houston DR, Riemen AHK, Eijsink VGH, van Aalten DMF. 2005b. Crystal Structure and Binding Properties of the Serratia marcescens Chitin-binding Protein CBP21. Journal of Biological Chemistry 280(12):11313-11319.
Vaaje-Kolstad G, Westereng B, Horn SJ, Liu Z, Zhai H, Sørlie M, Eijsink VGH. 2010. An Oxidative Enzyme Boosting the Enzymatic Conversion of Recalcitrant Polysaccharides. Science 330(6001):219-222.
Väljamäe P, Sild V, Pettersson G, Johansson G. 1998. The initial kinetics of hydrolysis by cellobiohydrolases I and II is consistent with a cellulose surface − erosion model. European Journal of Biochemistry 253(2):469-475.
Varrot A, Frandsen TP, von Ossowski I, Boyer V, Cottaz S, Driguez H, Schülein M, Davies GJ. 2003. Structural Basis for Ligand Binding and Processivity in Cellobiohydrolase Cel6A from Humicola insolens. Structure 11(7):855-864.
Viamajala S, Donohoe BS, Decker SR, Vinzant TB, Selig MJ, Himmel ME, Tucker MP. 2010. Heat and mass transport in processing of lignocellulosic biomass for fuels and chemicals. Sustainable Biotechnology. In: Singh OV, Harvey SP, editors: Springer Netherlands. p 1-18.
Viamajala S, Selig MJ, Vinzant TB, Tucker MP, Himmel ME, McMillan JD, Decker SR. 2006. Catalyst transport in corn stover internodes
Twenty-Seventh Symposium on Biotechnology for Fuels and Chemicals. In: McMillan JD, Adney WS, Mielenz JR, Klasson KT, editors: Humana Press. p 509-527.
Vidal B, Dien B, Ting K, Singh V. 2011. Influence of feedstock particle size on lignocellulose conversion—a review. Applied Biochemistry and Biotechnology 164(8):1405-1421.
Waharte F, Steenkeste K, Briandet R, Fontaine-Aupart M-P. 2010. Diffusion measurements inside biofilms by image-based fluorescence recovery after photobleaching (FRAP) analysis with a commercial confocal laser scanning microscope. Applied and Environmental Microbiology 76(17):5860-5869.
Walker LP, Belair CD, Wilson DB, Irwin DC. 1993. Engineering cellulase mixtures by varying the mole fraction of *Thermomonospora fusca* E5 and E3, *Trichoderma reesei* CBHI, and *Caldocellum saccharolyticum* beta-glucosidase. Biotechnology and Bioengineering 42:1019-1028.
Walker LP, Wilson DB. 1991. Enzymatic hydrolysis of cellulose: An overview. Bioresource Technology 36(1):3-14.
Walker LP, Wilson DB, Irvin DC, McQuire C, Price M. 1992. Fragmentation of cellulose by the major Thermomonospora fusca cellulases, Trichoderma reesei CBHI, and their mixtures. Biotechnology and Bioengineering 40(9):1019-1026.
Walker LP, Wilson DB, Irwin DC. 1990. Measuring fragmentation of cellulose by Thermomonospora fusca cellulase. Enzyme and Microbial Technology 12(5):378-386.

Walseth CS. 1952. The influence of the fine structure of cellulose on the action of cellulases. Tappi 35:233-236.
Walton JD. 1994. Deconstructing the plant cell wall. Plant Physiology 104:1113-1118.
Wang J, Dismer F, Hubbuch J, Ulbricht M. 2008. Detailed analysis of membrane adsorber pore structure and protein binding by advanced microscopy. Journal of Membrane Science 320(1-2):456-467.
Wang QQ, He Z, Zhu Z, Zhang YHP, Ni Y, Luo XL, Zhu JY. 2012. Evaluations of cellulose accessibilities of lignocelluloses by solute exclusion and protein adsorption techniques. Biotechnology and Bioengineering 109(2):381-389.
Warren RA. 1996. Microbial hydrolysis of polysaccharides. Annual Review of Microbiology 50:183-212.
Watson DL, Wilson DB, Walker LP. 2002. Synergism in binary mixtures of Thermobifida fusca cellulases Cel6B, Cel9A, and Cel5A on BMCC and Avicel. Appl Biochem Biotechnol 101(2):97-111.
Weimer PJ, Lopez-Guisa JM, French AD. 1990. Effect of cellulose fine structure on kinetics of its digestion by mixed ruminal microorganisms in vitro. Applied and Environmental Microbiology 56(8):2421-2429.
Weise U. 1998. Hornification : mechanisms and terminology. Helsinki, FINLANDE: Suomen paperi- ja puutavaralehti oy.
Wen Z, Liao W, Chen S. 2004. Hydrolysis of animal manure lignocellulosics for reducing sugar production. Bioresource Technology 91(1):31-39.
Wickholm K, Hult E-L, Larsson PT, Iversen T, Lennholm H. 2001. Quantification of cellulose forms in complex cellulose materials: a chemometric model. Cellulose 8(2):139-148.
Wilson D. 2012. Processive and nonprocessive cellulases for biofuel production—lessons from bacterial genomes and structural analysis. Applied Microbiology and Biotechnology 93(2):497-502.
Wilson DB. 2004. Studies of Thermobifida fusca plant cell wall degrading enzymes. The Chemical Record 4(2):72-82.
Wilson DB. 2008. Three microbial strategies for plant cell wall degradation. Ann NY Acad Sci 1125(1):289-297.
Wilson DB, Irwin DC. 1999. Genetics and properties of cellulases. Advances in Biochemical Engineering Biotechnology: Recent Progress in Bioconversion 65:1-21S.
Wiselogel AE, Agblevor FA, Johnson DK, Deutch S, Fennell JA, Sanderson MA. 1996. Compositional changes during storage of large round switchgrass bales. Bioresource Technology 56(1):103-109.
Wong KKY, Deverell KF, Mackie KL, Clark TA, Donaldson LA. 1988. The relationship between fiber-porosity and cellulose digestibility in steam-exploded Pinus radiata. Biotechnology and Bioengineering 31(5):447-456.

Wood TM, McCrae SI. 1979. Synergism between enzymes involved in the solubilization of native cellulose. In: Brown RD, Jurasek L, editors. Hydrolysis of Cellulose: Mechanisms of Enzymatic and Acid Catalysis. Washington, DC: American Chemical Society. p 181-209.

Wood TM, McCrae SI. 1986. The cellulase of Penicillium pinophilum. Synergism between enzyme components in solubilizing cellulose with special reference to the involvement of two immunologically distinct cellobiohydrolases. Biochem. J. 234(1):93-99.

Woodward J, Lima M, Lee NE. 1988a. The role of cellulase concentration in determining the degree of synergism in the hydrolysis of microcrystalline cellulose. Biochem. J. 255(3):895-899.

Woodward J, Lima M, Lee NE. 1988b. The role of cellulase concentration in determining the degree of synergism in the hydrolysis of microcrystalline cellulose. Biochemical Journal 255:895-899.

Wyman CE, Dale BE, Elander RT, Holtzapple M, Ladisch MR, Lee YY. 2005. Coordinated development of leading biomass pretreatment technologies. Bioresource Technology 96(18):1959-1966.

Xu G-Y, Ong E, Gilkes NR, Kilburn DG, Muhandiram DR, Harris-Brandts M, Carver JP, Kay LE, Harvey TS. 1995. Solution Structure of a Cellulose-Binding Domain from Cellulomonas fimi by Nuclear Magnetic Resonance Spectroscopy. Biochemistry 34(21):6993-7009.

Yang D, Moran-Mirabal JM, Parlange J-Y, Walker LP. 2013. Investigation of the porous structure of cellulosic substrates through confocal laser scanning microscopy. Biotechnology and Bioengineering:n/a-n/a.

Zeng M, Mosier NS, Huang C-P, Sherman DM, Ladisch MR. 2007. Microscopic examination of changes of plant cell structure in corn stover due to hot water pretreatment and enzymatic hydrolysis. Biotechnology and Bioengineering 97(2):265-278.

Zeng M, Ximenes E, Ladisch MR, Mosier NS, Vermerris W, Huang C-P, Sherman DM. 2012a. Tissue-specific biomass recalcitrance in corn stover pretreated with liquid hot-water: Enzymatic hydrolysis (part 1). Biotechnology and Bioengineering 109(2):390-397.

Zeng M, Ximenes E, Ladisch MR, Mosier NS, Vermerris W, Huang C-P, Sherman DM. 2012b. Tissue-specific biomass recalcitrance in corn stover pretreated with liquid hot-water: SEM imaging (part 2). Biotechnology and Bioengineering 109(2):398-404.

Zhang S, Wolfgang DE, Wilson DB. 1999. Substrate heterogeneity causes the nonlinear kinetics of insoluble cellulose hydrolysis. Biotechnology and Bioengineering 66(1):35-41.

Zhang Y-HP, Lynd LR. 2004. Toward an aggregate understanding of enzymatic

hydrolysis of cellulose: noncomplexed cellulase systems. Biotechnology and Bioengineering 88:797-824.

Zhang Y, Xu J-L, Xu H-J, Yuan Z-H, Guo Y. 2010. Cellulase deactivation based kinetic modeling of enzymatic hydrolysis of steam-exploded wheat straw. Bioresource Technology 101(21):8261-8266.

Zhang Z, Nadezhina E, Wilkinson KJ. 2011. Quantifying Diffusion in a Biofilm of Streptococcus mutans. Antimicrobial Agents and Chemotherapy 55(3):1075-1081.

Zhou W, Hao Z, Xu Y, Schüttler H-B. 2009. Cellulose hydrolysis in evolving substrate morphologies II: Numerical results and analysis. Biotechnology and Bioengineering 104(2):275-289.

Zhu JY, Wang GS, Pan XJ, Gleisner R. 2009a. Specific surface to evaluate the efficiencies of milling and pretreatment of wood for enzymatic saccharification. Chemical Engineering Science 64(3):474-485.

Zhu L, O'Dwyer JP, Chang VS, Granda CB, Holtzapple MT. 2008. Structural features affecting biomass enzymatic digestibility. Bioresource Technology 99(9):3817-3828.

Zhu P, Moran-Mirabal J, Luterbacher J, Walker L, Craighead H. 2011. Observing Thermobifida fusca cellulase binding to pretreated wood particles using time-lapse confocal laser scanning microscopy. Cellulose 18(3):749-758.

Zhu Z, Sathitsuksanoh N, Percival Zhang YH. 2009b. Direct quantitative determination of adsorbed cellulase on lignocellulosic biomass with its application to study cellulase desorption for potential recycling. Analyst 134(11):2267-2272.

Zhu Z, Sathitsuksanoh N, Vinzant T, Schell DJ, McMillan JD, Zhang YHP. 2009c. Comparative study of corn stover pretreated by dilute acid and cellulose solvent-based lignocellulose fractionation: Enzymatic hydrolysis, supramolecular structure, and substrate accessibility. Biotechnology and Bioengineering 103(4):715-724.

Zou J-y, Kleywegt GJ, Ståhlberg J, Driguez H, Nerinckx W, Claeyssens M, Koivula A, Teeri TT, Jones TA. 1999. Crystallographic evidence for substrate ring distortion and protein conformational changes during catalysis in cellobiohydrolase Ce16A from Trichoderma reesei. Structure 7(9):1035-1045.

3. INVESTIGATION OF THE POROUS STRUCTURE OF CELLULOSIC SUBSTRATE THROUGH CONFOCAL LASER SCANNING MICROSCOPY

3.1 Introduction

Despite the current uncertainty and challenges to the development of second generation biofuels and bioproducts, there remains considerable global interest in the biochemical conversion of biomass into fermentable sugars (Harris et al., 2013). Progress has been made in lowering the cost of biomass saccharification through process engineering and the innovative application of genomics, protein engineering and other molecular biology approaches (Gusakov et al., 2005; Irwin et al., 1993; Karlsson et al., 2001; Santhanam and Walker, 2008; Snow and O'Dea, 1981; Wilson, 2012). However, the saccharification of lignocellulosic biomass remains one of the most expensive steps in the production of advanced biofuels (Luterbacher et al., 2010; Lynd et al., 2008; Wang et al., 2012). This is primarily due to the cost associated with high enzyme loadings commonly required for efficient saccharification (Jeoh et al., 2002; Wilson, 2004). Thus, the successful commercialization of fuels derived from lignocellulosic biomass hinges on lowering the cost of the enzymes through a reduction of enzyme loadings or an increase in the activities of enzyme cocktails (Arantes and Saddler, 2011).

At the most fundamental level, saccharification occurs when cell wall degrading enzymes

(CWDEs) diffuse, bind to, and react on readily accessible cellulose fibrils (Chanzy et al., 1984; Langan et al., 2001). The available surface area for enzymatic hydrolysis and the ease of transport of the enzyme through the porous cellulosic structure are critical in assessing the activities of CWDEs. Grethlein obtained an excellent linear correlation between the surface area available to probes with molecular diameter of 51Å and the initial glucose yield for acid pretreated mixed hardwood (Grethlein, 1985; Grethlein et al., 1984). The transport of CWDEs to reactive cellulose surfaces area can be influenced by steric hindrance within the porous structure of cellulosic materials. This is especially relevant for accessibility to pores with dimensions comparable to those of CWDEs (micropores), where "traffic jams" can occur due to interactions between CWDEs and the micropore walls and due to collisions between CWDE molecules in crowded environments. Furthermore, these limitations are expected to play a major role in the ability of CWDEs to cooperate in the synergistic degradation of cell wall materials. Pore size and steric hindrance could act as a sieving mechanism that limits synergistic activities, since synergism can only occur when CWDEs with complementary activities occupy the same reaction space. Therefore, the hydrodynamic radius of CWDEs is a key factor in assessing their diffusion into the porous structure of biomass. Previous biomass accessibility studies often focused on the structure change of pretreated biomass in general, instead of the structure influence on CWDEs or equivalent size probes. For example, research using NMR showed a broken down and loosing cellulosic

ultrastructure for acid pretreated lignocellulosic biomass (Foston and Ragauskas., 2010). A semiquantitative Simons' stain method has been developed to estimate the porous structure and surface area (Chandra et al., 2008). However, the cellulose accessibility based on dye adsorption is different from those determined using enzymes because the molecular sizes of the dyes are often significantly smaller than those of enzymes. In addition, the process of teasing out diffusive mechanism strictly based on molecular diameter is complicated by the high binding affinity of CWDEs and dyes (Jeoh et al., 2007). A key goal of this research was to gain insight into the diffusion hindrance that CWDEs may encounter in the complex porous structure of cellulosic materials by visualizing the diffusion of non-binding molecular probes of different sizes into the pore space of cellulosic biomass.

Our effort to explore diffusive behavior strictly based on molecular diameter relies on the use of a high-resolution fluorescence microscopy platform, which has been used to visualize and measure the diffusion of non-binding probes in the porous structure of filter paper particles. In essence, this platform constitutes a micro-scale solute exclusion technique that employs confocal laser scanning microscopy (CLSM) to visualize and quantify the three dimensional concentration of fluorescently-labeled dextrans. Fluorescence microscopy in combination with high numerical aperture objectives and highly sensitive cameras has allowed high resolution imaging of enzyme-surface

interactions (Moran-Mirabal et al., 2011; Moran-Mirabal et al., 2009; Zhu et al., 2011). The approach presented in this manuscript provides high spatial and temporal resolution of the three dimensional distribution of fluorescence-labeled dextran probes inside biomass pore space. This distribution coupled with mathematical models is used to assess the influence of pore size distribution on steric hindrance and mass transport limitations.

3.2 Materials and Methods

Fluorescently-labeled dextrans with molecular weights ranging from 20kDa to 150kDa were used as probes to assess the porous structure of filter paper. The hydrodynamic radius of the Fluorescein isothiocyanate (FITC)-dextran probes were obtained from light scattering measurements by Zhu (Zhu, 2012). These probes have hydrodynamic radii that are comparable to the size of CWDEs and can provide insight into the diffusion hindrance and entrapment encountered as these enzymes hydrolyze cellulosic particles. Filter paper particles were lightly dried onto the bottom plate of a microfluidic chamber. The particles were incubated with dextran solution to allow the probes to diffuse into the pore structure over a period of 24 hours. This process was followed by flushing the chamber with phosphate buffer saline (PBS) to remove free dextran. The fluorescent intensity of remaining labeled dextran contained in cellulosic structures was monitored by CLSM. Two diffusion rate models were constructed to predict the pore-hindered diffusivities of the dextran probes and the pore size distribution.

3.2.1 Sample Preparation

Whatman #1 filter paper (GE Healthcare, Kent, UK) was hand cut and milled (IKA Wilmington, NC) with a 1 mm screen. The resulting biomass was sieved to obtain particles collected through 75 μm mesh screens (U.S. Standard 200 sieve, E. H Sargent and Co., Chicago, IL). Deionized water was added to form a stock containing 1 mg/ml milled filter paper. The filter paper stock was stored at 4 °C until use.

Commercially available FITC labeled dextran molecules with molecular weights ranging from 20 to 150 kDa (TdB consultancy, Uppsala, Sweden) were acquired and used as test probes in the diffusion studies. FITC- dextran solutions were prepared separately in 10 μM PBS buffer supplemented with 5 mM ascorbic acid to reduce dissolved oxygen content and decrease fluorophore photo-degradation. The solution was made the day before imaging and stored at 4 °C.

Forty millimeter round glass wafers (Bioptechs, Butler, PA) were cleaned through successive immersion in acetone, isopropanol (10 min each), 5 M sodium hydroxide (60 min), 5 M hydrochloric acid and deionized water baths (10 min each), followed by drying under nitrogen stream. Organic residues were removed by 5 min exposure to low power oxygen plasma (Harrick, Ithaca, NY) prior to filter paper immobilization.

3.2.2. Dextran diffusion imaging

Sixty microliters of the suspended filter paper stock were pipetted on the glass wafer and dried at 70 °C for 30 minutes. The glass wafer was used as the viewing window in a Focht Chamber System 2 (FCS2) temperature-controlled microfluidic chamber with a capacity of 1ml (Bioptechs, Butler, PA), as previously described (Luterbacher et al., 2012). Buffer and dextran solutions (2.5 μM) were perfused into the chamber using a syringe pump (Harvard Apparatus, Boston, MA). The filter paper immobilized on the glass wafer was then rehydrated and rinsed with MilliQ water to wash off any filter paper particles that were not strongly adhered (Figure 3.1A). To minimize non-specific adsorption of dextrans onto the chamber surface, the sample was incubated for 8 h with 5% bovine serum albumin (BSA) (Fisher Scientific, Pittsburgh, PA) and rinsed again with 40 ml of PBS buffer with 5 mM ascorbic acid. Then, the fluidic chamber was mounted on the confocal laser scanning microscope (CLSM), where temperature was held constant at 25°C.

Fluorescence images of the filter paper particles were taken using an Olympus Fluoview 1000 system equipped with a 60X/0.9NA UPLFLN objective. Auto fluorescence excited at 405 nm was used to identify the filter paper using a 430-470 emission filter (Olympus, Center Valley, PA). Figure 3.1B shows an axial projection of a typical autofluorescence

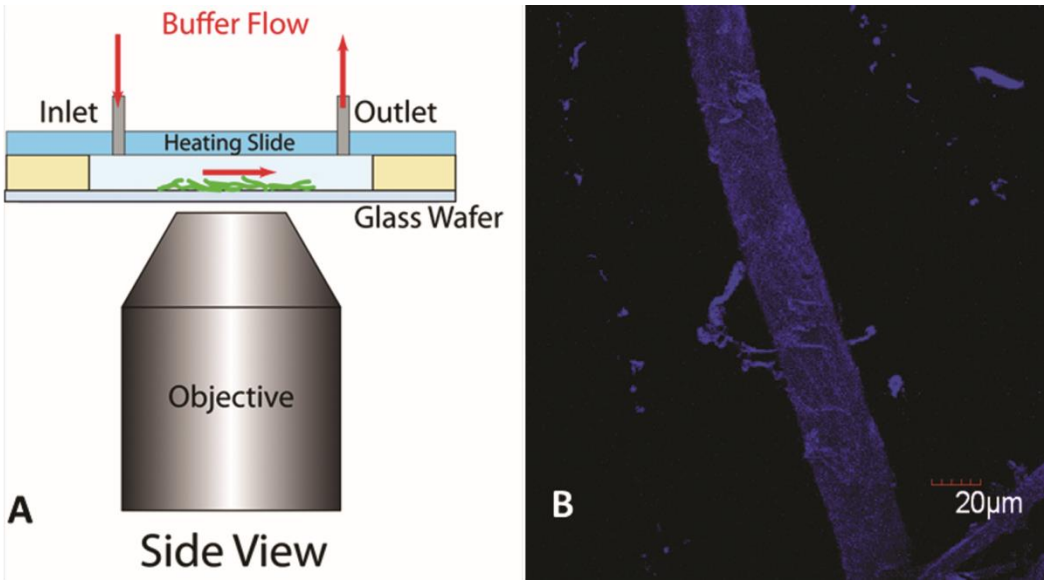

Figure 3.1. CLSM imaging system setup (A) and a typical reconstructed image of filter paper particle (B)

image obtained from a filter paper particle. After acquiring the reference image, 5 ml of 2.5 μM FITC-dextran solution in PBS buffer was incubated with the sample for the dextrans to diffuse into the accessible pores. After 24 h, the sample was washed with PBS buffer for 2 min at 4 ml/min to remove FITC-dextrans in the chamber, followed by a steady buffer flow at 1 ml/h to wash away FITC-dextran molecules as they diffused out of the filter paper particle. The filter paper particles and FITC-dextrans were imaged throughout this process using a 488 nm excitation laser, a dichroic mirror SDM-560, and a 505-525AF45 emission filter (Chroma Technology Corp., Rockingham, VT). Auto-fluorescence from the filter paper particle accounted for less than 0.5% of the initial FITC- dextran fluorescence intensity inside the particle and it was constant during the whole imaging process. Therefore, no adjustment was applied to correct the auto-fluorescence for FITC-dextran fluorescence. Individual areas of interest were located and imaging planes were selected to give a complete profile of the fluorescence intensity distribution inside the particle. Time-lapse experiments were run for 1000-1500 min, with 20-30 data points taken at evenly space over time. The 150kDa time-lapse experiment was stopped after 1000 min because of an air bubble interruption in the microfluidic chamber during imaging. The areas of interest were exposed to light only during image acquisition to minimize photobleaching. To assess the effect of photobleaching, control imaging experiments were run on FITC-dextran under the same conditions (i.e. same laser intensity and microscope settings) and showed no marked decrease in fluorescence

intensity as the experiment proceeded.

3.2.3. Image processing

Fluorescence images of the filter paper particles before dextran infusion were combined into a z-axis sum projection that was used as reference to define the profile of the particles. During this process, the intensity for each pixel within the z-stack of images was integrated to create a two-dimensional sum projection. The rest of the images from the time course experiments were combined along the z-axis in the same way and aligned to the reference image using a customized macro "BatchSUM&MAX" in Image J (NIH, Bethesda, Maryland). In addition, a two-dimensional maximum intensity projection image was created for each z-stack to identify the saturated pixels. The aligned images were analyzed by a custom Matlab script (The Mathworks, Natick, MA). Otsu's algorithm was applied in this Matlab program to separate signal from background (Otsu, 1979). This algorithm set a threshold to separate all pixels into two classes, signal (fluorescence from FITC-dextran) and background (areas devoid of FITC-dextran). Then, a background area was selected and a mask was generated representing the signal pixels. At the same time, saturated pixels were removed and the mean background was subtracted from the signal pixels. The corrected average intensities of the signal pixels, which reflected the amount of FITC-dextran inside the filter paper particle, were plotted against time elapsed after chamber flushing to show the fluorescence signal decay over

time.

3.2.4. Diffusion model development

Figure 3.2A shows a schematic diagram of a filter paper structure with a length scale of ~200μm and a height and width of ~20 μm. To reduce the mathematical complexity of the problem, the particle was modeled as infinitely long. Therefore, this problem could be simplified to a two-dimensional problem with FITC-dextran diffusing out from the boundary of the particle's cross section. The filter paper particle was taken as a rectangular cuboid with one of its six faces sitting on "pillars" (small filter paper residues), which stuck on the glass wafer (Figure 3.2B). This allows the assumption that all four boundaries in one cross section have similar diffusion behavior. This assumption reflects our experimental observations and simulates the practical scenario where biomass particles seldom attach seamlessly to the walls of the reactor (Figure 3.3).

Transient diffusion from a quarter of the rectangular cross section is a well-defined physical problem for which an analytical solution is available (Carslaw and Jaeger, 1959)**.** A slow buffer flow, 1 ml/h, was applied during imaging to keep the free dextran concentration in the chamber to negligible levels. The flow was also slow enough to avoid other mass transfer mechanisms (*i.e.,* convection) from obscuring diffusive processes. Therefore, diffusion in the quarter cross section of a rectangular particle can be

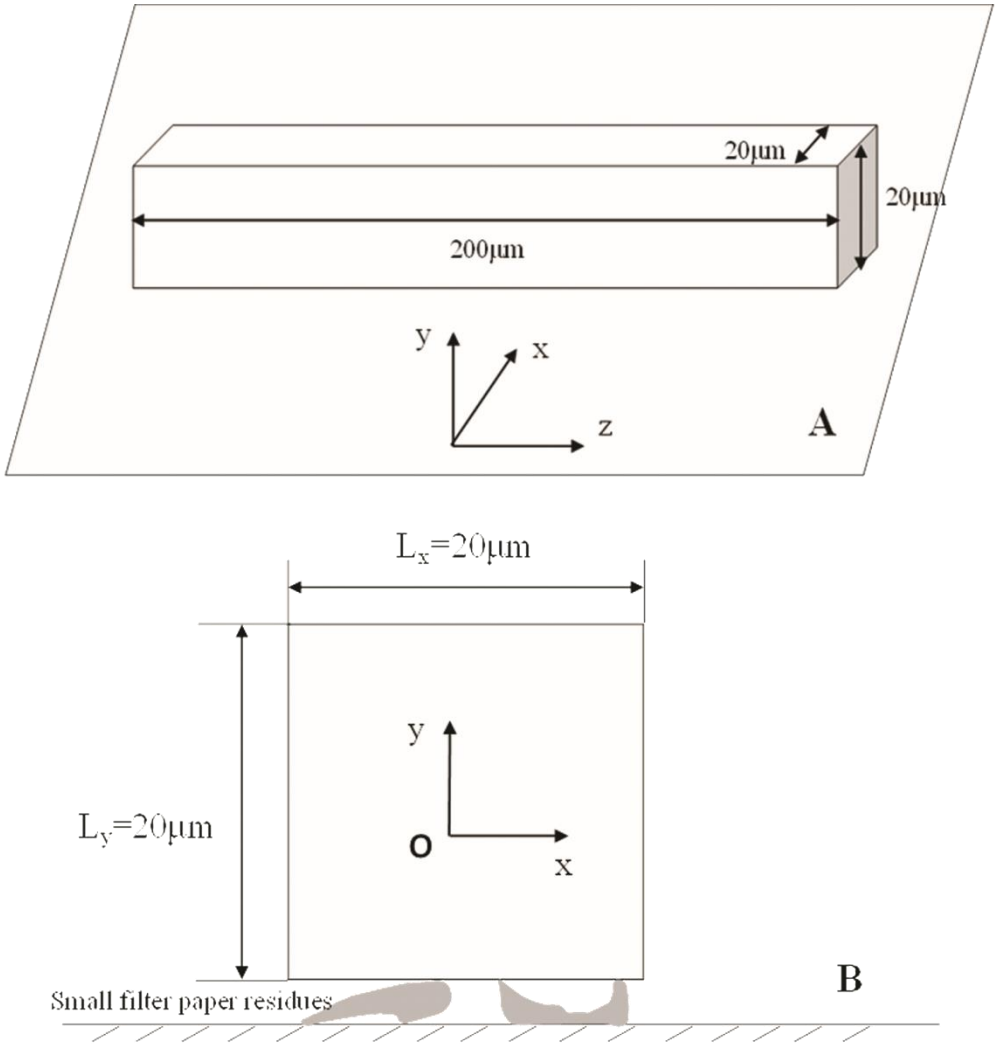

Figure 3.2. Schematic diagram of the filter paper on the glass wafer. A 200 μm long filter paper lies on top of a glass slide (A); the cross section of the filter paper particle (B), in which the light gray areas underneath are small filter paper residues.

described by the following partial differential equation:

$$\frac{\partial C}{\partial t} = D\left(\frac{\partial^2 C}{\partial x^2} + \frac{\partial^2 C}{\partial y^2}\right) \tag{3.1}$$

The above equation can be solved using boundary and initial conditions:

$$\frac{dC}{dx} = 0, \qquad x = 0, \qquad t > 0 \tag{3.2}$$

$$C = 0, \qquad x = \frac{L_x}{2}, \qquad t > 0 \tag{3.3}$$

$$\frac{dC}{dy} = 0, \qquad y = 0, \qquad t > 0 \tag{3.4}$$

$$C = 0, \qquad y = \frac{L_y}{2}, \qquad t > 0 \tag{3.5}$$

$$C = C_0, \quad 0 \le x \le \frac{L_x}{2}, \quad 0 \le y \le \frac{L_y}{2}, \quad t = 0 \tag{3.6}$$

The solution for this PDE is

$$C(x, y, t) = \tag{3.7}$$

$$C_0 * \sum_{n=1}^{\infty}\left\{\frac{4}{\pi} * \frac{(-1)^{n-1}}{(2n-1)} * exp\left[-\frac{(2n-1)^2\pi^2}{4{L_x}^2}Dt\right] * cos\left(\left(\frac{2n-1}{2L_x}\right)\pi x\right)\right\} * \sum_{n=1}^{\infty}\left\{\frac{4}{\pi} *\right.$$

$$\left.\frac{(-1)^{n-1}}{(2n-1)} * exp\left[-\frac{(2n-1)^2\pi^2}{4{L_y}^2}Dt\right] * cos\left(\left(\frac{2n-1}{2L_y}\right)\pi y\right)\right\}$$

Since at low concentrations we don't expect quenching of the fluorophores, the mass of the remaining dextrans is expected to be proportional to the observed fluorescence.

Therefore, Equation 3.7 is integrated to determine the mass, M, of the FITC-dextran

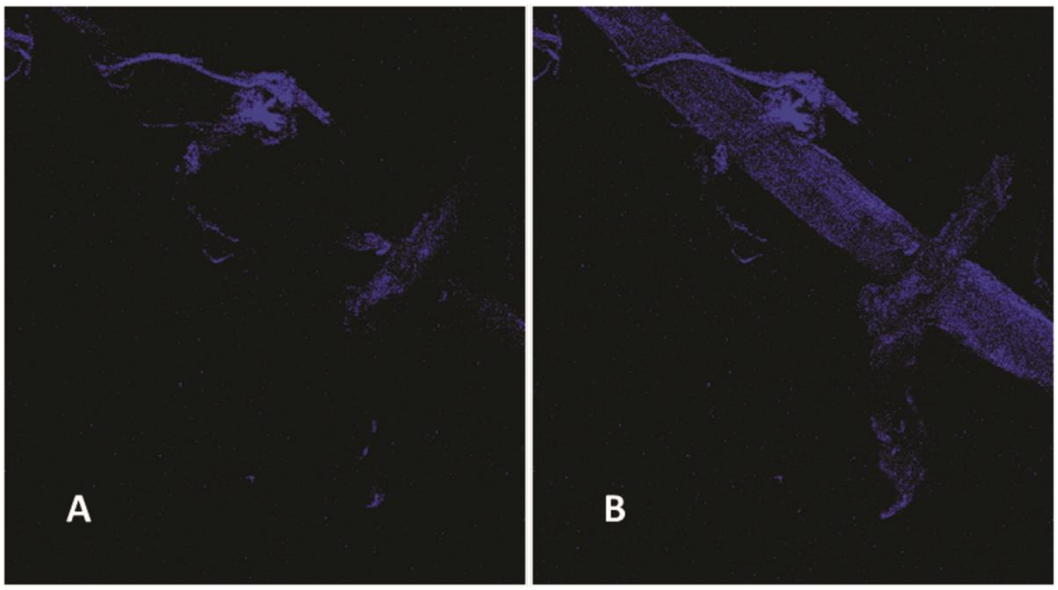

Figure 3.3. Filter paper residues on glass wafer (“pillars”, A) and filter paper particle together with these residues (B).

remaining inside filter paper particle. Thus, the percentage of dextran remaining inside filter paper particle at time t is

$$\frac{M}{M_{initial}} = \sum_{n=1}^{\infty}\left\{\frac{8}{\pi^2} * \frac{1}{(2n-1)^2} * exp\left[-\frac{(2n-1)^2\pi^2}{4{L_x}^2} Dt\right]\right\} * \sum_{n=1}^{\infty}\left\{\frac{8}{\pi^2} * \frac{1}{(2n-1)^2} * exp\left[-\frac{(2n-1)^2\pi^2}{4{L_y}^2} Dt\right]\right\} \quad (3.8)$$

Because of the symmetry imposed by assuming an infinitely long particle, the relative signal intensity in one cross section is representative to that of the whole particle. This means the model can be fitted to the experimental data and key parameters can be estimated. For this study, diffusion coefficients were estimated by minimizing the difference between the predicted and experimentally observed amount of dextran remaining inside filter paper particles at certain time points. Nonlinear parameter estimation was done using the *lsqnonlin* function in Matlab® (R2011B, Mathworks, Natick, MA) with Trust-region-reflective algorithm.

3.3 Results and Discussion

3.3.1. Diffusion model boundary conditions

Figure 3.4 shows three examples of fluorescence intensity maps reconstructed from z-stacks of fluorescence images obtained from cellulosic particles. The contour lines show

regions of equal fluorescence intensity inside the filter paper particle, with colors representing different intensity levels (see scale bar). Higher intensity indicates higher dextran concentrations in the center of the filter paper particle. These are consistent with other particles we observed.

Figure 3.4 provides evidence that supports the assumption that all boundary conditions of the filter paper particles are the same. In fact, two representative filter paper layouts on glass wafer have been observed. Some imaged filter paper particles lie on top of small residues positioned on the surface of the glass wafer, showing very limited contact areas between filter paper particles and the residues. Other particles are suspended rigid structures that contact the surface at some points but lie above the surface for the particular region imaged. In either case, filter paper particles are not seamlessly adhered to the surface of glass wafer. This justifies the assumption that all four boundaries in a cross section have similar diffusion behaviors.

To validate whether the Equation 3.8 would yield similar pattern of fluorescent intensity than those observed experimentally and reported in Figure 3.4, a Matlab simulation of a 20μm by 20μm filter paper cross section particle was conducted using a diffusion coefficient of $0.01\mu m^2/s$, which is in line with the estimated diffusion coefficient values presented later (Figure 3.5). The pattern of the simulated normalized fluorescence

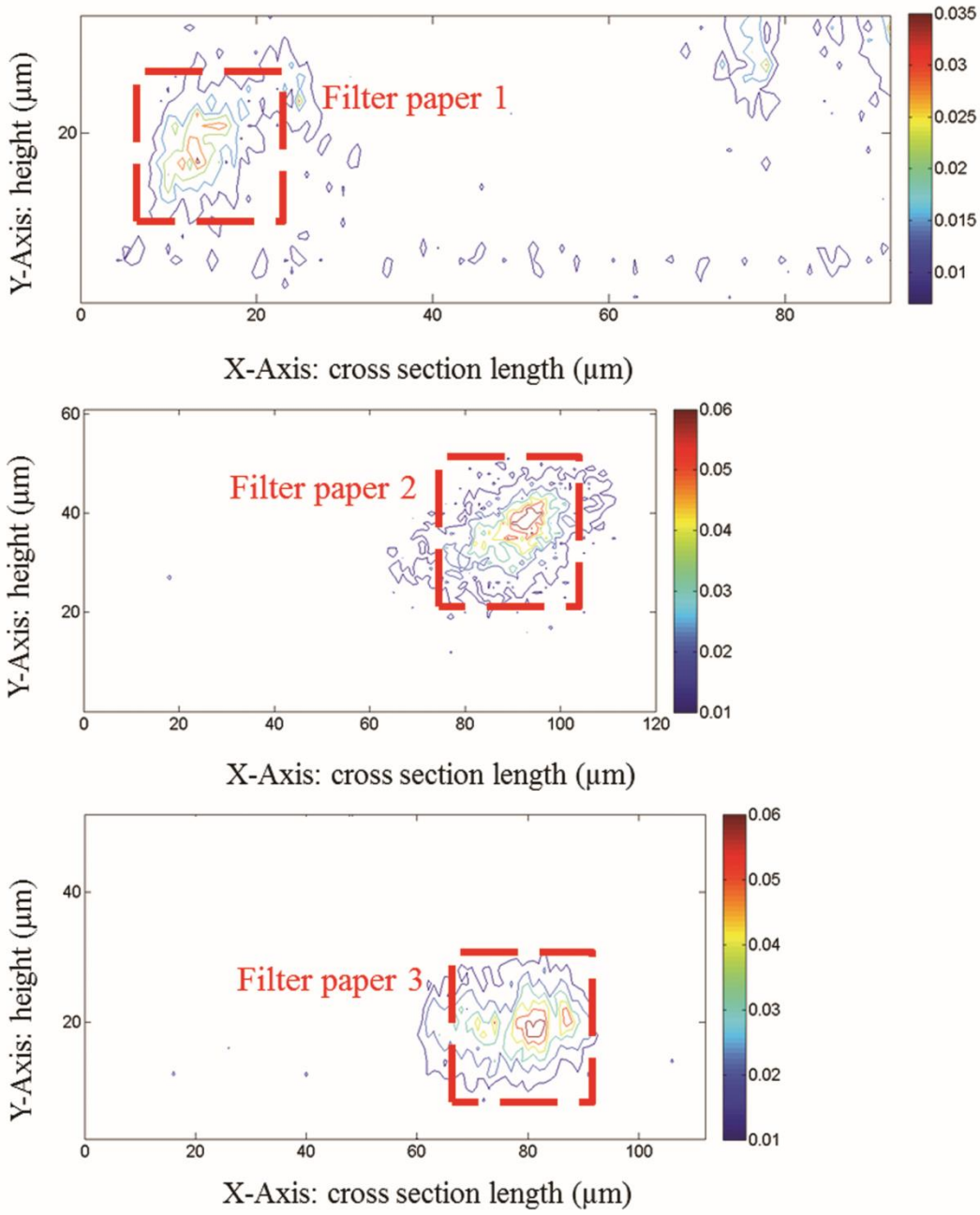

Figure 3.4. Fluorescence intensity distributions in chosen image scanning cross sections of filter paper (inside red dashed line). X axis is the horizontal length of one image scanning cross section. Y axis is the vertical height from the bottom of the glass wafer. Different colors of contour lines refer to different fluorescence intensities from FITC-dextran inside filter paper in arbitrary units.

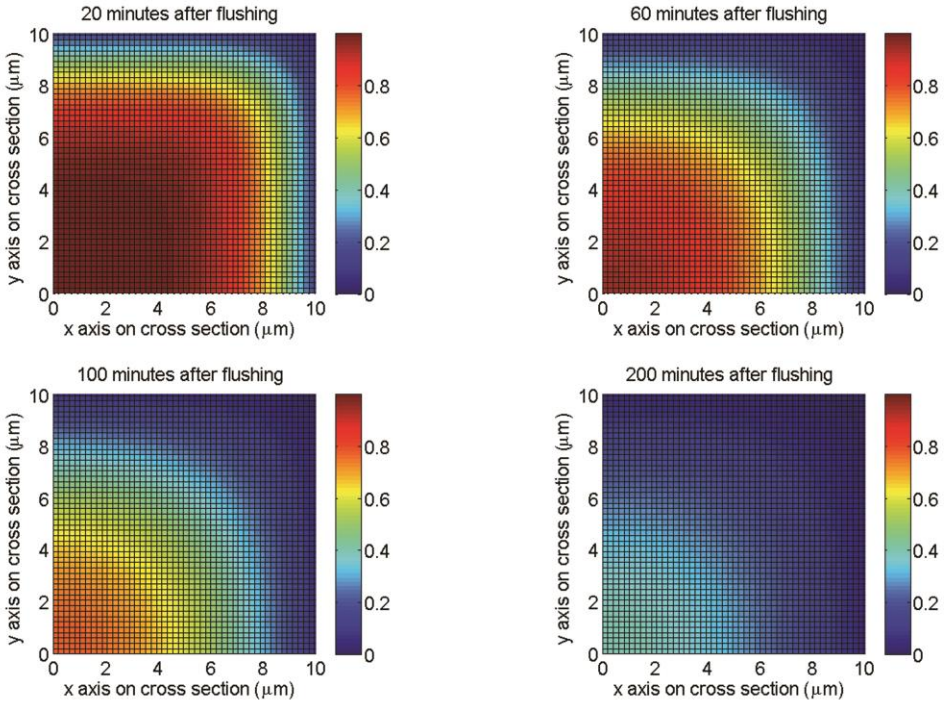

Figure 3.5. Model predicted dextran distribution in the upper right quarter of a filter paper's cross section ($D = 0.01\mu m^2/s$). Different colors in the cross section indicate the remaining portions of dextran at a specific time after diffusion starts.

intensities agrees quite well with the measured ones, where higher dextran signal was observed in the center of the particle than on the layers closer to the boundaries. In the simulation, it took less than 200 min for 90% of the dextran to diffuse out.

3.3.2. Observation and analysis of the fast and slow diffusion mechanism

Different size dextran probes (20, 70, 150 kDa) were used to study molecular diffusion in filter paper particles. Due to the time needed to qualify particles for imaging and the aperture speed, first fluorescent intensity profiles were acquired 20-30 min after elution. Figure 3.6 shows z-stack projections of confocal fluorescence images taken from experiments that tracked the diffusion of 20k and 150k Da dextran probes. It is clear that the fluorescent intensity of the particle decreases rapidly over time and that rate at which the intensity decreases is a function of the dextran size.

A more quantitative assessment of the decrease is shown in Figure 3.7 where the average pixel intensity obtained from axial projections of images taken from different filter paper particles over time are plotted. For each of the three data sets for a particular size dextran probe the average pixel intensity in the time-lapse experiment was normalized to the initial intensity. This allowed for the comparison of the temporal evolution of the relative intensities (Y axis in Figure 3.7) across different particles. Fluorescence signal decayed 75%, 74% and 52% in the first 20-30 min. The observed decay in fluorescent intensity

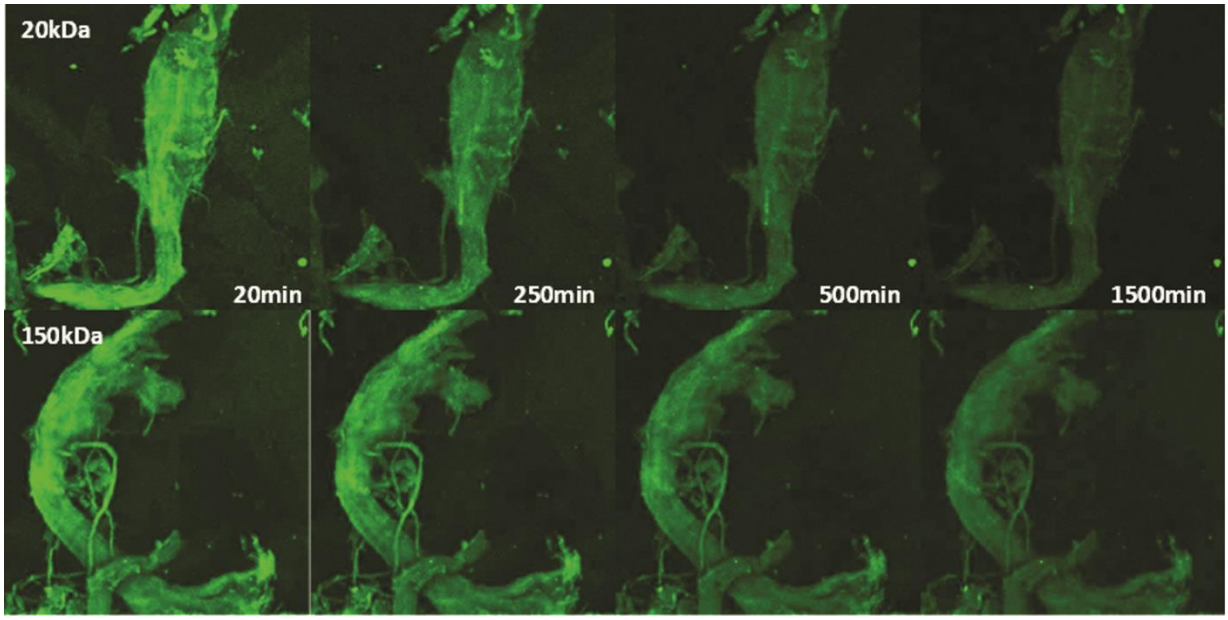

Figure 3.6. Diffusion images of 20kDa (top frames) and 150kDa (bottom frames) dextran probes by fluorescence confocal microscopy. The green color shows FITC-dextran remaining in the filter paper particles.

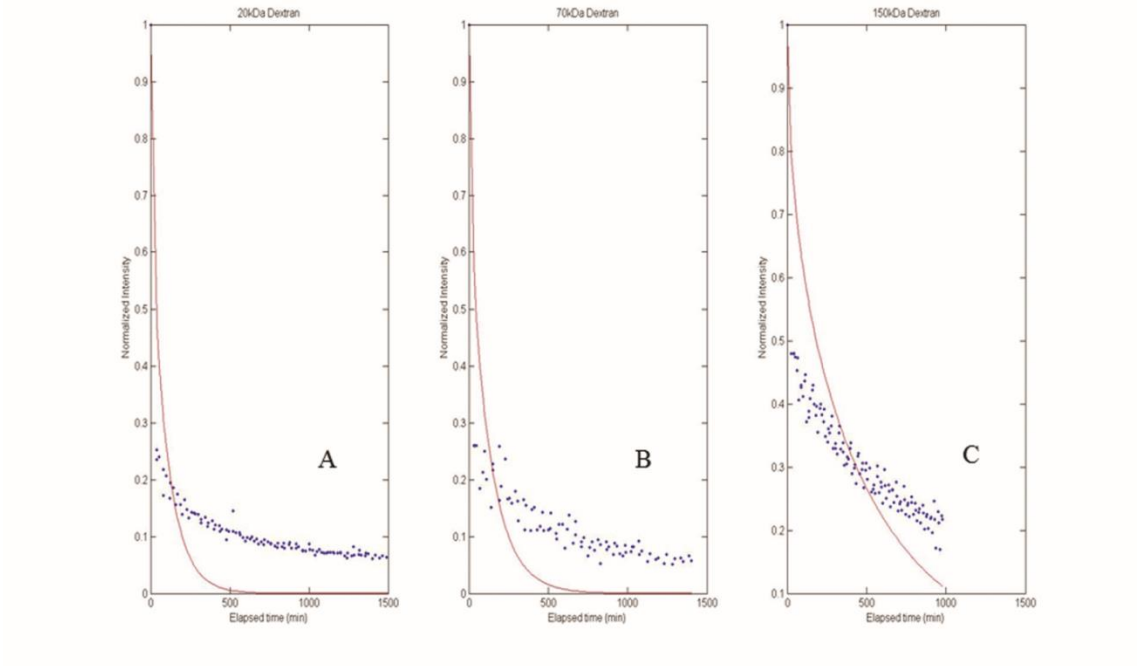

Figure 3.7. Measured and estimated normalized intensity curves obtained from the diffusion model with one diffusion coefficient. Blue dots show the average pixel intensity obtained from axial projections of images taken from different filter paper particles over time.

revealed a fast diffusion in the initial phase followed by a much slower diffusion process in the later phase. To estimate the pore diffusion coefficients (D_p) for all data, Equation 3.8 was fitted to these data sets using Matlab Trust-region-reflective algorithm. The resulting curves obtained for the best fit are presented in red in Figure 3.7 A-C. The estimated pore diffusion coefficients for the three dextrans were found to be 0.0137, 0.0109, 0.0026 $\mu m^2/s$ with R^2 values 0.67, 0.66, and 0.42, respectively. It appears that the model, Equation 3.8, is not adequate for describing both the initial fast diffusion rates and the later slow diffusion rates observed in Figure 3.7.

3.3.3. Pore grouping diffusion model

The diffusion model described by Equation 3.8 was based on the assumption of uniform particle pore size distribution. However, the pore size in untreated and treated biomass is poly-disperse, as reported by Grethlein (Grethlein, 1985). Thus, a range of diffusion rates should be expected requiring some type of semi-continuous or continuous relationship between pore size distribution and pore diffusion to adequately model transport. Here, we used a semi-continuous approach to group all pores into four sizes: 4.4, 6.6, 9.9 and 14.9 nm (Figure 3.8). These sizes are consistent with the hydrodynamic molecular diameter of the 20, 70, 150 kDa dextrans of 4, 6, 9 nm, respectively (Zhu, 2012). The volume proportions of the four clusters are w_1, w_2, w_3 and w_4, respectively. Thus, pores exactly 10% larger in width than the probes are defined to be micropores with diffusion

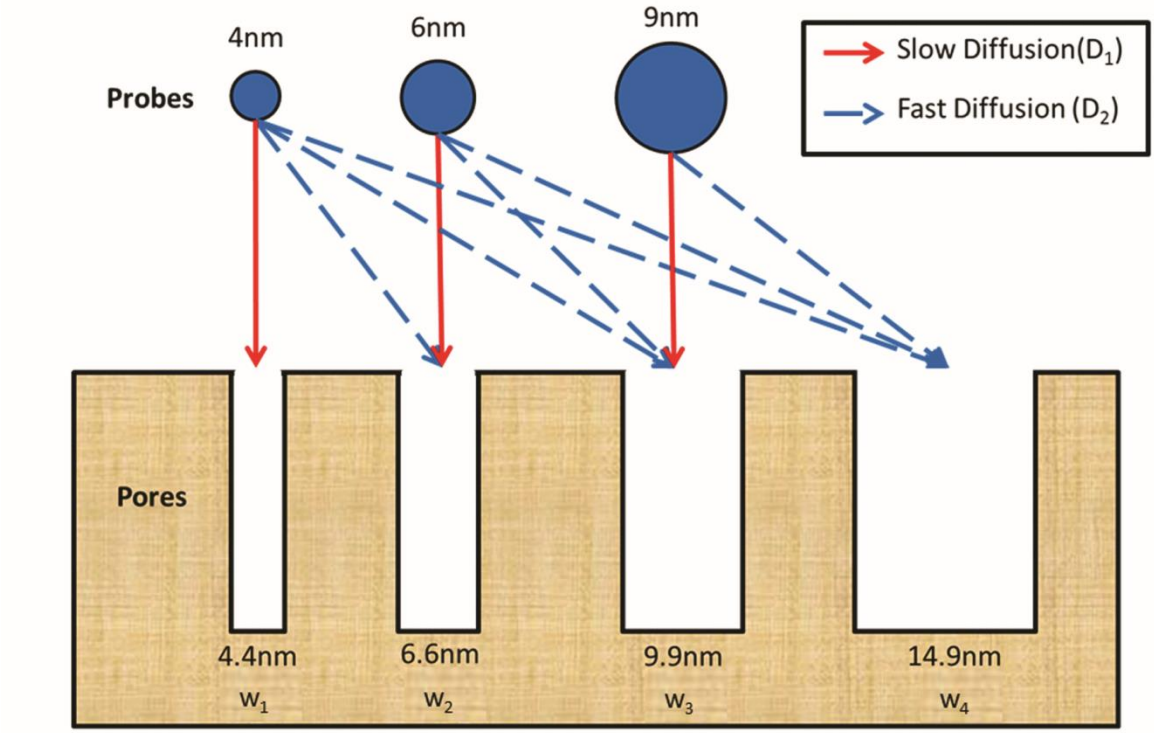

Figure 3.8. Proposed diffusion scenario for different probe sizes and pore diameters.

coefficient D_1 (e.g. 4, 6, 9 nm probe in 4.4, 6.6, 9.9 nm pores, respectively). Other pores, which are 1.65 times or larger than probes, are defined to be macropores with a bulk diffusion coefficient (D_2). Bulk diffusion coefficients (D_2) were calculated using Stokes-Einstein equation (Table 3.1).

$$D_2 = \frac{kT}{6\pi\eta R_H} \tag{3.9}$$

Where k = Boltzmann constant (N m/K),

T = absolute temperature of the buffer (K),

η = viscosity of the solution (10^{-3} N s/m^2), and

R_h = hydrodynamic radius (m).

Equations 3.10-3.12 are the weighted models used to describe the diffusion behavior of the three dextran probes (20,70 and 150kDa) in filter paper particles.

$$\left[\frac{M}{M_0}\right]_{20kDa} = w_1 f(D_1) + (1 - w_1) f(D_2) \tag{3.10}$$

$$\left[\frac{M}{M_0}\right]_{70kDa} = \frac{w_2}{1 - w_1} f(D_1) + \frac{1 - w_1 - w_2}{1 - w_1} f(D_2) \tag{3.11}$$

$$\left[\frac{M}{M_0}\right]_{150kDa} = \frac{w_3}{1 - w_1 - w_2} f(D_1) + \frac{1 - w_1 - w_2 - w_3}{1 - w_1 - w_2} f(D_2) \tag{3.12}$$

Table 3.1. Adjusted volume proportions (β_1, β_2, β_3) and slow diffusion coefficients (D_1) estimated from Equation 3.13 -3.15 and bulk diffusion coefficient D_2 calculated by Stokes-Einstein equation for all three probes

	β_1	β_2	β_3	D_1 ($\mu m^2/s$)	D_2 ($\mu m^2/s$)
20kDa	0.2516			0.0011	52
Confidence Interval	(0.2417,0.2614)			(0.0010,0.0012)	
70kDa		0.3099		0.0015	35
Confidence Interval		(0.2914,0.3284)		(0.0013,0.0017)	
150kDa			0.5609	0.0009	23
Confidence Interval			(0.5487,0.5731)	(0.0008,0.0009)	

The function 'f' corresponds to the right hand term of Equation 3.8, which is evaluated using the slow and fast diffusion coefficients (D_1 and D_2). The first and second terms of Equations 3.10-3.12 describe slow and fast diffusion, respectively. They can be further simplified to Equation 3.13-3.15.

$$\text{20kDa dextran(4nm):} \quad \beta_1 f(D_1) + (1-\beta_1) f(D_2) \tag{3.13}$$

$$\text{70kDa dextran(6nm):} \quad \beta_2 f(D_1) + (1-\beta_2) f(D_2) \tag{3.14}$$

$$\text{150kDa dextran(9nm):} \quad \beta_3 f(D_1) + (1-\beta_3) f(D_2) \tag{3.15}$$

Adjusted volume proportions (β_1, β_2 and β_3) and slow diffusion coefficient (D_1) were estimated for each of the three dextran probes using Matlab (R2011B, Mathworks, Natick, MA) nonlinear parameter estimation program *lsqnonlin*. Efforts to obtain unique estimates of D_1 and D_2 were unsuccessful as indicated by the large confidence intervals obtained. Thus, D_2 was estimated using the Equation 3.9. Listed in Table 3.1 are the estimated values for the β's and D_1 along with confidence intervals. Plotted in Figure 3.9 are dextran concentrations versus time curves obtained from this curve fitting effort. The use of bulk diffusivity values for D_2 was successful in capturing the rapid drop in normalized intensity observed in the first thirty minutes of the experiment, while the much lower estimated D_1 values were successful in capturing the leveling off of normalized intensity during the remaining time course. By incorporating fast and slow diffusive processes into our model we were able to better model the experimental data.

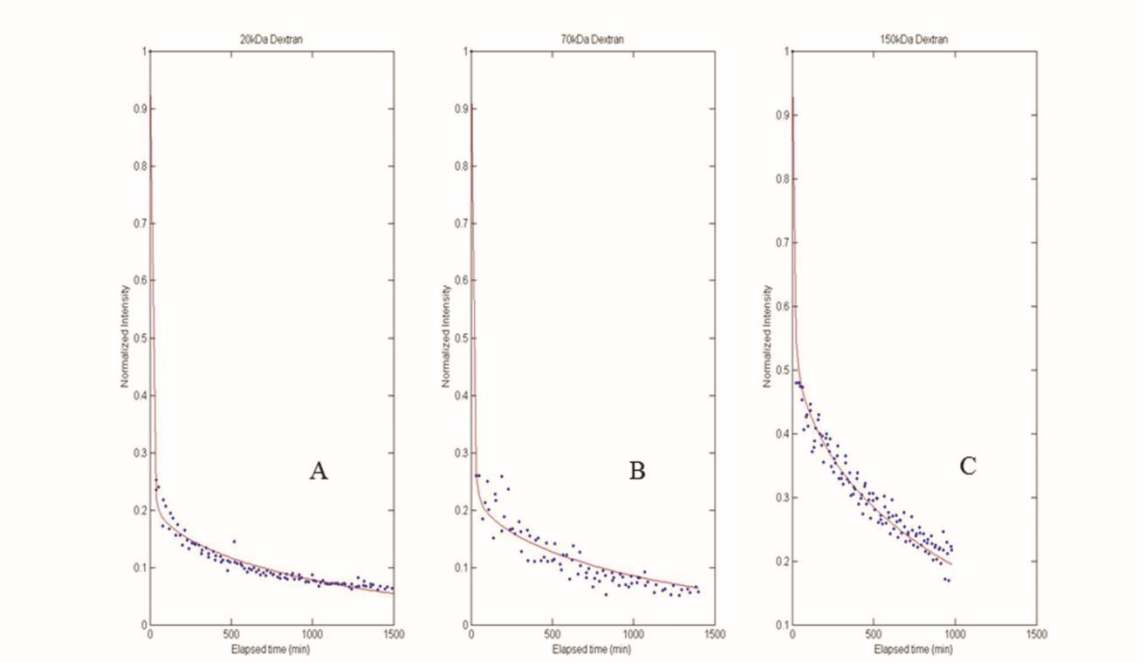

Figure 3.9. Measured and estimated normalized intensity curves obtained from the pore-cluster diffusion model. Blue dots show the average pixel intensity obtained from axial projections of images taken from different filter paper particles over time.

Estimates of D_1 are much smaller than D_2 values. This is consistent with our hypothesis that strong steric hindrance of the solute is occurring in the micropores. As noted earlier, this hindrance is caused by the interactions between probes and micropore wall and collisions between probes in crowded environments. Diffusivity would be expected to decrease with increasing solute/pore diameter ratio. Harriot (Harriott, 2003) reported the following relationship that relates the ratio of D_{pore} and D_{bulk} to the ratio of solute/pore diameters (d_{solute} and d_{pore}) :

$$\frac{D_{pore}}{D_{bulk}} = \left(1 - \frac{d_{solute}}{d_{pore}}\right)^4 \qquad (3.16)$$

Equation 3.16 yields estimates of solute diffusivities that are four or five orders of magnitude lower than those calculated for bulk solution. The ratios of our estimates of D_1 and D_2 are in the order of 1/10,000, which is consistent with Equation 3.16. Thus, our estimation of D_1 is consistent with our original hypothesis that the transport of probes to some cellulose surfaces area can be influenced by steric hindrance within the porous structure of cellulosic materials.

Volume fractions were estimated to be 0.25, 0.23, 0.29 and 0.23 for w_1, w_2, w_3 and w_4, respectively. These results indicate that micropores represent, on average, 25% of the

accessible pore volume. In addition, the first terms of Equation 3.10 - 3.12 indicating the slow diffusion in micropores, were found to be $0.25f(D_1)$, $0.30f(D_1)$ and $0.56f(D_1)$. This explains the similar rapid drop pattern for the first two probes (20kDa and 70kDa) in normalized intensity observed in the first thirty minutes of the experiment and the following level-off during the remaining time course (Figure 3.9A, B). It is also equivalent to say that 20kDa and 70kDa dextran probes diffuse much slower in 25% and 30% of the pores they can enter than in the rest of the pores.

3.4 Conclusions

The diffusion of dextrans in the porous structure of cellulosic particles derived from biomass can be influenced by steric hindrance, mainly by the interactions between the diffusing solute and micropore wall and collisions between solutes. Given the poly-disperse pore size distribution that is characteristic of untreated and treated biomass (Grethlein, 1985), non-binding dextran probes of different sizes can exhibit different diffusion behaviors in these porous structures. Observing diffusion into the pore space of cellulosic biomass allows us to evaluate the influence of pore size distribution on rates of probe diffusion. A semi-continuous pore size distribution model grouping all pores into four size clusters shows that 75% of the accessible pore volume is from easily accessible pores and the rest from diffusion-hindered pores for 6 nm probes, which is about the size of an enzyme.

Dextran probes with hydrodynamic radii comparable to the size of CWDEs are capable of providing insight into the diffusion hindrance encountered as these enzymes diffuse into and bind to cellulosic substrate. However, our observations and modeling activities do not tell the complete story of CWDEs transport and binding. The reactive domains of CWDEs diffusing through the pore structure would bind to the substrate as the enzymes interact with the reactive pore wall; thus, further reducing the rate of diffusion through the substrate. Despite this limitation of our research approach, our micro-scale solute exclusion technique does provide important insights into the mass transport challenges associated with CWDEs gaining access to reactive surfaces. It provides a quantitative measure of the fraction of the substrate structure that is accessible to CWDEs based on their relative size. In addition, our approach provides the foundation for future studies with fluorescently-labeled native CWDEs and CWDEs that have been engineered to exhibit no binding affinity for the substrate. These future studies are possible because of the reduced quantity of enzymes needed to probe the substrate as opposed to the larger volume needed for macro-scale solute exclusion studies using CWDEs (Corner, 2003; Neuman and Walker, 1992a; Neuman and Walker, 1992b).

3.5 References

Arantes V, Saddler J. 2011. Cellulose accessibility limits the effectiveness of minimum cellulase loading on the efficient hydrolysis of pretreated lignocellulosic substrates. Biotechnol Biofuels 4(1):3.

Carslaw HS, Jaeger JC. 1959. Conduction of heat in solids. Oxford: Clarendon Press. p 176-188.

Chandra R, Ewanick, S, Hsieh, C, Saddler, JN. 2008. The characterization of pretreated lignocellulosic substrates prior to enzymatic hydrolysis, Part 1: a modified Simons' staining technique. Biotechnol Prog 24(5):1178-1185.

Chanzy H, Henrissat B, Vuong R. 1984. Colloidal gold labelling of l,4-β-D-glucan cellobiohydrolase adsorbed on cellulose substrates. FEBS Letters 172(2):193-197.

Corner CV. 2003. A size-exclusion chromatography system for observing the transport and weak binding of Thermobifida Fusca catalytic domains: Experiemntal and theoretical investigation. [Ph.D. thesis]. Ithaca. Cornell University.193 p.

Foston M, Ragauskas, AJ. 2010. Changes in the structure of the cellulose fiber wall during dilute acid pretreatment in populus studied by 1H and 2H NMR. Energy Fuels 24(10):5677-5685.

Grethlein HE. 1985. The effect of pore size distribution on the rate of enzymatic hydrolysis of cellulosic substrates. Nat Biotech 3(2):155-160.

Grethlein HE, Allen DC, Converse AO. 1984. A comparative study of the enzymatic hydrolysis of acid-pretreated white pine and mixed hardwood. Biotechnol Bioeng 26(12):1498-1505.

Gusakov AV, Sinitsyn AP, Salanovich TN, Bukhtojarov FE, Markov AV, Ustinov BB, Zeijl Cv, Punt P, Burlingame R. 2005. Purification, cloning and characterisation of two forms of thermostable and highly active cellobiohydrolase I (Cel7A) produced by the industrial strain of *Chrysosporium lucknowense*. Enzyme Microb Tech 36(1):57-69.

Harriott P. 2003. Chemical reactor design: New York: Marcel Dekker. 143 p.

Harris D, Petti C, DeBolt S. 2013. The Synthesis, regulation and modification of lignocellulosic biomass as a resource for biofuels and bioproducts. In: Lee JW, editor. Biofuels and bioproducts. New York: Springer. p 281-314.

Irwin DC, Spezio M, Walker LP, Wilson DB. 1993. Activity studies of eight purified cellulases: Specificity, synergism, and binding domain effects. Biotechnol Bioeng 42(8):1002-13.

Jeoh T, Ishizawa CI, Davis MF, Himmel ME, Adney WS, Johnson DK. 2007. Cellulase digestibility of pretreated biomass is limited by cellulose accessibility. Biotechnol Bioeng 98(1):112-122.

Jeoh T, Wilson DB, Walker LP. 2002. Cooperative and competitive binding in synergistic

mixtures of *Thermobifida fusca* Cel5A, Cel6B and Cel9A. Biotechnol Prog 18(4):760-769.

Karlsson J, Saloheimo M, Siika-aho M, Tenkanen M, Penttilä M, Tjerneld F. 2001. Homologous expression and characterization of Cel61A (EG IV) of Trichoderma reesei. Eur J Biochem 268(24):6498-6507.

Langan P, Nishiyama Y, Chanzy H. 2001. X-ray Structure of Mercerized Cellulose II at 1 Å Resolution. Biomacromolecules 2(2):410-416.

Luterbacher JS, Tester JW, Walker LP. 2010. High-solids biphasic CO2–H2O pretreatment of lignocellulosic biomass. Biotechnol Bioeng 107(3):451-460.

Luterbacher JS, Walker LP, Moran-Mirabal JM. 2012. Observing and modeling BMCC degradation by commercial cellulase cocktails with fluorescently labeled Trichoderma reseii Cel7A through confocal microscopy. Biotechnol Bioeng 110(1):108-117.

Lynd LR, Laser MS, Bransby D, Dale BE, Davison B, Hamilton R, Himmel M, Keller M, McMillan JD, Sheehan J and others. 2008. How biotech can transform biofuels. Nat Biotech 26(2):169-172.

Moran-Mirabal JM, Bolewski JC, Walker LP. 2011. Reversibility and binding kinetics of Thermobifida fusca cellulases studied through fluorescence recovery after photobleaching microscopy. Biophys Chem 155(1):20-28.

Moran-Mirabal JM, Corgie SC, Bolewski JC, Smith HM, Cipriany BR, Craighead HG, Walker LP. 2009. Labeling and purification of cellulose-binding proteins for high resolution fluorescence applications. Anal Chem 81(19):7981-7987.

Neuman RP, Walker LP. 1992a. Solute exclusion from cellulose in packed columns: Experimental investigation and pore volume measurements. Biotechnol Bioeng 40(2):218-225.

Neuman RP, Walker LP. 1992b. Solute exclusion from cellulose in packed columns: Process modeling and analysis. Biotechnol Bioeng 40(2):226-234.

Otsu N. 1979. A threshold selection method from gray-level histograms. IEEE Trans 9(1):62-66.

Santhanam N, Walker LP. 2008. A high throughput assay to measure cellulose binding and synergism in ternary mixtures. Biol Eng 1(1):1-19.

Snow P, O'Dea K. 1981. Factors affecting the rate of hydrolysis of starch in food. Am J Clin Nutr 34(12):2721-7.

Wang QQ, He Z, Zhu Z, Zhang YHP, Ni Y, Luo XL, Zhu JY. 2012. Evaluations of cellulose accessibilities of lignocelluloses by solute exclusion and protein adsorption techniques. Biotechnol Bioeng 109(2):381-389.

Wilson D. 2012. Processive and nonprocessive cellulases for biofuel production—lessons from bacterial genomes and structural analysis. Appl Microbiol Biotechnol 93(2):497-502.

Wilson DB. 2004. Studies of Thermobifida fusca plant cell wall degrading enzymes.

Chem Rec 4(2):72-82.
Zhu P. 2012. Signal Processing In Single Molecule Studies. [Ph.D. thesis]. Ithaca. Cornell University. 192 p.
Zhu P, Moran-Mirabal J, Luterbacher J, Walker L, Craighead H. 2011. Observing Thermobifida fusca cellulase binding to pretreated wood particles using time-lapse confocal laser scanning microscopy. Cellulose 18(3):749-758.

4. REVISITING SIZE-EXCLUSION CHROMATOGRAPHY FOR MEASURING STRUCTURAL CHANGES IN RAW AND PRETREATED MIXED HAEDWOODS AND SWITCHGRASS

4.1 Introduction

Cellulosic feedstocks are complex physical materials that have complex pore structures. Their pore size distributions and the molecular diameters of the CWDEs define the reaction volume and surface area for the heterogeneous catalysis system of cellulase-cellulose reaction (Fan et al., 1980; Fan et al., 1981; Grethlein, 1985; Lee et al., 1982; Moran-Mirabal et al., 2011; Walker and Wilson, 1991; Yang et al., 2013). The reactive surface area of insoluble cellulosic particle can be divided into two categories: external surface area, and internal or pore surface area. The external surface area depends on the size and shape of the cellulose particle, while the pore surface area is determined by the accessible pore volume of the cellulose particle (Zhu et al., 2009). Of the two categories the pore surface area is the most important because it is generally much larger, by one or two orders of magnitude, than external surface area (Grethlein, 1985; Park et al., 2007; Walker et al., 1992). Wang et al (Wang et al., 2012) showed that over 90% of the substrate enzymatic hydrolysis extent is contributed by the accessible pore surface area, while external particle surface area plays only a minor role. Therefore, the accessible pore surface area is a major factor in defining the rate and extent of hydrolysis (Arantes and

Saddler, 2011; Bothwell et al., 1997).

The strong correlation between accessible pore surface area and the rate and extent of hydrolysis has been documented for a wide range of substrates, pretreatment technologies, enzymes and their loadings (Grethlein, 1985; Grous et al., 1986; Lin et al., 1987; Mansfield et al., 1999; Mooney et al., 1998; Thompson et al., 1992; Wang et al., 2012). Stone and Scallan reported a linear relationship between the initial cellulase reaction rate and the surface area inside the cellulose that was accessible to a molecule with 4 nm in diameter (Stone et al., 1969). Grethlein obtained an excellent linear correlation between available surface area to probes with molecular diameter of 5.1 nm and the initial glucose yield for acid pretreated mixed hardwood. Other studies where the initial rate of hydrolysis and binding shows a positive correlation to the available specific area include steam exploded pine (Wong et al., 1988) , acid/alkali/oxidative pretreated sugar cane bagasse (Sinitsyn et al., 1991), SO_2/steam pretreated wheat and spruce (Piccolo et al., 2010) and organosolv pretreated cedar (Kawakubo et al., 2010). Thus a major objective of thermal chemical pretreatment is to significantly increase the accessible surface area for CWDEs such as cellulases (Grethlein, 1985; Weimer et al., 1990)**.** In addition, the pore surface area is important for defining the degree of synergism that can occur because CWDEs must occupy the same surface area for synergism to occur (Jeoh et al., 2007; Jeoh et al., 2002; Zhu et al., 2011).

Early cellulose hydrolysis researchers used nitrogen adsorption to estimate pore surface area (Fan et al., 1980; Fan et al., 1981). However nitrogen is a much smaller molecule than CWDEs, and it more easily diffuses into pore volumes of the substrate and has a higher accessibility (Mansfield et al., 1999; Tanaka et al., 1988). In addition, the intensive drying of the biomass needed for using this method tends to collapse internal pore structure thus limiting its accuracy for estimating accessible pore surface area (Esteghlalian et al., 2001; Luo and Zhu, 2011; Neuman and Walker, 1992a). Another approach for estimating accessible surface area uses Simons' stain. This is a semi-quantitative method based on the competitive adsorption of two dyes in an aqueous environment and can provide useful information about both internal and external accessible surface areas of a porous substrate (Chandra et al., 2008).

Solute exclusion has proven to be an effective and low cost method for estimating pore volume and subsequently pore surface area that overcomes some of the limitations of nitrogen adsorption methods (Corner, 2003; Lin et al., 1987; Neuman and Walker, 1992a; Neuman and Walker, 1992b). This technique uses non-reactive molecular probes such as dextrans and polyethylene glycol probes (PEGs) to explore the pore volume of insoluble substrates (Grethlein, 1985; Lin et al., 1987). It is more representative of the actual surface area accessible to the CWDEs because the probes can be comparable in size.

Early efforts to use solute exclusion to measure pore size distribution and to estimate specific surface area were done in batch process (Grethlein, 1985; Lin et al., 1987; Stone et al., 1969; Weimer et al., 1990). In this process wet cellulose were immersed in different solutions of probes at known concentration until equilibrium was reached. Based on probe concentration in supernatant, the accessible pore volume could be calculated by performing a mass balance based on the assumption that the concentration of the probe in the pores is the same as the bulk solution probe concentration. The problem with this technique is that the changes in bulk probe concentrations are small leading to large measurement error (Neuman and Walker, 1992a; Tanaka et al., 1988). Using the elution profile from a column packed with pure cellulose is a more precise way to measure pore volume distribution (Corner, 2003; Lin et al., 1987; Neuman and Walker, 1992a; Neuman and Walker, 1992b).

Many of the previous efforts to use solute exclusion chromatography to investigate pore structure used pure and more mono-dispersed cellulose particles. Here we reported on our effort to use the solute exclusion chromatography for untreated and pretreated mixed-hardwoods (MHW) and switchgrass (SG) at particle sizes more aligned with those that would be used by the bioprocessing industry. We also wanted to assess the necessity for particle size reduction for uniform column packing. Finally, we provided specific pore volume and specific surface area distribution for the raw and pretreated biomass, and

specific surface area estimates.

4.2. Materials and Methods

4.2.1. PEG probe solution and size check by Dynamic Light Scattering

Polyethylene glycol probes (Sigma-Aldrich, St. Louis, Missouri) with molecular weights ranging from 1kDa to 35kDa (PEG1000, PEG3350, PEG8000, PEG20000, PEG35000) were used in this study. PEG size measurements obtained from different methods showed that these probes have hydrodynamic radii that are comparable to the size of CWDEs (Armstrong et al., 2004; Corner, 2003; Gokarn, 2003; Neuman and Walker, 1992a). PEG probes were measured into five-hundred milliliters glass bottles (New Brunswick Scientific, Enfield, CT) with deionized water to obtain a concentration of 4g/L.

The hydrodynamic radii of the PEG probes were obtained by dynamic light scattering (DLS) measurements using a Zetasizer Nano ZS (Malvern Instruments, Worcestershire, UK). DLS analyzes the velocity distribution of particle movement by measuring dynamic fluctuations of light scattering intensity caused by the Brownian motion of the particles. Fluctuations are correlated with diffusion rates, which can be used to estimate hydrodynamic radius from the Stokes-Einstein equation (Murdock et al., 2008; Zhu, 2012). In these experiments, different PEG solutions made at concentrations between 1 g/l to 20 g/l were vortexed to provide a homogeneous solution, and then 1 ml was

transferred to a square glass cuvette for DLS measurements. They were incubated at 20 °C in a temperature-controlled Zetasizer Nano ZS that was equipped with a 4 mW He−Ne laser at 633 nm. Intensity data were collected at a fixed angle of 90 degrees. Samples with counting rates of 10^5 counts/s were analyzed to ensure the measurement sensitivity. The Zetasizer Software (V7.02) was used for particle size data analysis.

4.2.2. Biomass particle size reduction and size distribution measurement

MHW (Auburn, NY, 2009) and SG (Ithaca, NY, 2009) were air dried in the field to 10% moisture content and used in this study. A hammer mill (Schutte Buffalo LLC, Buffalo, NY) with 9.5 mm screen was used to reduce the initial biomass particle size. The biomass particle size was further reduced using a cutting mill (IKA1, Wilmington, NC) with either a 2 mm or 0.5 mm screen to produce particles smaller than 2 mm or 0.5 mm. Biomass was then sieved with a 76 μm mesh screen to remove dust-like particles (E. H. Sargent and Co., Chicago, IL).

Biomass particle size distribution was obtained by using Sonic sifter model L3P (Advantech Manufacturing, Inc, New Berlin, WI). A vertical column of air separated particles by oscillating in a periodic vertical motion. This sifting method can produce very little abrasion which is important for retaining the biomass integrity used in the experiment (Yan and Barbosa-Cánovas, 1997). Five sieves with opening sizes from 75

μm to 5000 μm were used with amplitude of eight on the sifter. Eight to ten grams of biomass were loaded and sieved for 3 min. The mass difference of each sieve before and after sieving was determined for retained biomass.

4.2.3. Biomass pretreatment

Biphasic pretreatment using CO_2 and H_2O was used to process the size reduced MHW and SG using the method of Luterbacher *et al* (Luterbacher et al., 2012). Sixty grams of MHW or SG particles that had passed through a 9.5 mm screen was mixed with deionized water to obtain the desired dry solids content of 40 wt%. The resulting 150 g slurry was loaded into a 1 L stirred reactor and purged with CO_2 at 15 BAR and vented. Liquid CO_2 was then loaded into the reactor to achieve a pressure of 200 BAR and heated to 210°C. The reactor contents were mixed with a propeller to ensure uniform reactor conditions. The reactor pressure was maintained at 200 BAR using a backpressure regulator. The inner reactor temperature was maintained at 210 ± 3°C for 10 min before the reaction was stopped by flowing cold water through a cooling coil within the reactor to rapidly drop the reactor temperature. All raw and pretreated biomass samples were washed with deionized water extensively and kept in the refrigerator overnight as slurries with 90% moisture content before loading in to the solute exclusion column.

4.2.4. Column preparation

LRC chromatography column with 25 mm inner diameter and 330 mm length (Pall Corp., Port Washington, NY**)** was packed with either raw or pretreated biomass (i.e. MHW and SG). A flow adapter with 10 µm frit screens was attached to the bottom of the column. Four types of MHW and SG slurries were studied: 9.5 mm milled raw biomass, 2 mm milled raw biomass, 0.5 mm milled raw biomass, and pretreated biomass from 9.5 mm raw biomass. Biomass slurry was poured into the column through a funnel connected to the top of the column. Approximately 30 to 40 g of dry biomass was packed into the column depending on their particle sizes. As the slurry came to the top of the column, the excess liquid was removed using a syringe. When the column was filled to within about 0.5 cm of the top, the funnel was removed and the top flow adapter with 10 µm frit screens was attached. The column was then mounted on a rack and stored in the refrigerator at 4°C for use.

4.2.5. Elution volume measurements

Figure 4.1 shows the various components and connections of the measurement system. Polyethylene tubing (0.24 cm O.D. X 0.16 cm I.D.) was connected from a 2 L glass feed bottle (New Brunswick Scientific, Enfield, CT) to an online degasser (DGU-20A, Shimadzu Corp., Columbia, MD) and pump module (LC-20AD, Shimadzu Corp., Columbia, MD) to remove gas bubbles from the system. Narrow diameter fluorinated

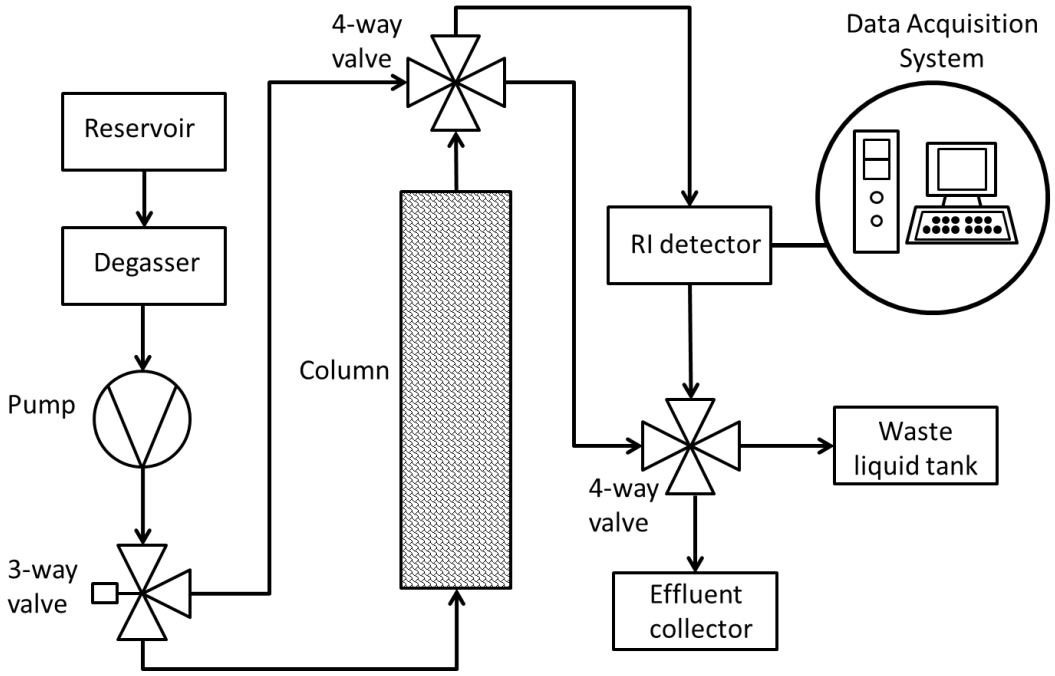

Figure 4.1. Layout for the solute exclusion system.

ethylene propylene (FEP) tubing (0.32 cm O.D. X 0.16 cm I.D.) was used to connect the pump module to the bottom of the column, and the top of the column to the refractive index detector (RID-10A, Shimadzu Corp., Columbia, MD) to measure the refraction index (RI) of the effluent from the column. The total volume of the tubing was 3 ml, resulting in 1.5 min lag time when for the 2 ml/min pump speed.

Before loading the column, 4 L of degassed MilliQ water was pumped through the column to remove trapped air and soluble materials which might contribute a signal as the elute volume passed the refractive index detector (RID). Then the feed bottle was filled with an aqueous 4 g/L (C_0) PEG solution. The data acquisition system was initiated when the pump module started to deliver PEG solutions from a feed bottle at 2 ml/min. Although the data collected during loading was not used for pore volume measurement, it was collected to determine the amount of probes remaining in the column after elution. The pump and data acquisition was stopped when the concentration of the effluent reached a constant peak value of about 400 mV, which correspondent to 4 g/L PEG solution. Then the feed bottle was filled with MilliQ water and the pump was turned on to start the elution process. The elution data was monitored until RI was less than 2 mv, which corresponded to less than 0.5% of the peak concentration for our threshold error. This approach was used to measure elution volumes for all of the PEGs and blue dextran. After completing the measurements with the probes the biomass was dried and weighed.

4.2.6. Pore volume determination

At low concentrations RI measurements, RI_i, are directly proportional to the solute concentration, C_i. This proportionality coupled with the initial value, RI_0, yields the following relationship: $RI_i/RI_0 = C_i/C_0$. The total mass for each specific solute is the summation of the solute mass in the substrate pore volume (V_p) and the solute mass in the external void volume (V_e). A mass balance on the system yields the following mass, M, relationship for the packed column:

$$M = C_0 \left(V_p + V_e\right) = C_0 V_T \tag{4.1}$$

Thus the total accessible volume (V_T) for a certain solute is

$$V_T = \frac{M}{C_0} = \sum_{i=1}^{m} \frac{C_i}{C_0} V_i = \sum_{i=1}^{m} \frac{RI_i}{RI_0} V_i \tag{4.2}$$

Where m is the number of elution aliquots measured for RI and V_i is a constant volume for each elution aliquot. The external void volume, V_e, was estimated using the elution volume of the largest probe, blue dextran at 1 MDa; thus V_p for a pore was determined by subtracting V_e from V_T (Neuman and Walker, 1992a; Neuman and Walker, 1992b).

4.3. Results and Discussions

4.3.1. PEG probe diameter measurement

Software provided with the Zetasizer (V7.02) was used to calculate bulk diffusion coefficient (D_b) by fitting an exponential function scattering intensity and elapsed time data. Then hydrodynamic radius (R_H) was calculated using the Stokes-Einstein equation:

$$R_H = \frac{kT}{6\pi\eta D_b} \tag{4.3}$$

Where k is the Boltzmann constant (N m/K), T is the absolute temperature of the buffer (K), η is the viscosity of the solution (10^{-3} N s/m^2), and D_b is the bulk diffusion coefficients of PEGs in pure water (m^2/s). The resulting probe diameters are listed in Table 4.1 and compared with those obtained from other studies (Armstrong et al., 2004; Corner, 2003; Gokarn, 2003; Neuman and Walker, 1992a). The probe diameters are very comparable to values reported in the literature varying not more that 4% despite the different methods used.

4.3.2. Biomass particle size distribution

Presented in Figure 4.2 are MHW and SG weight fractions retained by sieving screens. Four screens are used (75 μm, 500 μm, 1000 μm and 2000 μm) and biomass weight

Table 4.1. PEG diameter measurements and comparison

Probe	Probe diameter measured by different method (nm)			
	DLS method, this study	Viscosity method (Neuman and Walker, 1992)	Viscosity and DLS method (Armstrong et al, 2004)	DLS method (Gokarn, 2003)
PEG1000	1.89 ±0.02	1.85	-	-
PEG3350	3.68 ±0.08	3.63	3.58	-
PEG8000	5.43 ±0.07	5.96	5.76	-
PEG20000	8.98 ±0.12	-	-	8.6
PEG35000	12.78 ±0.08	-	13.18	-

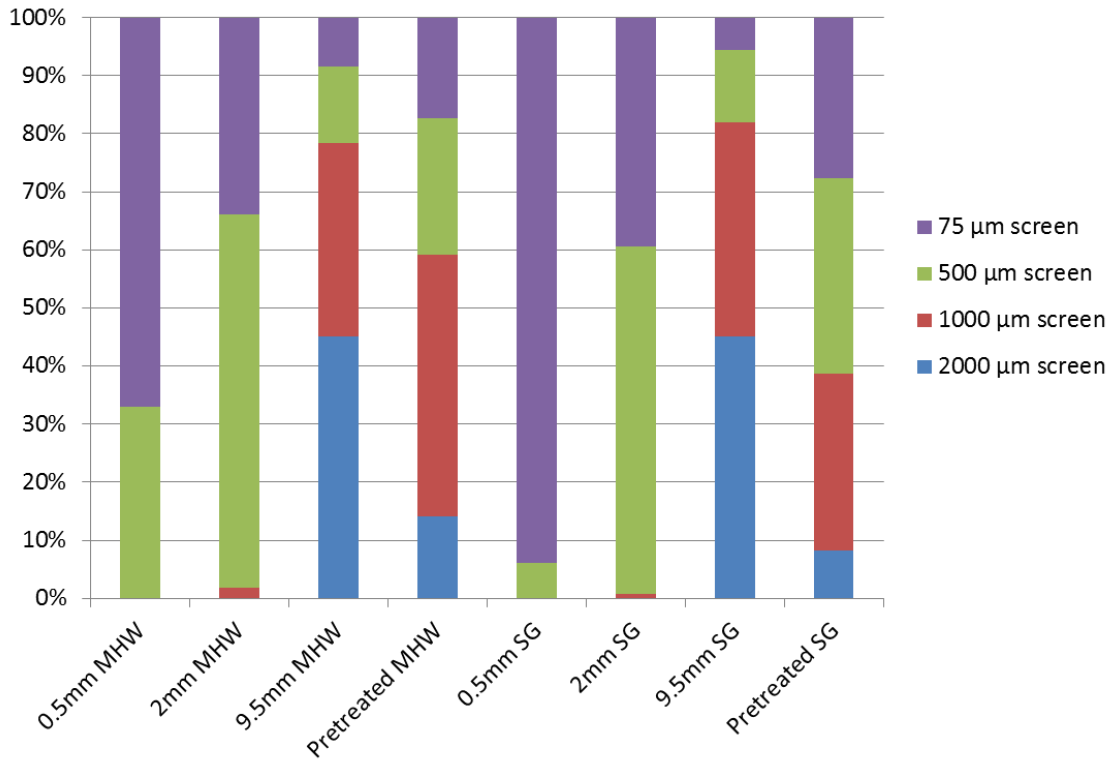

Figure 4.2. Weight percentages of biomass materials retained on different screen sizes (75 µm, 500 µm,100 µm and 2000 µm).

proportions retained on each screen are shown in different colors. Pretreated and 9.5 mm screened MHW and SG showed more size heterogeneity than biomass in smaller sizes (i.e. 2mm and 0.5mm screened). Rosin-Rammler (RR) function is applied to describe the biomass particle size distribution for all biomass types. RR distribution function was used widely for representing particle size distributions generated by grinding and milling operations (Bitra et al., 2009; Rosin and Rammler, 1933; Vaezi et al., 2013). It can be expressed as follows:

$$w = 1 - exp\left(-\left(\frac{x}{x_R}\right)^m\right) \tag{4.4}$$

Where w is the weight fraction of biomass finer than screen size x; x_R and m are two independent variables that describe particle size at e^{-1} = 36.8% of the total weight and the steepness of the cumulative curve. Their values are reported in Table 4.2. The function fits the experimental data very well with R^2 values for all the samples higher than 0.99. Utilizing the curve fits, Table 4.3 shows the mass weighted average sizes for 0.5 mm, 2 mm and 9.5 mm raw and the 9.5 mm pretreated MHW particle sizes samples were 0.41 mm, 0.59 mm, 1.8 mm and 1.1 mm, respectively. Similarly the estimated mass weighted average particle sizes for the 0.5 mm, 2 mm, 9.5 mm raw and pretreated SG samples were 0.32 mm, 0.55 mm, 1.9 mm and 0.8 µm, respectively. Since the pretreated biomass was created from 9.5 mm screened raw biomass, we observed 40% and 55% size reduction

Table 4.2. Values of x_R and m in equation 4.4 for different biomass after nonlinear data fitting

Biomass Types	0.5 mm raw		2mm raw		9.5 mm raw		Pretreated biomass	
	x_R (mm)	m	x_R (mm)	m	x_R (mm)	m	x_R (mm)	m
MHW	0.48	2.34	0.65	3.28	2.25	1.72	1.39	1.76
SG	0.36	3.02	0.62	3.27	2.24	1.97	1.05	1.5

Table 4.3. Mass weighted average particle sizes of raw and pretreated MHW and SG

Biomass Types	Mass weighted average particle sizes (mm)			
	0.5 mm raw	2 mm raw	9.5 mm raw	Pretreated biomass
MHW	0.41	0.59	1.8	1.1
SG	0.32	0.55	1.9	0.8

for pretreated MHW and SG compared to raw biomass. In other words, pretreatment can significantly reduce the biomass particle size.

4.3.3. Elution curve reproducibility and probe entrapment study

For both raw and pretreated biomass the resulting elution curves were highly reproducible. This is illustrated in Figure 4.3 PEG1000 and blue dextran elution curves, with error bars, for 9.5 mm raw and pretreated MHW. Tabulated in Table 4.4 are the total accessible volumes for raw MHW and pretreated MHW obtained from the different PEGs. The low standard deviations and coefficient of variance for the triplicate runs illustrate the high level of reproducibility that can be obtained with this chromatography approach.

To assess whether there was any entrapment of PEGs in the column during the elution of the probes, mass balances were determined for the loading and elution profiles. Probe entrapment ratio (PE%) can be calculated as follows:

$$PE\% = 1 - \frac{M_2}{M_1} = 1 - \frac{C_0 V_{t,2}}{C_0 V_{t,1}} = 1 - \frac{V_{t,2}}{V_{t,1}} \quad (4.5)$$

Where M_1 is the total solute mass loaded in the column (mg), M_2 is the total solute mass eluted out of the column (mg), C_0 is the bulk solute concentration (mg ml^{-1}), $V_{t,1}$ is the

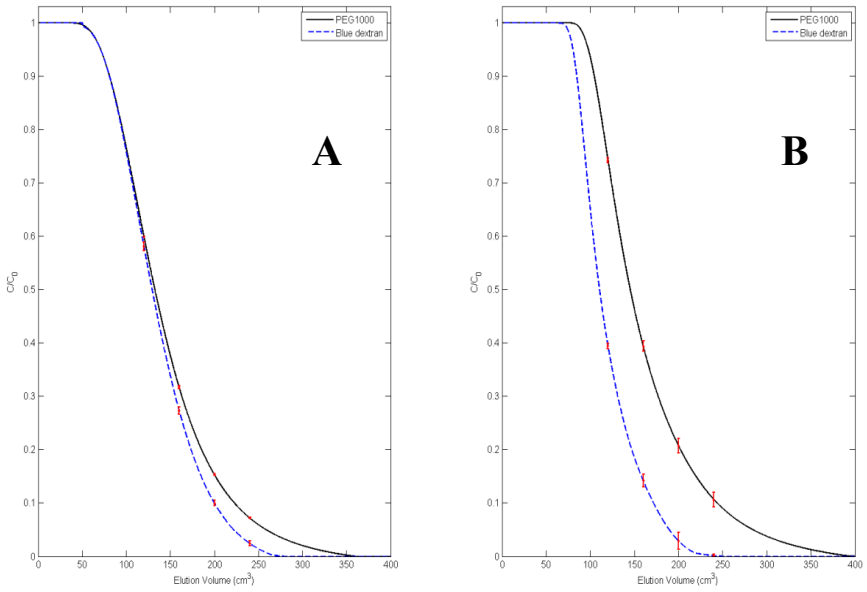

Figure 4.3. PEG1000 and blue dextran elution curves with error bars for 9.5 mm raw (A) and pretreated (B) MHW.

Table 4.4. Total accessible volume (V_{total}) in columns packed with raw and pretreated MHW

Probe	Raw MHW (9.5mm)			Pretreated MHW		
	Mean V_{total} (cm^3)	Standard deviation (cm^3)	Coefficient of Variance	Mean V_{total} (cm^3)	Standard deviation (cm^3)	Coefficient of Variance
PEG1000	149.0	1.8	1.2%	167.6	3.2	1.9%
PEG3350	143.6	0.1	0.1%	161.7	2.5	1.5%
PEG8000	141.1	0.7	0.5%	151.5	0.8	0.5%
PEG20000	137.6	0.3	0.2%	138.0	0.7	0.5%
PEG35000	136.8	0.7	0.5%	133.8	2.0	1.5%
Blue Dextran	135.1	1.6	1.2%	119.7	1.0	0.8%

total accessible volume (TAV) calculated from loading curves (ml), and $V_{t,2}$ is the total accessible volume (TAV) calculated from elution curves (ml). The bulk solute concentration is assumed to be the same before and after elution. Therefore, entrapment ratio is related to the ratio of $V_{t,2}$ to $V_{t,1}$. Integrating over the loading and elution curves can generate the values of $V_{t,1}$ and $V_{t,2}$. The results of this calculation are reported in Table 4.5 showing no significant probe entrapment. For all eight types of biomass measured, on average 1% probe entrapment ratio is observed. This low probe entrapment ratio was demonstrated throughout the entire range of PEG molecules and all measured biomass types, allowing for a precise characterization of elution volumes.

4.3.4. Specific pore volume

Illustrated in Figure 4.4 are the elution curves for the smallest, PEG1000, and the largest probe, PEG35000. Total accessible pore volume of the packed biomass can be calculated from those curves. Specific pore volume is defined as the pore volume per gram of dry biomass accessible to a certain probe. Presented in Figure 4.5 are the specific pore volume results obtained for mixed MHW (A) and SG (B) for all biomass and probes. As the solute size increases, the specific pore volume of all types of biomass decreases. For MHW, size reduction yields a modest gain in specific pore volume accessible for probes of 5.43 nm and larger but comparable specific pore. It is clear that pretreatment significantly increased specific pore volume for both MHW and SG. Over the probe size

Table 4.5. Solute retention ratio in column packed with MHW and SG for different probes

Probes	Solute retention ratio in MHW				Solute retention ratio in SG			
	Raw (9.5mm)	Raw (2mm)	Raw (0.5mm)	Pretreated	Raw (9.5mm)	Raw (2mm)	Raw (0.5mm)	Pretreated
PEG1000	0.38%	0.52%	3.00%	0.20%	1.63%	0.63%	0.43%	2.10%
PEG3350	1.67%	-0.20%	-0.30%	1.38%	1.41%	0.25%	1.78%	1.06%
PEG8000	0.99%	1.40%	1.90%	0.59%	0.84%	0.81%	0.90%	0.95%
PEG20000	1.35%	1.33%	1.10%	0.56%	1.29%	-0.28%	0.56%	0.45%
PEG35000	1.68%	0.84%	1.10%	0.98%	0.37%	0.75%	0.03%	0.71%
Blue dextran	0.69%	0.33%	1.50%	2.73%	0.93%	1.98%	1.78%	3.20%

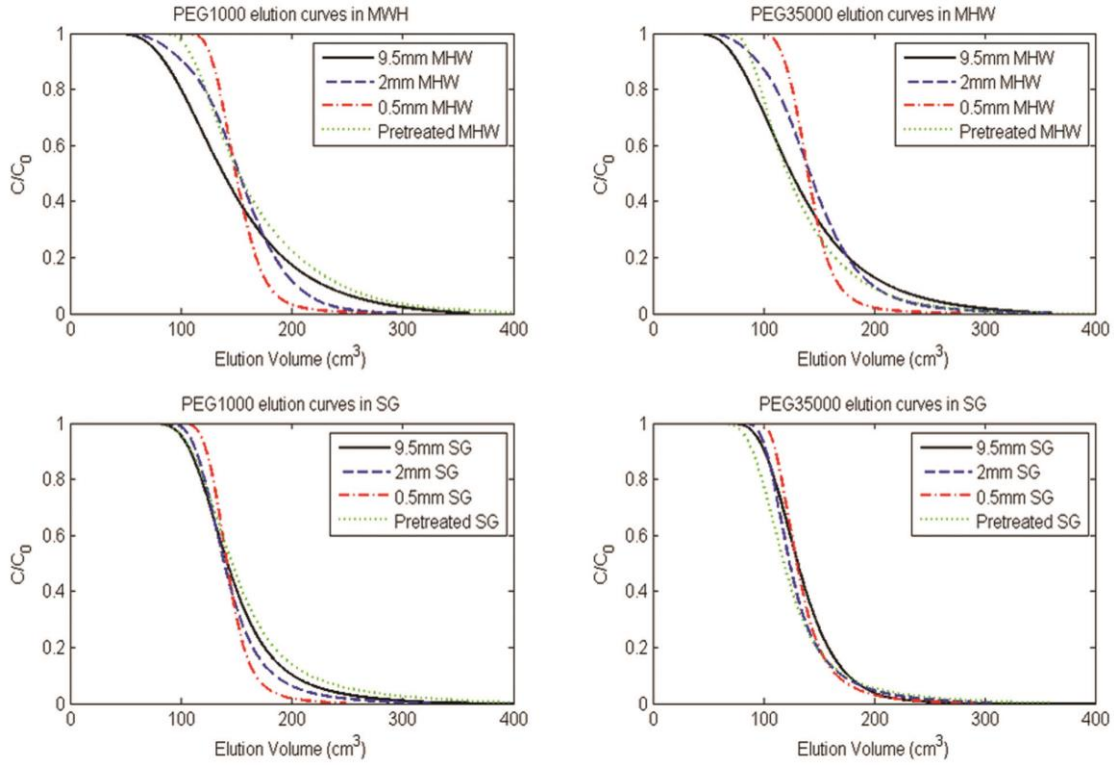

Figure 4.4. Elution curves obtained for PEG1000 and PEG35000 for several raw and pretreated biomass materials.

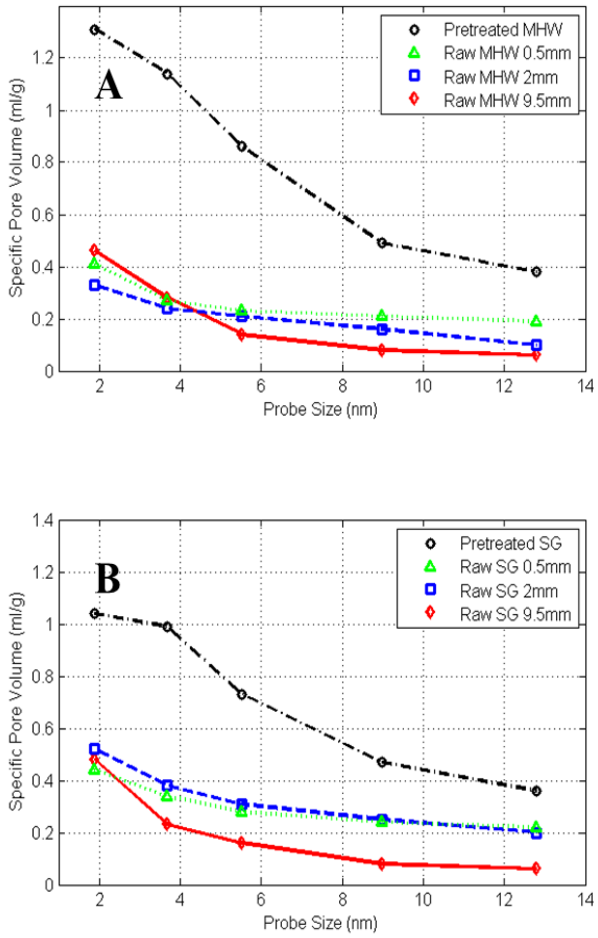

Figure 4.5. Specific pore volume distribution for size reduced and pretreated MHW (A) and SG (B) volume accessible for smaller probes.

range of 1.89 nm to 12.78 nm, specific pore volumes for pretreated MHW increased by a factor of 3 to 2, while for SG over the same range increased by a factor of 2 to 1.5. The measured specific pore volumes for MHW are comparable to those obtained by Grethlein (Grethlein, 1985) where dilute acid pretreatment of MHW yielded a specific pore volume of 0.69 ml/g accessible for 5.1 nm probe compared to 0.71 ml/g based on extrapolation of results. Specific pore volume data was fitted to the following power function using nonlinear regression to generate equation for estimating accessible pore volume for different size probes:

$$V_p = a * \emptyset_p{}^b \tag{4.6}$$

Where V_p is the specific pore volume accessible for a certain probe (ml/g), and $\emptyset_p$ is the probe diameter (nm). Nonlinear parameter estimation was performed using the *lsqnonlin* function in Matlab® (R2011B, Mathworks, Natick, MA) with Trust-region-reflective algorithm. Listed in Table 4.6 are the estimates for "a" and "b" for the eight different biomass studied. The fitted equations resulting from all eight types of biomass are shown in Figure 4.6(A) and Figure 4.6(B). In general, this parameter estimation exercise yields good R^2 values.

From Figure 4.5 it is clear that the 9.5 mm raw MHW and SG materials exhibited a much more rapid decrease in pore volume with increasing probe size. Table 4.6 shows that

Table 4.6. Values of a, b, and r in Equation 4.6 for the pore volume distributions

Type of biomass	a (ml/g)	b	R^2
Raw MHW (9.5mm)	0.898	-1.016	0.978
Raw MHW (2mm)	0.467	-0.516	0.964
Raw MHW (0.5mm)	0.521	-0.436	0.949
Pretreated MHW	1.998	-0.557	0.897
Raw SG (9.5mm)	0.958	-1.086	0.998
Raw SG (2mm)	0.710	-0.485	0.998
Raw SG (0.5mm)	0.557	-0.381	0.994
Pretreated SG	1.532	-0.480	0.857

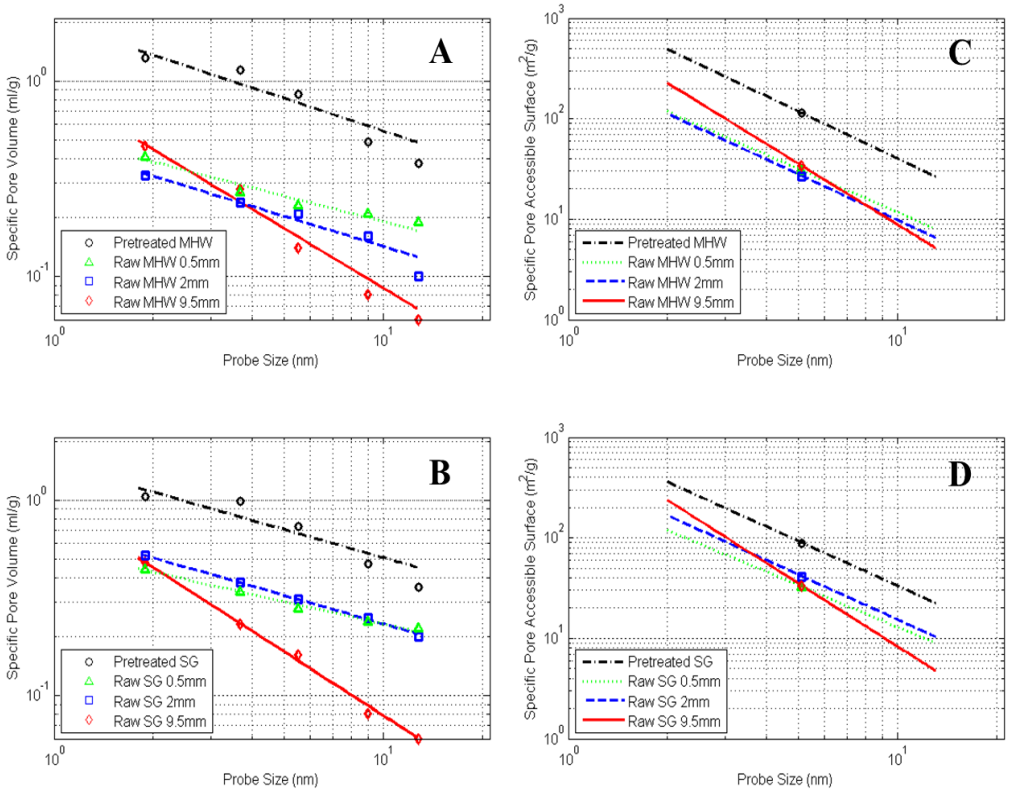

Figure 4.6. Specific pore volume as a function of probe size for MHW (A) and SG (B), and specific pore accessible surface as a function of probe size for MHW (C) and SG (D).

estimates of "b" for the 9.5 mm materials, which represent the slope of the lines in Figure 4.6(A) and Figure 4.6(B), are twice that of the smaller particles. However, pretreated biomass showed a comparable "b" values to those of 2 mm and 0.5 mm biomass. This may due to the combined effects from size reduction and chemical reaction during pretreatment process. As we showed earlier the average sizes of pretreated biomass were smaller than the average sizes of 9 mm biomass particles. Meanwhile the biphasic pretreatment created larger pores everywhere and vertically shift the curves upward in Figure 4.6(A) and Figure 4.6(B).

4.3.5. Specific pore surface area

It is important to quantify the specific pore surface area in biomass since CWDEs need to bind to these areas to start hydrolysis reaction. In order to compare estimated surface area data to those in previous publications, we assumed parallel plate pore geometry, in which the pore surface area is related to pore volume as follows (Stone et al., 1969),

$$\Delta A_{m\to n} = \frac{2000 * \Delta V_{m\to n}}{(\emptyset_m + \emptyset_n)/2} \tag{4.7}$$

Where $\Delta A_{m\to n}$ is the incremental pore surface area when pore width increases from m to n (m^2/g), $\Delta V_{m\to n}$ is the incremental pore volume when pore width increases from m to n (ml/g), $\emptyset_m$ and $\emptyset_n$ are the sizes of two neighbor probes used and $(\emptyset_m+\emptyset_n)/2$ is the average pore width over this size range (nm). After substituting dV_p from the derivative

of Equation 4.6 for $\Delta V_{m\rightarrow n}$ in Equation 4.7, Equation 4.7 can be integrated to obtain the surface area as a function of probe diameter. The result is shown in the following equation:

$$A = a_1 * \emptyset_p{}^{b_1} = \frac{2000ab}{b-1} * \emptyset_p{}^{b-1} \tag{4.8}$$

Where A is the specific pore surface area (m^2/g) accessible to probe with diameter $\emptyset_p$ (nm). a and b are parameters fitted from Equation 4.6. Figure 4.6(C) and Figure 4.6(D) showed a plot of the accumulative accessible surface area for all eight types of biomass as a function of probe size. Minimal or no surface area increase from size reduction is observed for both MHW and SG. However, pore surface area increase due to pretreatment was observed. Pore surface areas accessible to 5.1 nm probes are marked in Figure 4.6(C) and Figure 4.6(D). For pretreated MHW, this area is 120 m^2/g compared to 20-30 m^2/g for raw MHW with different sizes. For pretreated SG, this area is 90 m^2/g compared to 20-30 m^2/g for raw SG with different sizes. As a basis for comparison, literature values for surface area accessible to a 5.1 nm probe are provided in Table 4.7. The biomass particle sizes in those experiments are in the range of 0.25 mm to 0.5 mm, which is significantly smaller than the first two particle sizes (9.5 mm, 2 mm) in this study. Despite this size difference, these surface area values are in fairly good agreement with our results.

Table 4.7. Values of the specific surface area for 5.1 nm probes in lignocellulosic biomass

Substrate	Specific Surface Area (m^2/g)	Particle size (mm)	References
Acid swollen cotton	10-100	0.42	(Stone et al., 1969)
Steam treated wood pulp	55-61	0.42	(Stone et al., 1969)
Untreated hardwood	10.5	0.25	(Grethlein, 1985)
Acid pretreated hardwood	37-140	0.25	(Grethlein, 1985)
Alkaline peroxide treated mixed hardwood	66-71	0.25	(Thompson et al., 1992)
Dilute acid treated mixed hardwood	86-128	0.25	(Thompson et al., 1992)
Sulfite pretreated (SPORL) lodgepole pine	32-40	<1mm	(Wang et al., 2012)

4.3.6. Pore size change mechanism

We observed increasing pore volume accessible to larger probes caused by biomass particle size reduction from 9.5 mm to 2 mm. One hypothesis for this result is that there are two types of pores, types A and B, as illustrated in Figure 4.7. Type A pores have narrow tunnels connecting to the outside space ("ink bottle"). These tunnels are not wide enough for large probes (i.e. PEG8000, PEG20000, PEG35000) to enter the more spacious inner space. Type B pores have large pore entrances to accommodate large probes. However, the pore width decreases as it goes deeper inside the biomass ("wine glass"). These entrance areas are connected by a narrow tunnel which does not allow larger probes to enter. During the size reduction process, the large biomass particles are broken up into smaller ones and the spacious inner space in type A pores is then exposed and becomes accessible to large probes. However no additional pore space to large probes is created from type B pores because the new exposed inner tunnel is still too narrow. Meanwhile the total volume accessible to small probes (i.e. PEG1000, PEG3350) is not influenced by size reduction. This agrees with the experimental result shown in Figure 4.5. During the pretreatment process, the chemical reagents can diffuse into all pore spaces and create larger pores, which lead to larger pore volume accessibility to both small and large probes than raw biomass. Pretreatment can also reduce the average particle size by 40% to 55% as shown earlier. The combination of these two effects from pretreatment leads to a much higher accessible pore volume than raw biomass.

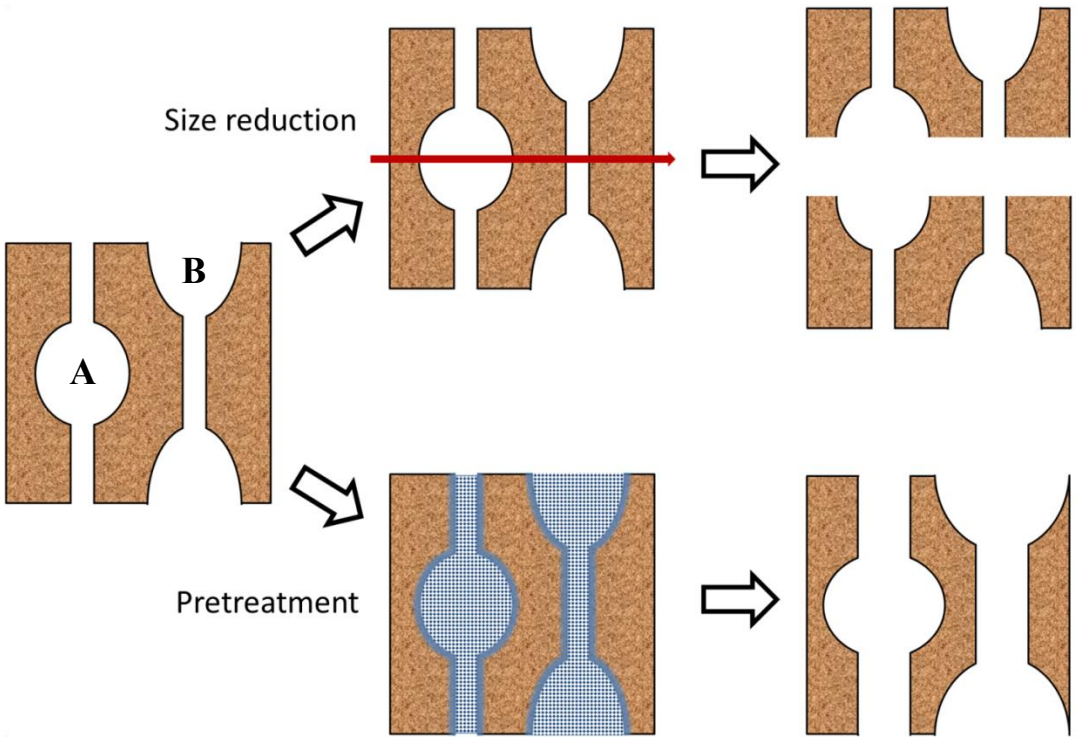

Figure 4.7. Proposed pore volume increase mechanisms resulting from size reduction and pretreatment.

4.4. Conclusions

Experimental results showed size reduction from 2 mm to 0.5 mm did not increase pore volume in either MHW or SG. This means that very little surface area is created for enzyme binding, and that the energy investment to reduce the particle size can be avoided. Besides, Vidal et al. reported that milling mixed hardwood and switchgrass to pass through 2 mm screen requires up to 130 kWh/ton dry biomass, which is equivalent to more than 5% of the energy theoretically recovered from ethanol if it is produced (Vidal et al., 2011). Further size reduction of the 2 mm biomass can increase the energy consumption to an even higher level (Zhang et al., 2012; Zhu et al., 2010). Therefore, it is not recommended that biomass particle size be reduced below 2 mm.

The solute exclusion technique developed in this paper is a fast and precise method for measuring accessible pore volumes and surface area in raw and pretreated lignocellulosic biomass. Elution curves are highly reproducible and probe entrapment is negligible. Further size reduction of the biomass to less than 2 mm cannot significantly alter the pore size distribution. Pretreatment can increase accessible pore volume by 200% and 100% for MHW and SG over the whole measurement range, respectively. The method we developed can be applied in future research to assess biomass morphology changes during hydrolysis and build relationship between pore structure changes and hydrolysis rate/extent.

4.5. References

Arantes V, Saddler J. 2011. Cellulose accessibility limits the effectiveness of minimum cellulase loading on the efficient hydrolysis of pretreated lignocellulosic substrates. Biotechnology for Biofuels 4(1):3.

Armstrong JK, Wenby RB, Meiselman HJ, Fisher TC. 2004. The Hydrodynamic Radii of Macromolecules and Their Effect on Red Blood Cell Aggregation. Biophysical Journal 87(6):4259-4270.

.

Bitra VSP, Womac AR, Yang YT, Igathinathane C, Miu PI, Chevanan N, Sokhansanj S. 2009. Knife mill operating factors effect on switchgrass particle size distributions. Bioresource Technology 100(21):5176-5188.

Bothwell MK, Daughhetee SD, Chaua GY, Wilson DB, Walker LP. 1997. Binding capacities for Thermomonospora fusca E3, E4 and E5, the E3 binding domain, and Trichoderma reesei CBHI on Avicel and bacterial microcrystalline cellulose. Bioresource Technology 60(2):169-178.

Chandra R, Ewanick S, Hsieh C, Saddler JN. 2008. The characterization of pretreated lignocellulosic substrates prior to enzymatic hydrolysis, part 1: A modified Simons' staining technique. Biotechnology Progress 24(5):1178-1185.

Corner CV. 2003. A size-exclusion chromatography system for observing the transport and weak binding of Thermobifida Fusca catalytic domains: Experiemntal and theoretical investigation. Ph.D. Dissertation, Cornell University, Ithaca.

Esteghlalian AR, Bilodeau M, Mansfield SD, Saddler JN. 2001. Do enzymatic hydrolyzability and simons' stain reflect the changes in the accessibility of lignocellulosic substrates to cellulase enzymes? Biotechnology Progress 17(6):1049-1054.

Fan LT, Lee Y-H, Beardmore DH. 1980. Mechanism of the enzymatic hydrolysis of cellulose: Effects of major structural features of cellulose on enzymatic hydrolysis. Biotechnology and Bioengineering 22(1):177-199.

Fan LT, Lee YH, Beardmore DR. 1981. The influence of major structural features of cellulose on rate of enzymatic hydrolysis. Biotechnology and Bioengineering 23(2):419-424.

Gokarn YR. 2003. Hydrodynamic Behavior and Thermal Stability of a PEGylated Protein: Studies with Hen Egg Lysozyme: University of New Hampshire (Department of Biochemistry and Molecular Biology).

Grethlein HE. 1985. The effect of pore size distribution on the rate of enzymatic hydrolysis of cellulosic substrates. Nat Biotech 3(2):155-160.

Grous WR, Converse AO, Grethlein HE. 1986. Effect of steam explosion pretreatment on pore size and enzymatic hydrolysis of poplar. Enzyme and Microbial Technology 8(5):274-280.

Jeoh T, Ishizawa CI, Davis MF, Himmel ME, Adney WS, Johnson DK. 2007. Cellulase digestibility of pretreated biomass is limited by cellulose accessibility. Biotechnology and Bioengineering 98(1):112-122.

Jeoh T, Wilson DB, Walker LP. 2002. Cooperative and Competitive Binding in Synergistic Mixtures of Thermobifida fuscaCellulases Cel5A, Cel6B, and Cel9A. Biotechnology Progress 18(4):760-769.

Kawakubo T, Karita S, Araki Y, Watanabe S, Oyadomari M, Takada R, Tanaka F, Abe K, Watanabe T, Honda Y and others. 2010. Analysis of exposed cellulose surfaces in pretreated wood biomass using carbohydrate-binding module (CBM)–cyan fluorescent protein (CFP). Biotechnology and Bioengineering 105(3):499-508.

Lee SB, Shin HS, Ryu DDY, Mandels M. 1982. Adsorption of cellulase on cellulose: Effect of physicochemical properties of cellulose on adsorption and rate of hydrolysis. Biotechnology and Bioengineering 24(10):2137-2153.

Lin JK, Ladisch MR, Patterson JA, Noller CH. 1987. Determining pore size distribution in wet cellulose by measuring solute exclusion using a differential refractometer. Biotechnology and Bioengineering 29(8):976-981.

Luo X, Zhu JY. 2011. Effects of drying-induced fiber hornification on enzymatic saccharification of lignocelluloses. Enzyme and Microbial Technology 48(1):92-99.

Luterbacher JS, Tester JW, Walker LP. 2012. Two-temperature stage biphasic CO2–H2O pretreatment of lignocellulosic biomass at high solid loadings. Biotechnology and Bioengineering 109(6):1499-1507.

Mansfield SD, Mooney C, Saddler JN. 1999. Substrate and enzyme characteristics that limit cellulose hydrolysis. Biotechnology Progress 15(5):804-816.

Mooney CA, Mansfield SD, Touhy MG, Saddler JN. 1998. The effect of initial pore volume and lignin content on the enzymatic hydrolysis of softwoods. Bioresource Technology 64(2):113-119.

Moran-Mirabal JM, Bolewski JC, Walker LP. 2011. Reversibility and binding kinetics of Thermobifida fusca cellulases studied through fluorescence recovery after photobleaching microscopy. Biophysical Chemistry 155(1):20-28.

Murdock RC, Braydich-Stolle L, Schrand AM, Schlager JJ, Hussain SM. 2008. Characterization of Nanomaterial Dispersion in Solution Prior to In Vitro Exposure Using Dynamic Light Scattering Technique. Toxicological Sciences 101(2):239-253.

Neuman RP, Walker LP. 1992a. Solute exclusion from cellulose in packed columns: Experimental investigation and pore volume measurements. Biotechnology and Bioengineering 40(2):218-225.

Neuman RP, Walker LP. 1992b. Solute exclusion from cellulose in packed columns: Process modeling and analysis. Biotechnology and Bioengineering 40(2):226-234.

Park S, Venditti RA, Abrecht DG, Jameel H, Pawlak JJ, Lee JM. 2007. Surface and pore structure modification of cellulose fibers through cellulase treatment. Journal of Applied Polymer Science 103(6):3833-3839.

Piccolo C, Wiman M, Bezzo F, Lidén G. 2010. Enzyme adsorption on SO2 catalyzed steam-pretreated wheat and spruce material. Enzyme and Microbial Technology 46(3–4):159-169.

Rosin P, Rammler E. 1933. The laws governing the fineness of powdered coal. Journal of the Institute of Fuel 7:29-36.

Sinitsyn A, Gusakov A, Vlasenko E. 1991. Effect of structural and physico-chemical features of cellulosic substrates on the efficiency of enzymatic hydrolysis. Applied Biochemistry and Biotechnology 30(1):43-59.

Stone JE, Scallan AM, Donefer E, Ahlgren E. 1969. Digestibility as a simple function of a molecule of similar size to a cellulase enzyme. Cellulases and Their Applications: AMERICAN CHEMICAL SOCIETY. p 219-241.

Tanaka M, Ikesaka M, Matsuno R, Converse AO. 1988. Effect of pore size in substrate and diffusion of enzyme on hydrolysis of cellulosic materials with cellulases. Biotechnology and Bioengineering 32(5):698-706.

Thompson DN, Chen H-C, Grethlein HE. 1992. Comparison of pretreatment methods on the basis of available surface area. Bioresource Technology 39(2):155-163.

Vaezi, Mahdi, Pandey, Vivek, Kumar, Amit, Bhattacharyya, Souvik. 2013. Lignocellulosic biomass particle shape and size distribution analysis using digital image processing for pipeline hydro-transportation. Kidlington, ROYAUME-UNI: Elsevier. 16 p.

Vidal B, Dien B, Ting K, Singh V. 2011. Influence of feedstock particle size on lignocellulose conversion—a review. Applied Biochemistry and Biotechnology 164(8):1405-1421.

Walker LP, Wilson DB. 1991. Enzymatic hydrolysis of cellulose: An overview. Bioresource Technology 36(1):3-14.

Walker LP, Wilson DB, Irvin DC, McQuire C, Price M. 1992. Fragmentation of cellulose by the major Thermomonospora fusca cellulases, Trichoderma reesei CBHI, and their mixtures. Biotechnology and Bioengineering 40(9):1019-1026.

Wang QQ, He Z, Zhu Z, Zhang YHP, Ni Y, Luo XL, Zhu JY. 2012. Evaluations of cellulose accessibilities of lignocelluloses by solute exclusion and protein adsorption techniques. Biotechnology and Bioengineering 109(2):381-389.

Weimer PJ, Lopez-Guisa JM, French AD. 1990. Effect of cellulose fine structure on kinetics of its digestion by mixed ruminal microorganisms in vitro. Applied and Environmental Microbiology 56(8):2421-2429.

Wong KKY, Deverell KF, Mackie KL, Clark TA, Donaldson LA. 1988. The relationship between fiber-porosity and cellulose digestibility in steam-exploded Pinus radiata. Biotechnology and Bioengineering 31(5):447-456.

Yan H, Barbosa-Cánovas GV. 1997. Size characterization of selected food powders by five particle size distribution functions Caracterización del tamaño de partícula de alimentos en polvo mediante cinco funciones de distribuciones de tamaño. Food Science and Technology International 3(5):361-369.

Yang D, Moran-Mirabal JM, Parlange J-Y, Walker LP. 2013. Investigation of the porous structure of cellulosic substrates through confocal laser scanning microscopy. Biotechnology and Bioengineering 110(11):2836-2845.

Zhang M, Song X, Deines TW, Pei ZJ, Wang D. 2012. Biofuel Manufacturing from Woody Biomass: Effects of Sieve Size Used in Biomass Size Reduction. Journal of Biomedicine and Biotechnology 2012:9.

Zhu JY, Wang GS, Pan XJ, Gleisner R. 2009. Specific surface to evaluate the efficiencies of milling and pretreatment of wood for enzymatic saccharification. Chemical Engineering Science 64(3):474-485.

Zhu P. 2012. Signal Processing In Single Molecule Studies. Ithaca: Cornell University.

Zhu P, Moran-Mirabal J, Luterbacher J, Walker L, Craighead H. 2011. Observing Thermobifida fusca cellulase binding to pretreated wood particles using time-lapse confocal laser scanning microscopy. Cellulose 18(3):749-758.

Zhu W, Zhu JY, Gleisner R, Pan XJ. 2010. On energy consumption for size-reduction and yields from subsequent enzymatic saccharification of pretreated lodgepole pine. Bioresource Technology 101(8):2782-2792.

5. ASSESSMENT OF PORE SIZE DISTRIBUTION CHANGE DURING THE HYDROLYSIS PROCESS TO ELUCIDATE THE INTRINSIC HYDROLYSIS MECHANISMS OF CWDEs

5.1. Introduction

A strong linear correlation between accessible pore surface area and the initial rate and extent of hydrolysis has been documented for a wide range of biomass substrates (Grethlein, 1985; Grous et al., 1986; Mansfield et al., 1999; Mooney et al., 1998). This is consistent with the heterogeneous catalysis framework that defines the transport and binding of cell-wall-degrading-enzymes (CWDEs) to the various insoluble cellulosic fibers, mats and particles that represent the three dimensional structure of cellulosic biomass (Walker and Wilson, 1991; Moran-Mirabal et al. 2011; Luterbacher et al. 2013; Yang et al 2013). However, the CWDEs-cellulose reaction system differs from classical heterogeneous catalysis framework in that the CWDEs are modifying the three dimensional structure of the particles through the fragmentation of cellulosic particles (Walker et al., 1992; Walker et al., 1990) and through altering the localize density of the biomass (Luterbacher et al., 2013). This would imply that the accessibility of the biomass to CWDEs is likely to change dramatically over the course of enzymatic hydrolysis, and that understanding the temporal changes in accessibility is essential for elucidating the CWDEs-cellulose reaction system.

Physical and morphological modifications of biomass substrate during enzymatic hydrolysis process have been investigated using different technologies (Eibinger et al.,

2014; Luterbacher et al., 2013; Walker et al., 1992). Using a particle counter it was found that Avicel PH102 particles, which passed through the 150 mesh sieve and collected on the 200 mesh sieve, underwent physical fragmentation. This was observed by the increase in the numbers of cellulose particles and the shift in the particle volume distribution towards the smaller size range. It was also reported that endoglucanases played the main role in cellulose fragmentation although both endoglucanases and exoglucanases are capable of fragmenting cellulose (Walker et al., 1992; Walker et al., 1990). Another study, using fluorescence imaging and a confocal microscopy system, observed smaller particle being generated but also a 40% reduction in the BMCC particle density without significant change in the particle shape after 8 hr of hydrolysis (Luterbacher et al., 2013; Moran-Mirabal, 2013). From these observation it was concluded that the density of the BMCC decrease over the course of the reaction. Atomic force microscopy (AFM) has also been used to visualize the biomass surface modification by CWDEs (Bubner et al., 2013). An AFM study revealed the CWDES traffic jams on the cellulose fibrils and attributed it to the roughness of the crystalline cellulose surface (Igarashi et al., 2011). Other AFM studies showed the CWDEs system preferentially degraded the amorphous regions over the high crystalline regions of the ionic liquid treated Avicel, thus yielding a change in the surface morphology of cellulose microfibrils (Eibinger et al., 2014; Goacher et al., 2014).

Solute exclusion has been proven to be a particularly effective method for estimating accessible pore volume and pore surface area (Corner, 2003; Grethlein, 1985; Lin et al., 1987; Neuman and Walker, 1992; Yang et al., 2014). Inert probes are eluted through a

column packed with the substrate of interest. Analysis of the elution data can yield accessible pore volume of the packed substrate of interest for different size polyethylene glycol probes (PEGs), the most commonly used inert probes, that are comparable in size with CWDEs. In addition, this method avoids the intensive drying of the biomass, which is required for nitrogen adsorption surface area measurement, that can cause internal pore structure collapsing (Esteghlalian et al., 2001; Luo and Zhu, 2011; Neuman and Walker, 1992).

Many of the previous efforts to use solute exclusion chromatography investigated the relationship between initial pore structure and the initial hydrolysis extent of conversion. Here we reported on temporal changes in pore volume distribution during the course of enzymatic hydrolysis for pretreated and hydrolyzed mixed-hardwoods (MHW) and switchgrass (SG). A biomass hydrolysis model is proposed that integrated pore structure changes and the hydrolysis mechanisms. In addition, we assessed and quantified the influence of drying on biomass pore structure.

5.2. Method

5.2.1. Biomass pretreatment and enzymatic hydrolysis

Sized reduced MHW and SG was pretreated using bi-phasic CO_2 and H_2O (Luterbacher et al., 2012). Sixty grams of MHW or SG biomass that had passed through a 9.5 mm screen was mixed with deionized water to obtain the desired solids content of 40 wt%. The resulting 150 g slurry was loaded into a 1 L stirred reactor. Liquid CO_2 was then loaded into the reactor to achieve a pressure of 200 BAR and heated to 210°C. The

reactor contents were mixed to ensure uniform reactor conditions. The inner reactor temperature was maintained at 210 ± 3°C for 10 min before the reaction was stopped by flowing cold water through a cooling coil within the reactor to rapidly drop the reactor temperature and pressure before venting the CO_2.

Pretreated biomass samples (20 g wet) were extensively washed with deionized water, and hydrolyzed in a 10% (wt) solution of 50 mM sodium acetate buffer (pH 4.8) with 15 FPU/(g cellulose) of spezyme CP1 cellulases, 30 (mg protein)/(g cellulose) of Multifect1 xylanase (both from Genecor, Copenhagen, DK), and 30 CBU/(g cellulose) of Novo188 β-glucosidase (Novozyme, Davis, CA) at 50 °C. Samples of 150 µL were taken at 1, 2, 4, 6, 8, 12, 24 and 48 h. Hydrolysis was ended by heating the samples at 95°C for 5 min. Samples were analyzed for glucose, xylose, mannose, arabinose, furfural, and 5-hydroxymethylfurfural (5-HMF) using a Shimadzu liquid chromatography system (Shimadzu, Kyoto, Japan) with an Aminex P-Column (Biorad, Hercules, CA).

5.2.2. Biomass Proteinase K treatment and separation

Hydrolyzed biomass samples were loaded onto a Millipore glass vacuum filtration system with 0.2 um filter (EMD Millipore, Billerica, MA) to separate the biomass solids from the samples. The biomass solids were washed with 100 ml deionized water. This process was repeated three times before the biomass solids were rinsed with 30 mM Tris-HCl buffer (pH 8.2). The collected liquid samples were washed and kept for protein determination. The biomass solids were then treated with 0.1mg/ml Proteinase K (Thermo Scientific, Waltham, MA) in 100 ml Tris-HCl buffer (pH 8.2) at 37°C for 2 hr

to remove bound CWDEs. $CaCl_2$ (3 mM) was added to the buffer to increase the stability of Proteinase K. The 100 ml Proteinase K treated biomass solids were loaded onto the vacuum filtration system to separate the solids, which were washed with 100 ml deionized water. The process was repeated three times and the resulting wash solution samples were collected and assayed to determine protein concentration. The biomass solids were collected and prepared for solute exclusion column packing. To assess the degree of CWDEs removal by proteinase K, one tenth of the biomass samples were incubated with 10 ml Tris-HCl buffer only at 37°C for 2 hr again. Liquid was separated by vacuum filter and the solids were washed with 10 ml deionized water for two times and separated for solids and stored at 4°C before column packing. All the resulting wash solution samples were collected for protein measurement.

5.2.3. Determination of residual protein concentration

Liquid samples were filtered through 0.22 µm Spin-X® centrifuge tube filter (Swedesboro, NJ) and prepared for loading on a SDS-PAGE and for protein determination using Bradford reagent (Bradford, 1976; Rath et al., 2009; Shapiro et al., 1967). Thirty micro-liter liquid samples were mixed with 10 µL 4X SDS loading dye (4% β-mercaptoethanol, 0.16% bromophenol blue, 24% glycerol, 8% sodium dodecyl sulfate, 0.4M DL-Dithiothreitol, 200 mM Tris-Cl and 0.02M PMSF) and heat up to 95°C for 3 min using a heating block. Electrophoresis was performed in a vertical precast Ready Gel® (BioRad, Hercules, CA). Amounts of 10 µL samples were loaded into each well of the gel. The same volume of SeeBlu Plus-2 pre-stained standard marker (Life Technologies, Carlsbad, CA) was added in a separate well along with the samples. The

gels were composed of 12% resolving gel and 4% stacking gel and run at constant voltage of 120 volts for 40 min. After electrophoretic separation, the gel was stained with Coomassie Brilliant Blue R250® (Bio-Rad Laboratories, Inc., Hercules, CA) for 30 min at room temperature and subsequently destained in DI water over night.

The concentration of CWDEs in liquid samples was also quantitatively determined by Bradford assay using Coomassie Plus protein assay reagent and bovine serum albumin standards (Thermo Scientific, Waltham, MA). Amounts of 150 µl dye reagent and 150 µl standard/unknown sample solution were transferred and mixed into Costar® microplate (Corning, NY) wells and incubate at room temperature for 15 min. The absorbances at 595 nm of the standards, blanks, and unknown samples were measured by Synergy 2 spectrophotometer (Biotek, Winooski, VT). A standard curve was created by plotting the 595 nm absorbance of standard versus the protein concentration to determine the unknown sample concentration.

5.2.4. Biomass column packing and pore size measurements

Tricorn™ high performance column with 10 mm inner diameter and 100 mm length (GE Healthcare, Piscataway, NJ**)** was packed with pretreated and hydrolyzed biomass mixed-hardwood (PHMHW) and switchgrass (PHSG). A flow adapter with 7 µm frit screens was attached to the bottom of the column. Three hydrolysis times, 2, 8 and 48 hr, were used to generate PHMHW and PHSG for pore volume determination. Biomass separated by vacuum filtration was loaded into the column through a funnel connected to the top of the column. Approximately 3 g (dry weight) of biomass was packed into the column.

When the column was filled to within about 0.5 cm of the top, the funnel was removed and the top flow adapter with 7 μm frit screens was attached. The column was then mounted on a rack and stored in the refrigerator at 4°C for use.

The setup of solute exclusion column and pump/detector system is as described in Chapter 4. Polyethylene tubing was connected from a 2 L glass feed bottle to an online degasser and pump module to remove gas bubbles from the system. Fluorinated ethylene propylene (FEP) tubing was used to connect the pump module to the bottom of the column, and the top of the column to the refractive index (RI) detector to determine PEG concentrations.

Before loading solute into the column, 500 mL of degassed MilliQ water was pumped through the column to remove trapped air and soluble materials which might contribute a signal as the elute volume passed the refractive index detector (RID). The data acquisition system was initiated when the pump module started to deliver aqueous (4 g/L) PEG solutions from a feed bottle at 2 ml/min, and it was stopped when the concentration of the effluent reached a constant peak value. Then the feed bottle was filled with MilliQ water and the pump was turned on to start the elution process. The elution data was monitored until the RI value reached a constant value near 0. After completing the measurements with the probes the biomass was dried and weighed. Also as described in Chapter 4, the total accessible volume (V_T) for a certain solute is

$$V_T = \frac{M}{C_0} = \sum_{i=1}^{m} \frac{C_i}{C_0} V_i = \sum_{i=1}^{m} \frac{RI_i}{RI_0} V_i \qquad (5.1)$$

Where m is the number of elution aliquots measured for RI and V_i is a constant volume for each elution aliquot.

5.2.5. Biomass size distribution measurements

PHMHW and PHSG particle size distribution was obtained by using Sonic sifter model L3P (Advantech Manufacturing, Inc, New Berlin, WI). A vertical column of air separated particles by oscillating in a periodic vertical motion. This sifting method can produce very little abrasion which is important for retaining the biomass integrity used in the experiment (Yan and Barbosa-Cánovas, 1997). Five sieves with opening sizes from 75 μm to 2000 μm were used with amplitude of eight on the sifter. Two to three grams of biomass were loaded and sieved for 3 min. The mass difference of each sieve before and after sieving was determined for retained biomass.

5.3. Results

5.3.1. Enzymatic hydrolysis results for pretreated switchgrass and hardwood

Reported in Figure 5.1 are percent conversion of substrate into glucose values for PHSG and PHMHW measured over 48 hours. PHSG reached the plateau after 12 hr of hydrolysis, while it took 24 hr for PHMHW to reach the plateau. PHSG demonstrated faster initial hydrolysis rate for the first 6 hr with a percent conversion of 70% compared to 45% for PHMHW. At 48 hr PHSG had a 91% glucose conversion compared to 85% for PHMHW. Both substrates exhibited the standard drop-off in hydrolysis rate observed that has been extensive reported in the literature (Desai and Converse, 1997; Ohmine et al., 1983; van Zyl et al., 2011; Yang et al., 2006; Yu et al., 2012).

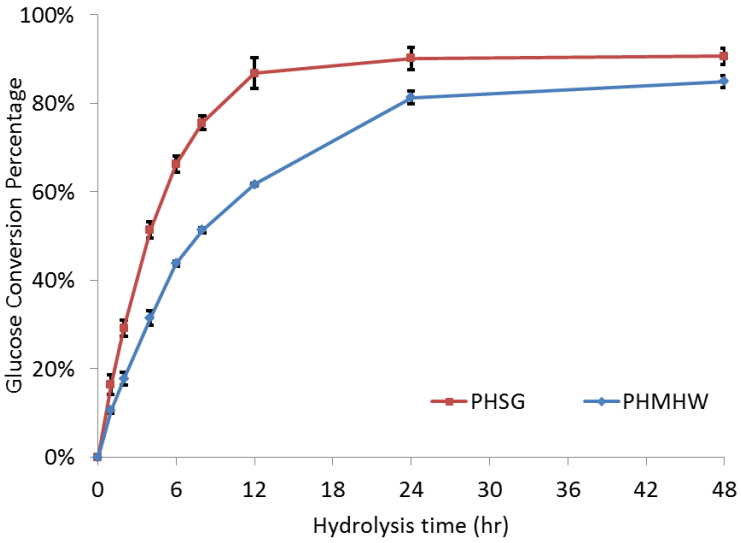

Figure 5.1. Glucose conversion percentages as function of hydrolysis time for both PHSG and PHMHW

A closer look at the PHMHW revealed that slopes of the curves in Figure 5.1 are changing rapidly over the course of the experiment. Three different hydrolysis rates can be extracted from the data set that would represent fast, moderate and slow reaction rates. For PHSG the time intervals that capture these rates are observed over 0 to 2, 2 to 6, and 6 to 12 hr for fast, moderate and slow rates, respectively. The three time intervals for PHMHW are 0 to 2, 2 to 6, and 6 to 24 hr. The resulting hydrolysis rates for these intervals are listed in Table 5.1. For PHSG the moderate rate is 36.3% lower than the fast hydrolysis rates, while for PHMHW the moderate rate is 26.3% lower. The slow hydrolysis rate is 76% lower than the fast rate for both PHSG and PHMHW. The fast rate for PHSG is 23% higher than that for PHMHW, where the differences in the hydrolysis rate between the moderate and slow rates for the two substrates are of the order of 5 to 8%. These results are consistent with Zhu *et al* that the plant biomass recalcitrance (PBR) of woody biomass is greater than herbaceous biomass (Zhu et al., 2010). PBR is related to the physical/pore structure, chemical components and their distributions within the plant cell wall, though it has never been quantitatively defined in the biomass research community (Silveira et al., 2013).

5.3.2. Proteinase K treatment of biomass to remove bound CWDEs

CWDEs treated biomass samples were loaded onto a Millipore All-Glass® vacuum filtration system with 0.22 um filter (EMD Millipore, Billerica, MA) to separate the liquid and solid fractions. The solids fractions were washed three times with deionized water. The liquid fractions were collected and filtered through 0.22 µm filter before loading on a SDS-PAGE gel and being compared with a SeeBlu Plus-2 marker to reveal

Table 5.1. Comparison of the hydrolysis rate of PHMHW and PHSG

PHMHW	Hydrolysis time interval (hr)	0 - 2	2-6	6-24
	Hydrolysis rate (g/l/hr)	2.97	2.19	0.70
PHSG	Hydrolysis time interval (hr)	0 - 2	2-6	6-12
	Hydrolysis rate (g/l/hr)	3.64	2.32	0.86

the unbound CWDEs (A1, A2, A3 in Figure 5.2). A2 and A3 showed significantly lighter band than the A1. It means after three washings most of the unbound CWDEs in the supernatant were removed.

Solid fraction samples were then treated with Proteinase K as described before. After the proteinase treatment, the solid and liquid fractions were separated using the vacuum filter system. The solids samples were washed twice with deionized water. The resulting three liquid samples were filtered and loaded on the SDS-PAGE gel (B1, B2, B3 in Figure 5.2). During the 2 hr Proteinase K treatment, it is expected that proteinase K degrades and fragments both the bound and unbound CWDEs. As a result, light-colored bands in Figure 5.2 (B1, B2, B3) indicated that only a very small amount of CWDEs existed in the supernatant after Proteinase K treatment and washing.

To assess the existence of bound CDWEs, the proteinase K treated and washed biomass was incubated with buffer in a shaker for 2 hr and then the solid was separated and washed two times following the same procedure as described before. The resulting three liquid samples were filtered and loaded on the SDS-PAGE gel (C1, C2, C3 in Figure 5.2). If significant amount of bound CWDEs still exist after proteinase K treatment, they would unbind and enter the supernatant in the aqueous system. In that case CWDEs bands should be observed on the SDS-PAGE gel as shown in Figure 5.2 A1 and B1. However, C1 in Figure 5.2 showed no CWDEs band. Thus it is reasonable for us to infer that most of the CWDEs have been removed by proteinase K.

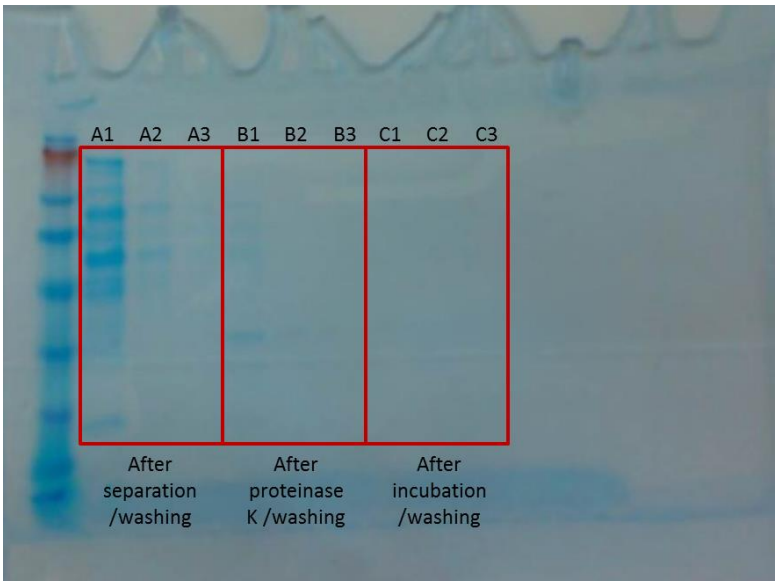

Figure 5.2. SDS-PAGE gel of supernatants separated from hydrolyzed switchgrass (A1-A3), proteinase treated switchgrass (B1-B3,C1-C3)

The CWDEs concentrations in all nine liquid samples were also quantitatively determined by Bradford assay using Coomassie Plus protein assay reagent. Protein concentration in supernatant after the first separation of hydrolyzed biomass (A1) is 176 µg/ml. After proteinase K treatment and buffer incubation the protein concentration in supernatant (C1) drops to 3.5 µg/ml, which means 98% decrease of proteins concentration. The Bradford assay results agree well with the results from SDS-PAGE gel. It showed that proteinase K treatment and washing can effectively remove CWDEs from the system.

5.3.3. Specific pore volume of hydrolyzed biomass

Presented in Figure 5.3 are the specific pore volume results obtained for hydrolyzed PHMHW (A) and PHSG (B) for all probes. As the solute size increases, the specific pore volumes decrease for both substrates. These results are consistent with those reported in Chapter 4, where the biomass pore volume was measured using a much larger solute exclusion column. The results in Figure 5.3 also show that the accessibility of the both substrate drops rapidly during the first 2 hr of hydrolysis. This drop is very acute for a probe of 5.4 nm, the nominal size of CWDEs, for both PHMHW and PHSG as shown in Figure 5.4. About 30% drop in the accessible pore volume was observed during the first 2 hr of hydrolysis for both substrates. However, after 2 hr the temporal patterns change dramatically for the two substrates with the accessible pore volume for PHMHW approaching a constant value (0.55 ml/g) while it continues to decrease for PHSG. Over a period of 48 hr the accessible pore volume for PHSG decreases by 60% to 0.28 ml/g.

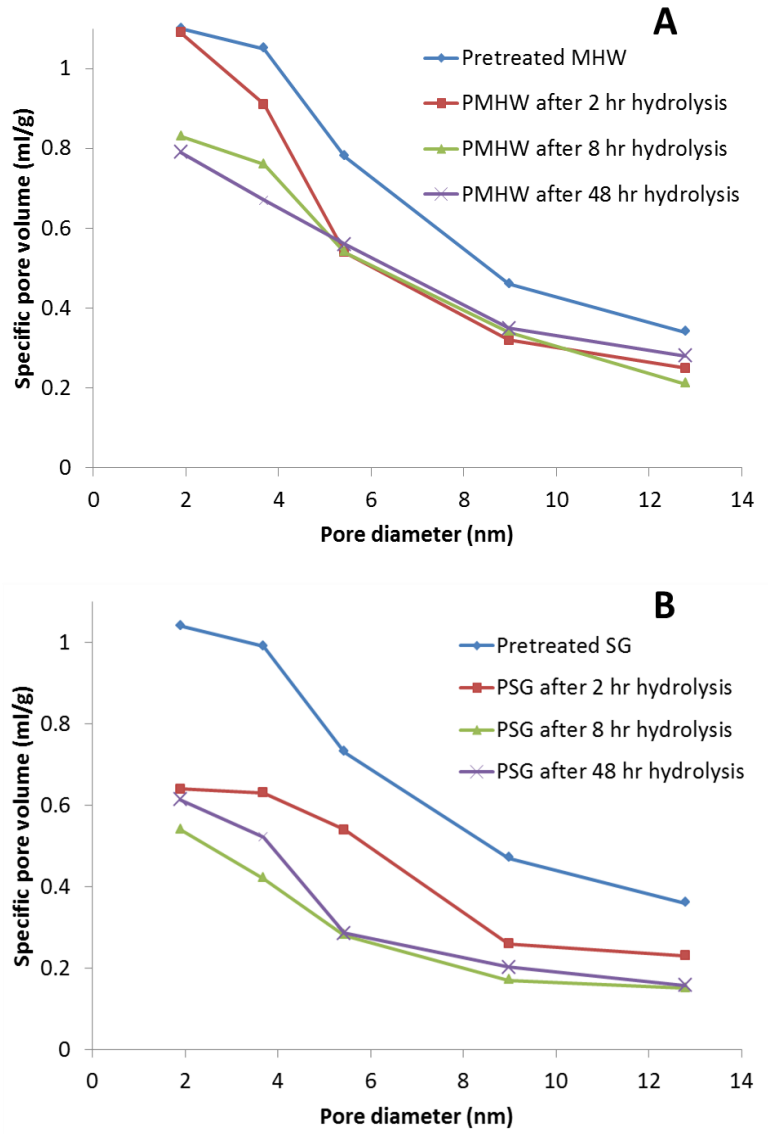

Figure 5.3. Specific pore volume as a function of probe size for pretreated and hydrolyzed HW (A) and SG (B)

As noted earlier, there is a strong correlation between the accessibility of the substrate and the rate of hydrolysis. This is evident when we compare the hydrolysis rate data in Table 5.1with the temporal change in specific pore volume report in Figure 5.4. The observed decrease in hydrolysis rate after 2hr, 26.3 and 36.3% for PHMHW and PHSG, respectively, correlates well with the 30% initial decrease in accessible pore volume reported in Figure 5.4. This is consistent with our heterogeneous catalysis framework where less accessible pore volume means less reactive surface area inside cellulose particle available for CWDEs to bind and react on, which leads to an overall decreasing in the reaction rate. Similarly, PHSG is consistent with our heterogeneous catalysis framework where the 60% decrease in the hydrolysis rates observed between the interval of 2-6 hr and 6-24 hr correlate well with the 54% accessible pore volume decrease. However, there was no such correlation with PHMHW where the pore volume did not change after 2 hr but the reaction rate drop 68%. This observation for PHMHW would suggest that some other factor is responsible for the decrease in the hydrolysis rate, such as enzyme deactivation and increasing cellulose crystallinity other than accessibility (Ciolacu et al., 2012; Eriksson et al., 2002; Fan et al., 1981; Ooshima et al., 1991; Ye et al., 2012; Zhang et al., 2010).

5.3.4. Biomass particle size distribution

Presented in Figure 5.5 are weight fractions retained by sieving screens for PHMHW and PHSG. Five screens were used (75 μm, 500 μm, 710 μm, 1000 μm and 2000 μm) and biomass weight proportions retained on each screen are shown in different colors. When pretreated MHW and SG are hydrolyzed for an extended time, the size distributions for

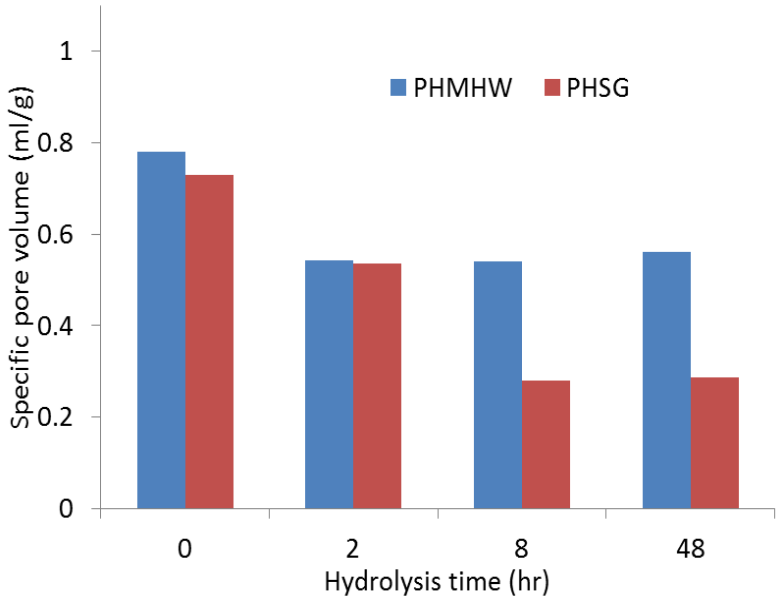

Figure 5.4. Relationship between specific pore volume available for 5.4 nm probe (PEG8000) and hydrolysis time for both pretreated MHW and SG

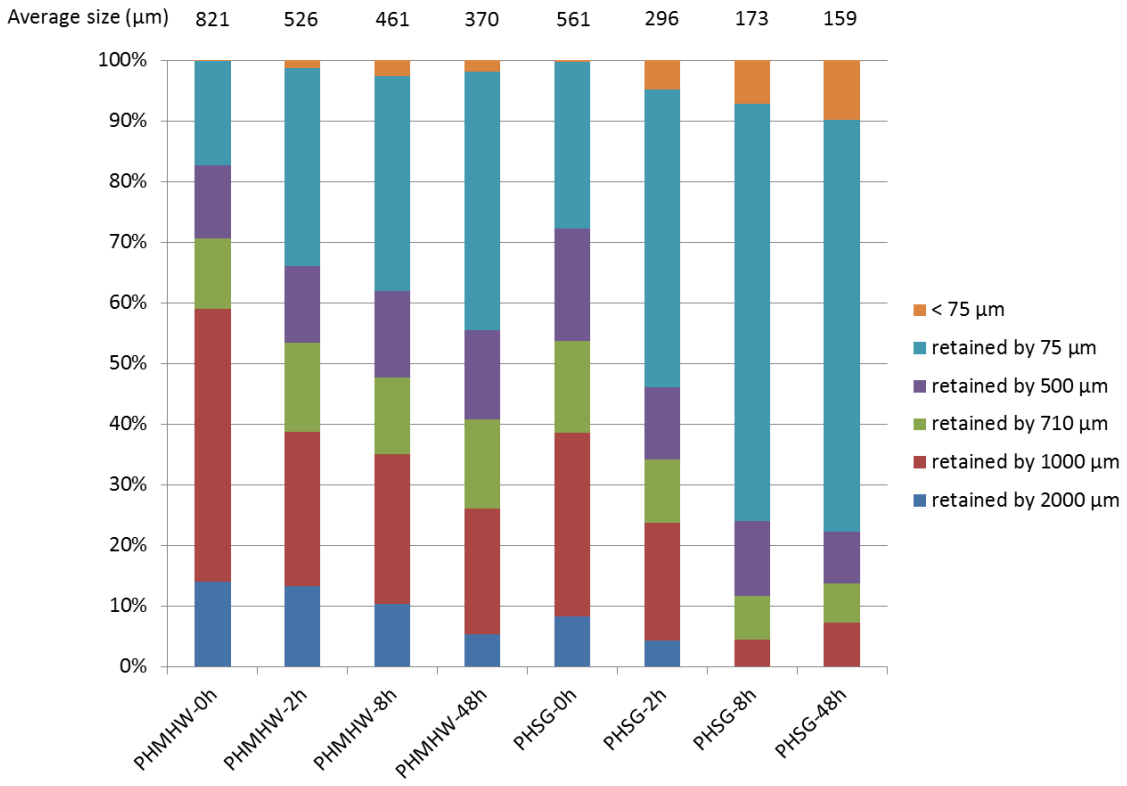

Figure 5.5. Weight percentages of biomass materials hydrolyzed for 0 to 48 hr retained on different screen sizes (75 µm, 500 µm, 710 µm, 1000 µm and 2000 µm). The mass weighted average sizes of the each biomass materials are listed on the top the bars.

both materials shift toward the smaller particle size range. A similar Rosin-Rammler (RR) approach as stated in Chapter 4 was used to calculate the mass weighted sizes for PHMHW and PHSG. The mass weighted average size for 0 h, 2 h, 8 h, 48 h hydrolyzed PHMHW were 821 μm, 526 μm, 461 μm and 370 μm, respectively. A 36% and 55% decrease in average particle size was observed after 2 h and 48 h of hydrolysis, which clearly showed that hydrolysis can significantly reduce the biomass particle size. Similarly the mass weighted average size for 0 h, 2 h, 8 h, 48 h hydrolyzed PHSG were 561 μm, 296 μm, 173 μm and 159 μm, respectively. Average particle size was reduced by 47% in 2 h and eventually 72% in 48 h.

The substrate size reduction during hydrolysis can be due to the combination of two effects. CWDEs bound to the substrate outer surface as visualized by AFM can degrade the surface layer and modify the surface morphology of cellulose microfibrils, thus reduce the size of substrate particles (Bubner et al., 2013; Eibinger et al., 2014; Goacher et al., 2014; Igarashi et al., 2011). CWDEs diffusing and binding to the substrate inner pore surface can initiate hydrolysis within the particle pores, leading to the density reduction and particle fragmentation (Luterbacher et al., 2012; Moran-Mirabal, 2013; Walker et al., 1992; Walker et al., 1990). Thus small particles can be released from the large biomass in this process.

5.3.5. The influence of drying

Presented in Figure 5.6 are plots of specific pore volume versus probe size for dried and un-dried PHMHW and PHSG, respectively, before hydrolysis and 2 hr after hydrolysis. It

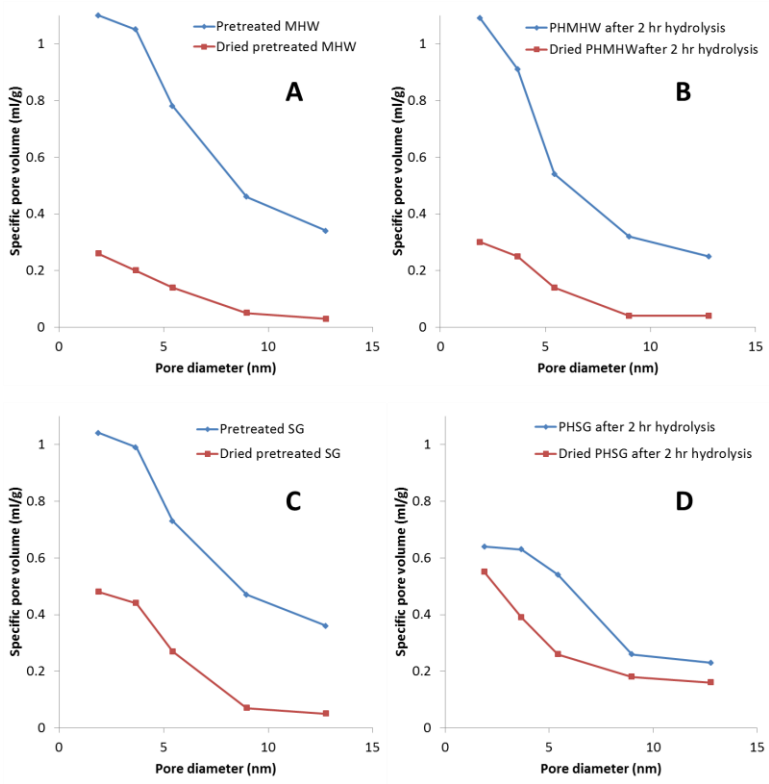

Figure 5.6. Specific pore volume as a function of probe size on Pretreated MHW (A), PHMHW after 2 hr hydrolysis (B), Pretreated SG (C) and PHSG after 2 hr hydrolysis (D) for assessing the influence of drying

is clear that drying significantly decreased specific pore volume for both PHMHW and PHSG. Over the probe size range of 1.89 nm to 12.78 nm, specific pore volumes for PHMHW decreased by 60% to 70%, while for PHSG over the same range most of the points saw a decrease by 30% to 50%.

Plotted in Figure 5.7 is the comparison of accessible pore volume accessible for 5.4 nm probe for wet and dried PHMHW and PHSG, which was used as an example to illustrate the pore collapsing effect. Over a period of 48 hr the accessible pore volume for dried PHMHW stays at 0.15 ml/g except the 48 hr point and for dried PHSG is almost constantly at 0.22 ml/g. These results reveal a 60 to 70% drop in the accessible pore volume for PHMHW. Due to the pore volume drop as hydrolysis continues for wet PHSG, the difference between the dried PHSG and wet PHSG is narrowed gradually. Since the dried biomass samples were rehydrated after packing into the column for solute exclusion measurement, this decrease in specific pore volume indicates that the pore structure collapsing due to drying is irreversible.

5.3.6. Possible hydrolysis model

The observed decrease in initial reaction rate correlates well with the decrease in accessible pore volume. Since it is necessary to form the enzyme-substrate complex for hydrolysis to occur, less accessible pore volume means less reactive surface area inside cellulose particle available for CWDEs to bind and react on, which leads to an overall decreasing in the reaction rate. The substrate size reduction during hydrolysis can be due to the combination effects of both CWDEs surface reaction and inner pore reaction. The

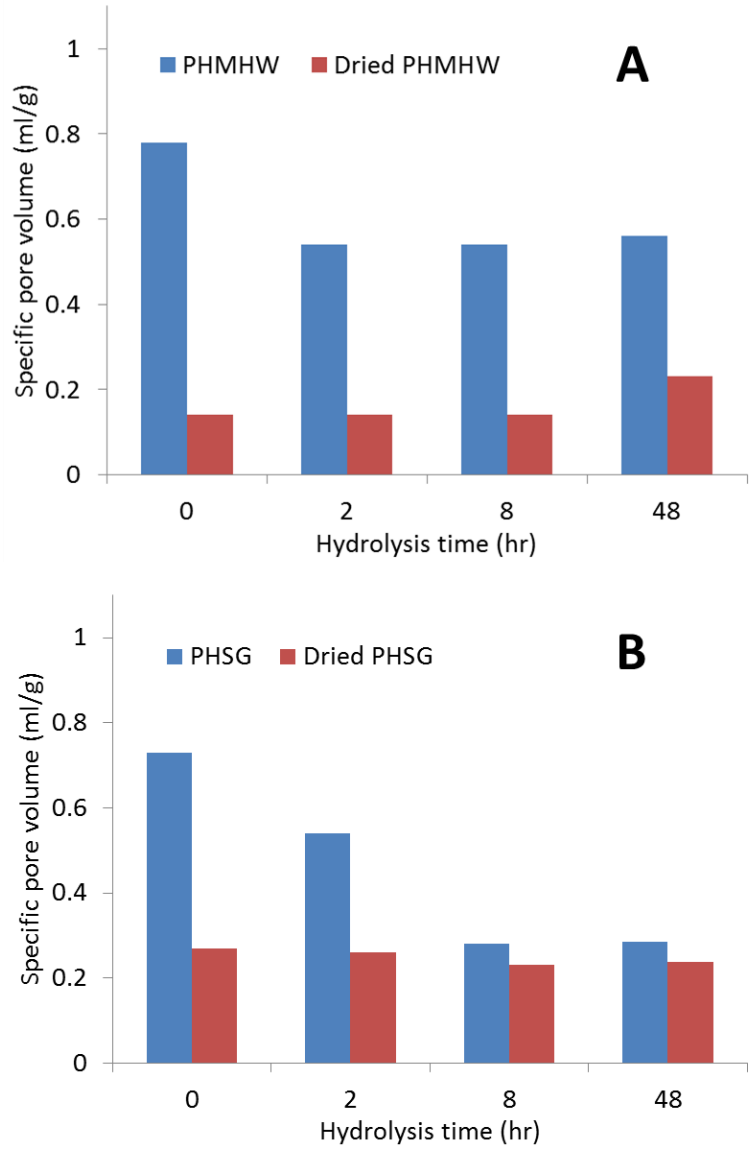

Figure 5.7. Relationship between specific pore volume available for 5.4 nm probe (PEG8000) and hydrolysis time for PHMHW (A) and PHSG (B) for assessing the influence of drying

latter reaction can release more particles, thus reduce the inner pore volume measured by solute exclusion system, since the old inner pore surface becomes outer surface of the newly released particles.

A possible hydrolysis model integrating porous structure change is proposed and illustrated in Figure 5.8. After the CWDEs are incubated together with pretreated biomass, pores are flooded with enzymes and hydrolysis initiates fast in those pores. During this process, pores accessible to CWDEs are enlarged temporally but simultaneously the biomass linkages connecting all the sub-particles are removed. This leads to the result that small biomass particles with less accessible pore volume are released from large biomass particles. From this point hydrolysis enters the slow phase due to the combined effects of limited surface area, enzyme deactivation, lignin and increasing crystallinity.

5.4. Conclusions

It has been shown consistently that CWDEs acting on cellulosic biomass yields an initial high rate of hydrolysis followed by declining rate (Desai and Converse, 1997; van Zyl et al., 2011; Yang et al., 2006; Yu et al., 2012). Enzyme deactivation (Eriksson et al., 2002; Ooshima et al., 1991; Ye et al., 2012; Zhang et al., 2010), increasing cellulose crystallinity (Chang and Holtzapple, 2000; Ciolacu et al., 2012; Fan et al., 1981; Lynd et al., 2002), and lignin content (Kumar et al., 2012; Lee et al., 1994; Mansfield et al., 1999; Zeng et al., 2012) have been proposed as potential reasons for this loss of activity. However, to our knowledge, there has been no study that has shown the decrease in

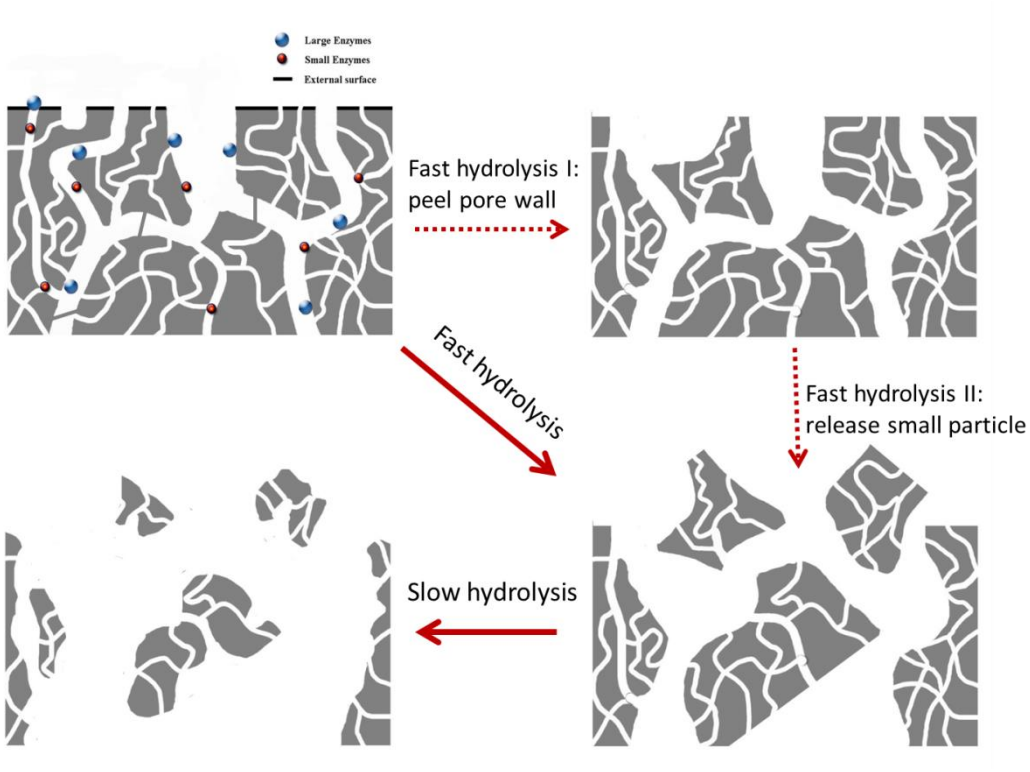

Figure 5.8. Proposed enzymatic hydrolysis model

accessible pore volume of biomass during enzymatic hydrolysis, and how this decrease is linked with the decrease in hydrolysis rate.

We found a strong correlation between the accessibility of the substrate and the rate of hydrolysis. Our results shows that hydrolysis rates decreased by 36.3% and 26.3% for PHSG and PHMHW 2 hr after reaction started, which correlated well with the 30% decrease in accessible pore volume for both PHSG and PHMHW. Reaction rate and surface area both decreased from 2 to 8 hr for PHSG, while only the reaction rate decreased for PHMHW. After 8 hr the reaction rate continues to decline but the accessible pore volume for both PHSG and PHMWH was constant. Our results also showed that 105 °C drying overnight can universally and irreversibly cause biomass pore collapsing and reduce the biomass pore size by up to 80%. Also, results demonstrate that the solute exclusion method is an effective method for measuring the accessibility of complex lignocellulosic materials, and provides a means for documenting the temporal changes in accessibility which is essential for strengthen our understanding of the cellulose-CWDEs reaction systems.

5.5. References

Bradford MM. 1976. A rapid and sensitive method for the quantitation of microgram quantities of protein utilizing the principle of protein-dye binding. Analytical Biochemistry 72(1–2):248-254.

Bubner P, Plank H, Nidetzky B. 2013. Visualizing cellulase activity. Biotechnology and Bioengineering 110(6):1529-1549.

Chang VS, Holtzapple MT. 2000. Fundamental factors affecting biomass enzymatic reactivity Applied Biochemistry and Biotechnology 84-86(1-9):5-37.

Ciolacu D, Pitol-Filho L, Ciolacu F. 2012. Studies concerning the accessibility of different allomorphic forms of cellulose. Cellulose:1-14.

Corner CV. 2003. A size-exclusion chromatography system for observing the transport and weak binding of Thermobifida Fusca catalytic domains: Experiemntal and theoretical investigation. Ph.D. Dissertation, Cornell University, Ithaca.

Desai SG, Converse AO. 1997. Substrate reactivity as a function of the extent of reaction in the enzymatic hydrolysis of lignocellulose. Biotechnology and Bioengineering 56(6):650-655.

Eibinger M, Bubner P, Ganner T, Plank H, Nidetzky B. 2014. Surface structural dynamics of enzymatic cellulose degradation, revealed by combined kinetic and atomic force microscopy studies. FEBS Journal 281(1):275-290.

Eriksson T, Karlsson J, Tjerneld F. 2002. A model explaining declining rate in hydrolysis of lignocellulose substrates with cellobiohydrolase I (Cel7A) and endoglucanase I (Cel7B) of Trichoderma reesei. Applied Biochemistry and Biotechnology 101(1):41-60.

Esteghlalian AR, Bilodeau M, Mansfield SD, Saddler JN. 2001. Do enzymatic hydrolyzability and simons' stain reflect the changes in the accessibility of lignocellulosic substrates to cellulase enzymes? Biotechnology Progress 17(6):1049-1054.

Fan LT, Lee YH, Beardmore DR. 1981. The influence of major structural features of cellulose on rate of enzymatic hydrolysis. Biotechnology and Bioengineering 23(2):419-424.

Goacher RE, Selig MJ, Master ER. 2014. Advancing lignocellulose bioconversion through direct assessment of enzyme action on insoluble substrates. Current Opinion in Biotechnology 27(0):123-133.

Grethlein HE. 1985. The effect of pore size distribution on the rate of enzymatic hydrolysis of cellulosic substrates. Nat Biotech 3(2):155-160.

Grous WR, Converse AO, Grethlein HE. 1986. Effect of steam explosion pretreatment on pore size and enzymatic hydrolysis of poplar. Enzyme and Microbial Technology 8(5):274-280.

Igarashi K, Uchihashi T, Koivula A, Wada M, Kimura S, Okamoto T, Penttilä M, Ando T, Samejima M. 2011. Traffic Jams Reduce Hydrolytic Efficiency of Cellulase on Cellulose Surface. Science 333(6047):1279-1282.

Kumar L, Arantes V, Chandra R, Saddler J. 2012. The lignin present in steam pretreated softwood binds enzymes and limits cellulose accessibility. Bioresource Technology 103(1):201-208.

Lee D, Yu A, Wong K, Saddler J. 1994. Evaluation of the enzymatic susceptibility of

cellulosic substrates using specific hydrolysis rates and enzyme adsorption. Applied Biochemistry and Biotechnology 45-46(1):407-415.
Lin JK, Ladisch MR, Patterson JA, Noller CH. 1987. Determining pore size distribution in wet cellulose by measuring solute exclusion using a differential refractometer. Biotechnology and Bioengineering 29(8):976-981.
Luo X, Zhu JY. 2011. Effects of drying-induced fiber hornification on enzymatic saccharification of lignocelluloses. Enzyme and Microbial Technology 48(1):92-99.
Luterbacher JS, Parlange J-Y, Walker LP. 2013. A pore-hindered diffusion and reaction model can help explain the importance of pore size distribution in enzymatic hydrolysis of biomass. Biotechnology and Bioengineering 110(1):127-136.
Luterbacher JS, Walker LP, Moran-Mirabal JM. 2012. Observing and modeling BMCC degradation by commercial cellulase cocktails with fluorescently labeled Trichoderma reseii Cel7A through confocal microscopy. Biotechnology and Bioengineering:n/a-n/a.
Lynd LR, Weimer PJ, van Zyl WH, Pretorius IS. 2002. Microbial Cellulose Utilization: Fundamentals and Biotechnology. Microbiol. Mol. Biol. Rev. 66(3):506-577.
Mansfield SD, Mooney C, Saddler JN. 1999. Substrate and enzyme characteristics that limit cellulose hydrolysis. Biotechnology Progress 15(5):804-816.
Mooney CA, Mansfield SD, Touhy MG, Saddler JN. 1998. The effect of initial pore volume and lignin content on the enzymatic hydrolysis of softwoods. Bioresource Technology 64(2):113-119.
Moran-Mirabal J. 2013. The study of cell wall structure and cellulose–cellulase interactions through fluorescence microscopy. Cellulose 20(5):2291-2309.
Neuman RP, Walker LP. 1992. Solute exclusion from cellulose in packed columns: Experimental investigation and pore volume measurements. Biotechnology and Bioengineering 40(2):218-225.
Ohmine K, Ooshima H, Harano Y. 1983. Kinetic study on enzymatic hydrolysis of cellulose by cellulose from Trichoderma viride. Biotechnology and Bioengineering 25(8):2041-2053.
Ooshima H, Kurakake M, Kato J, Harano Y. 1991. Enzymatic activity of cellulase adsorbed on cellulose and its change during hydrolysis. Applied Biochemistry and Biotechnology 31(3):253-266.
Rath A, Glibowicka M, Nadeau VG, Chen G, Deber CM. 2009. Detergent binding explains anomalous SDS-PAGE migration of membrane proteins. Proceedings of the National Academy of Sciences 106(6):1760-1765.
Shapiro AL, Viñuela E, V. Maizel Jr J. 1967. Molecular weight estimation of polypeptide chains by electrophoresis in SDS-polyacrylamide gels. Biochemical and Biophysical Research Communications 28(5):815-820.
Silveira RL, Stoyanov SR, Gusarov S, Skaf MS, Kovalenko A. 2013. Plant Biomass Recalcitrance: Effect of Hemicellulose Composition on Nanoscale Forces that Control Cell Wall Strength. Journal of the American Chemical Society 135(51):19048-19051.
van Zyl JM, van Rensburg E, van Zyl WH, Harms TM, Lynd LR. 2011. A Kinetic Model for Simultaneous Saccharification and Fermentation of Avicel With Saccharomyces cerevisiae. Biotechnology and Bioengineering 108(4):924-933.

Walker LP, Wilson DB, Irvin DC, McQuire C, Price M. 1992. Fragmentation of cellulose by the major Thermomonospora fusca cellulases, Trichoderma reesei CBHI, and their mixtures. Biotechnology and Bioengineering 40(9):1019-1026.
Walker LP, Wilson DB, Irwin DC. 1990. Measuring fragmentation of cellulose by Thermomonospora fusca cellulase. Enzyme and Microbial Technology 12(5):378-386.
Yang B, Willies DM, Wyman CE. 2006. Changes in the enzymatic hydrolysis rate of Avicel cellulose with conversion. Biotechnology and Bioengineering 94(6):1122-1128.
Yang D, Parlange J-Y, Walker LP. 2014. Revisiting size-exclusion chromatography for measuring structural changes in raw and pretreated mixed hardwoods and switchgrass. Biotechnology and Bioengineering. In press.
Ye Z, Hatfield KM, Eric Berson R. 2012. Deactivation of individual cellulase components. Bioresource Technology 106(0):133-137.
Yu Z, Jameel H, Chang H-m, Philips R, Park S. 2012. Evaluation of the factors affecting avicel reactivity using multi-stage enzymatic hydrolysis. Biotechnology and Bioengineering 109(5):1131-1139.
Zeng M, Ximenes E, Ladisch MR, Mosier NS, Vermerris W, Huang C-P, Sherman DM. 2012. Tissue-specific biomass recalcitrance in corn stover pretreated with liquid hot-water: SEM imaging (part 2). Biotechnology and Bioengineering 109(2):398-404.
Zhang Y, Xu J-L, Xu H-J, Yuan Z-H, Guo Y. 2010. Cellulase deactivation based kinetic modeling of enzymatic hydrolysis of steam-exploded wheat straw. Bioresource Technology 101(21):8261-8266.
Zhu JY, Pan X, Zalesny R, Jr. 2010. Pretreatment of woody biomass for biofuel production: energy efficiency, technologies, and recalcitrance. Applied Microbiology and Biotechnology 87(3):847-857.

6. CONCLUSIONS

Essential to CWDEs-cellulose reaction systems is the formation of an enzyme-substrate complex. Given the insoluble nature of lignocellulosic biomass, this complex is formed on the accessible reactive surface area of the substrate and the available surface area is a key factor in determining the rate and extent of catalysis (Fan et al., 1980; Grethlein, 1985; Walker and Wilson, 1991). The accessible internal pore surface area is the dominant fraction of the reactive surface area (Arantes and Saddler, 2011; Bothwell et al., 1997). Access to this surface area can be limited by steric hindrance within the pore structure of cellulosic materials. My research has been focused on the fundamental mechanisms that limit CWDEs accessibility to reactive surface area. Three different objectives were defined to addressed this problem: (1) the development of a high resolution microscopy platform to observe, measure and analyze diffusive transport for non-binding species in biomass; (2) the development of a solute exclusion system to measure the pore volume distribution for raw and pretreated mixed hardwoods (MHW) and switchgrass (SG); and (3) the measurement of the temporal changes in pore volume distribution caused by the activities of CWDEs on MHW and SG, and biomass drying.

A key research goal was to gain insights into the steric hindrance that CWDEs encounter in their diffusive movement into the biomass porous space. The diffusion of CWDEs into the porous structure of cellulosic particles was observed to be limited by steric hindrances mainly by the interactions between the diffusing CWDEs and the micropore wall, and collisions between CWDEs. Thus, the molecular diameter of the CWDEs has been shown to be a key factor in their diffusion into the pore structure. Because the high binding

affinity of CWDEs can complicate the process of teasing out diffusive mechanism strictly based on molecular diameter (Jeoh et al., 2002b; Jung et al., 2002; Wang et al., 2008), I chose to study the diffusion of a non-binding molecular probe, dextran, in different sizes into the pore space of cellulosic biomass. Dextran probes with hydrodynamic radii comparable to the size of CWDEs are capable of providing insight into the diffusion hindrance encountered when CWDEs diffuse into cellulosic substrate. My micro-scale solute exclusion technique using a high resolution CLSM microscopy platform allowed for the observation and measure of the diffusion of fluorescently-labeled dextran probes in pore space of filter paper particles. Fitting of the datasets to the simple transient model yielded diffusion coefficients that were inadequate for describing the initial fast diffusion and the later slow diffusion rates observed. A novel pore grouping diffusion model yielded estimations of the micro-pore diffusion coefficient that described the inherently porous structure of plant-derived cellulose. Modeling results showed that on average 75% of the accessible pore volume was available for fast diffusion without any significant pore hindrance. The micro-scale solute exclusion technique provides important insights in the diversity of the pore diameter and its influence on the transport of CWDEs.

The results from Objective 1 and the conclusion that the diversity of the pore diameter is an important factor in determining the transport of CWDEs into the pore structure of lignocellulosic materials lead to my second objective of measuring the accessibility of biomass using size exclusion chromatography. Specific pore volume and specific surface areas measurements were obtained for raw and pretreated mixed-hardwood (MHW) and switchgrass (SG). The measurements for the accessible pore volume available to PEGs

using this system proved to be highly reproducible. Replicate measurements of probe concentrations from this system consistently yielded coefficient of variance of less than 1.5%. This high level of reproducibility was obtained for three particle sizes (0.5, 2.0 and 9.5mm) of raw switchgrass and mixed hardwoods. Particle size reduction had a smaller influence on the specific pore volume distribution of raw biomass. Size reduction from 2 mm to 0.5 mm did not increase pore volume in either MHW or SG. From this I conclude that very little surface area is created for enzyme binding by reducing the particle size. In contrast, bi-phasic pretreated biomass yielded much larger increase in pore volume accessibility. Pore surface area accessible to 5.1 nm probe for pretreated MHW is 120 m^2/g compared to 20-30 m^2/g for raw MHW. For pretreated SG, this area is 90 m^2/g compared to 20-30 m^2/g for raw SG.

Objective 3 was met by successfully measuring the temporal changes in the pore size distribution of pretreated and hydrolyzed switch grass and mixed hardwoods using the methods developed for objective 2. CWDEs dramatically alter the pore volume distribution of lignocellulosic materials in the initial phase of hydrolysis. This conclusion is based on the results that the accessible pore volume in PHMHW and PHSG for probes over the range of 1.89 nm to 12.78 nm decreases by up to 60% after 48 hr hydrolysis. I also concluded that decrease accessibility observed is responsible for the decrease in the rate of hydrolysis. As results showed that hydrolysis rates decreased by 36.3% and 26.3% for PHSG and PHMHW 2 hr after reaction started, correlating well with the 30% decrease in accessible pore volume for 5.4 nm probe in both PHSG and PHMHW. Drying

105 °C overnight can universally and irreversibly cause biomass pore collapsing and reduce the biomass pore size by up to 80%.

Through those three studies, we developed two highly effective platforms, CLSM and solute exclusion column, to earn insights on the interactions of CWDEs and biomass. From the results we conclude that the diversified pore size distribution inside biomass strongly influences the CWDEs transport and hydrolysis. Bi-phasic pretreatment can alleviate this problem and increase the pore volume accessibility for CWDEs by 4 to 5 times. During the initial phase of hydrolysis, CWDEs can dramatically alter the pore volume distribution and reduce accessibility of lignocellulosic materials. This decrease accessibility can contribute to the decrease of the hydrolysis rate.

Suggestions for future work

Mixture of CWDEs, with different catalytic modes, exhibits higher hydrolysis rate and extent than would be predicted by summing their individual activities. This synergistic phenomenon has been strongly documented in the literature but very little is known regarding how the pore structure of biomass influences the degree of synergistic effect (Jeoh et al., 2002a; Ooshima et al., 1991; Walker et al., 1993). The solute exclusion approach we developed can be applied to study synergism and provides the foundation for future studies with CWDEs mixtures that have been engineered to exhibit no binding affinity for the substrate. The enzyme transport and hydrolysis can be studied by performing enzyme hydrolysis experiments in a packed column of cellulose. Solutions with CWDEs are fed to the column and the column effluent is analyzed for hydrolysis

products and CWDEs concentration. Those mutant non-binding CWDEs could be used to see how size-exclusion and pore filtering of molecules from the matrix affects synergism and would help predict the movement of native multi-domain CWDEs.

For CWDEs accommodated by micropores in certain size, their collisions with micropore wall and each other slow down the process for approaching reactive sites, while their binding with the reactive sites reduce the pore sizes and bring down the diffusivity during the initial phase of hydrolysis. These phenomena cannot be studied by using inert probes. Thus to elucidate the mechanistic framework for synergistic CWDEs mixtures, four CWDEs candidates include *T. fusca* Cel5A (endocellulase), Cel6B (exocellulase), Cel9A (processive endocellulase) and Cel61 (oxidative endocellulase) can be labeled with fluorophores in different colors. Those fluorephores serve as reporters to track cellulase diffusion and binding onto the internal physical structure of pretreated biomass by CLSM. This quadruple mixture can be used as CWDEs template to study the pore hindered synergistic effects. The traffic jam inside biomass micropores can be revealed by developing a time-lapsed confocal microscopy method to track fluorescence distributions of labeled CWDEs and pretreated biomass (Moran-Mirabal et al., 2009; Zhu et al., 2011). Meanwhile, the decreasing biomass auto-fluorescence intensity over time can be measured to generate additional information on biomass destruction process, together with sugar production data and temporal porous volume data to better model the biomass structure change during hydrolysis. Through all these measures, systematical understanding of interaction between substrate structure and the synergistic activities of CWDEs mixtures during hydrolysis process is expected to be obtained.

References

Arantes V, Saddler J. 2011. Cellulose accessibility limits the effectiveness of minimum cellulase loading on the efficient hydrolysis of pretreated lignocellulosic substrates. Biotechnology for Biofuels 4(1):3.

Bothwell MK, Daughhetee SD, Chaua GY, Wilson DB, Walker LP. 1997. Binding capacities for Thermomonospora fusca E3, E4 and E5, the E3 binding domain, and Trichoderma reesei CBHI on Avicel and bacterial microcrystalline cellulose. Bioresource Technology 60(2):169-178.

Fan LT, Lee Y-H, Beardmore DH. 1980. Mechanism of the enzymatic hydrolysis of cellulose: Effects of major structural features of cellulose on enzymatic hydrolysis. Biotechnology and Bioengineering 22(1):177-199.

Grethlein HE. 1985. The effect of pore size distribution on the rate of enzymatic hydrolysis of cellulosic substrates. Nat Biotech 3(2):155-160.

Jeoh T, Wilson DB, Walker LP. 2002a. Cooperative and competitive binding in synergistic mixtures of *Thermobifida fusca* Cel5A, Cel6B and Cel9A. Biotechnology Progress 18(4):760-769.

Jeoh T, Wilson DB, Walker LP. 2002b. Cooperative and Competitive Binding in Synergistic Mixtures of Thermobifida fuscaCellulases Cel5A, Cel6B, and Cel9A. Biotechnology Progress 18(4):760-769.

Jung H, Wilson DB, Walker LP. 2002. Binding of Thermobifida fusca CDCel5A, CDCel6B and CDCel48A to easily hydrolysable and recalcitrant cellulose fractions on BMCC. Enzyme and Microbial Technology 31(7):941-948.

Moran-Mirabal JM, Corgie SC, Bolewski JC, Smith HM, Cipriany BR, Craighead HG, Walker LP. 2009. Labeling and purification of cellulose-binding proteins for high resolution fluorescence applications. Analytical Chemistry 81(19):7981-7987.

Ooshima H, Kurakake M, Kato J, Harano Y. 1991. Enzymatic activity of cellulase adsorbed on cellulose and its change during hydrolysis. Applied Biochemistry and Biotechnology 31(3):253-266.

Walker LP, Belair CD, Wilson DB, Irwin DC. 1993. Engineering cellulase mixtures by varying the mole fraction of *Thermomonospora fusca* E5 and E3, *Trichoderma reesei* CBHI, and *Caldocellum saccharolyticum* beta-glucosidase. Biotechnology and Bioengineering 42:1019-1028.

Walker LP, Wilson DB. 1991. Enzymatic hydrolysis of cellulose: An overview. Bioresource Technology 36(1):3-14.

Wang J, Dismer F, Hubbuch J, Ulbricht M. 2008. Detailed analysis of membrane adsorber pore structure and protein binding by advanced microscopy. Journal of Membrane Science 320(1-2):456-467.

Zhu P, Moran-Mirabal J, Luterbacher J, Walker L, Craighead H. 2011. Observing Thermobifida fusca cellulase binding to pretreated wood particles using time-lapse confocal laser scanning microscopy. Cellulose 18(3):749-758.